

**SYNTHESIS AND CHARACTERIZATION OF SUPPORTED
NANO Pd-BASED CATALYST FOR CONVERSION OF
GLYCEROL TO VALUE ADDED CHEMICALS**

NORFATEHAH BINTI BASIRON

**INSTITUTE OF GRADUATE STUDIES
UNIVERSITY OF MALAYA
KUALA LUMPUR**

2016

**SYNTHESIS AND CHARACTERIZATION OF
SUPPORTED NANO Pd-BASED CATALYST FOR
CONVERSION OF GLYCEROL TO VALUE ADDED
CHEMICALS**

NORFATEHAH BINTI BASIRON

**DISSERTATION SUBMITTED IN FULFILLMENT OF
THE REQUIREMENTS FOR THE DEGREE OF MASTER
OF PHILOSOPHY**

**INSTITUTE OF GRADUATE STUDIES
UNIVERSITY OF MALAYA
KUALA LUMPUR**

2016

UNIVERSITY OF MALAYA
ORIGINAL LITERARY WORK DECLARATION

Name of Candidate: NORFATEHAH BINTI BASIRON

(I.C/Passport No:

Registration/Matric No: HGA130001

Name of Degree: Master of Philosophy

Title of Project Thesis ("this Work"): Synthesis and Characterization of Supported Nano Pd-based Catalyst for Conversion of Glycerol to Value Added Chemicals

Field of Study: Chemistry (Catalysis)

I do solemnly and sincerely declare that:

- (1) I am the sole author/writer of this Work;
- (2) This Work is original;
- (3) Any use of any work in which copyright exists was done by way of fair dealing and for permitted purposes and any excerpt or extract from, or reference to or reproduction of any copyright work has been disclosed expressly and sufficiently and the title of the Work and its authorship have been acknowledged in this Work;
- (4) I do not have any actual knowledge nor do I ought reasonably to know that the making of this work constitutes an infringement of any copyright work;
- (5) I hereby assign all and every rights in the copyright to this Work to the University of Malaya ("UM"), who henceforth shall be owner of the copyright in this Work and that any reproduction or use in any form or by any means whatsoever is prohibited without the written consent of UM having been first had and obtained;
- (6) I am fully aware that if in the course of making this Work I have infringed any copyright whether intentionally or otherwise, I may be subject to legal action or any other action as may be determined by UM.

Candidate's Signature

Date:

Subscribed and solemnly declared before,

Witness's Signature

Date:

Name:

Designation:

ABSTRACT

The abundance bio-availability of glycerol mostly due to biodiesel production, makes it a particularly attractive as feed for the synthesis of value-added chemicals where a series of very important valuable oxygenates can be obtained through selective oxidation of glycerol. The highly selective catalysts are stable for glycerol oxidation to produce valuable chemicals, which potential in industrial manufacturing and environmental applications. There are two main reaction pathways for the oxidation of glycerol, i.e. intermediates via primary hydroxyl or secondary hydroxyl group. The pathway of the reaction is favored by the reaction conditions since glycerol oxidation can occur in acidic or basic pH conditions when using palladium catalyst. The present study, focus on transformation of glycerol to glyceric acid over supported palladium catalysts. Catalyst supports; activated carbon and hydrotalcite were pre-treated and synthesized before adding to the palladium. The three different supported catalysts (1wt% Pd/AC1, 1wt% Pd/HTc and 1wt% Pd/HTc-AC1) were prepared through immobilization method by using poly vinyl alcohol as a surfactant. The catalysts were characterized using TGA, TPR, TPD-CO₂, N₂ Physisorption, XRD, XRF and HR-TEM for physical and morphological properties. These catalysts were subjected to glycerol oxidation to glyceric acid at mild condition (333 K, 3 bar of O₂, 180 minutes and 750 rpm). The obtained results showed better performance of 1wt% Pd/HTc. Further evaluation at various temperature (303-383 K), partial oxygen pressure (1-9 bar), molar ratio NaOH/Glycerol (0-4) showed that 1wt% Pd/HTc catalyst gave the highest conversion of 70.35% and 80.37% selectivity to glyceric acid. Both conversion and selectivity increase with the increase of reaction temperature and pressure. The results also showed that, the conversion increase with increase NaOH/glycerol molar ratio. However, as the NaOH/glycerol, molar ratio exceed two, more side products were generated. Other than that, as the temperature and molar ratio of base/glycerol increased, the selectivity decreases. In summary, oxidation of glycerol

mechanism is a dehydrogenation step, hence, the pH of the reaction medium is a crucial factor in this reaction. The temperature plays an important role in glycerol oxidation as palladium metal is non-active at a lower temperature. Furthermore, the influenced of catalyst amount and stirring rate were studied to understand the mass transfer limitation on this reaction. The stability of the catalyst was investigated by filtration experiments and the reaction were re-run three times. The glycerol conversion were reduced from 80.37% to 61.34% for final run suggesting inhomogeneous leaching of palladium could have occurred.

University of Malaya

ABSTRAK

Bio-ketersediaan gliserol disebabkan produksi biodisel menjadikan ianya sangat menarik sebagai bahan mentah untuk sintesis satu siri bahan kimia beroksigen yang berharga boleh diperolehi melalui proses pengoksidaan terpilih gliserol. Pemangkin yang sangat selektif dan stabil untuk pengoksidaan gliserol dalam menghasilkan bahan kimia adalah sesuai dan mempunyai potensi besar dalam industri pembuatan dan aplikasi untuk alam sekitar. Terdapat dua laluan utama untuk tindak balas pengoksidaan gliserol, iaitu perantaraan melalui kumpulan hidroksil pertama atau hidroksil kedua. Jenis laluan untuk tindak balas pengoksidaan gliserol adalah ditentukan daripada keadaan tindak balas, lantaran, pengoksidaan gliserol berlaku dalam keadaan pH berasid atau beralkali apabila menggunakan pemangkin palladium. Usaha telah dibuat untuk menukarkan gliserol ke gliserik asid oleh pemangkin tersokong paladium. Penyokong mangkin berasaskan karbon teraktif dan hidrotalsit; dirawat dan disintesis sebelum ia dicampur ke palladium. Ketiga-tiga pemangkin tersokong yang berbeza (1wt% Pd/AC1, 1wt% Pd/HTc dan 1wt% Pd/HTc-AC1) telah disediakan melalui kaedah “immobilization” dengan menggunakan poli vinil alkohol sebagai surfaktan. Pemangkin telah dicirikan dengan menggunakan kaedah TGA, TPR, TPD, N₂ Physisorption, XRD, XRF dan HR-TEM untuk sifat fizikal dan morfologi. Semua pemangkin digunakan untuk pengoksidaan gliserol ke gliserik asid pada keadaan sederhana (333 K, 3 bar O₂, 180 minit dan 750 rpm). Keputusan yang diperolehi menunjukkan prestasi yang paling baik untuk 1wt% Pd/HTc. Oleh yang demikian, pemangkin ini telah dinilai dengan lebih lanjut pada pelbagai suhu (303-383 K), tekanan oksigen (1-9 bar), nisbah molar NaOH/Glycerol (0-4). Untuk menyiasat kestabilan pemangkin, ianya terus digunakan untuk tindak balas pada masa yang tertentu. 1wt% Pd/HTc telah memberikan penukaran tertinggi iaitu 70.35% dan 80.37% pemilihan ke gliserik acid. Penukuran dan pemilihan meningkat dengan peningkatan suhu dan tekanan tindak balas. Keputusan ini juga menunjukkan bahawa penukaran gliserol

meningkat dengan peningkatan nisbah molar NaOH/glisserol. Walau bagaimanapun, apabila nisbah molar NaOH/glisserol meningkat lebih dari dua, lebih banyak produk sampingan terhasil. Selain daripada itu, apabila suhu dan nisbah molar alkali/glisserol meningkat, pemilihan berkurangan. Kesimpulannya, mekanisme pengoksidaan gliserol adalah langkah nyahhidrogenan, dengan itu pH medium tindak balas adalah merupakan faktor penting untuk tindak balas ini. Suhu memainkan peranan penting di dalam pengoksidaan gliserol kerana besi paladium tidak aktif pada suhu yang rendah. Tambahan pula, pengaruh jumlah pemangkin dan kadar kacau dipelajari untuk memahami had pemindahan jisim dalam tindak balas ini. Kestabilan pemangkin di kaji menggunakan kaedah penapisan dan mengulangi tindak balas sebanyak tiga kali dan didapati “inhomogeneous leaching” palladium terjadi. Penukaran gliserol berkurangan daripada 70.35% kepada 61.34% pada tindak balas yang terakhir, ini menunjukkan bahawa palladium berkemungkinan mengalami proses larut tak homogen.

ACKNOWLEDGEMENTS

A special Thank You to the people at the Nanotechnology and Catalysis Research Centre (NANOCAT) and my surrounding friends.

First of all, I would like to express my deepest gratitude to my first supervisor Prof Sharifah Bee Abd Hamid for her excellent cooperation and guidance, and the opportunities I was given to conduct my research and further my studies at NANOCAT. In addition, I would also like to thank my second supervisor Dr Wageeh Abdulhadi Yehya Dabdawb for his guidance, assistance and concern throughout my research project. Their wide knowledge and valuable comments have provided a good basis for my project and thesis. I extend my gratitude further for their willingness to spend their valuable time and tireless help in guiding me to complete this project. I deeply expressed my thanks to them for all help and guidance rendered to me until completion of this thesis.

Besides that, I would like to express a special thanks to all staffs in NANOCAT, departments of physics and chemistry in University Malaya (UM), respectively for their continuous guidance and assistance during all the samples preparation and testing. Most importantly, I would like to greatly acknowledge my colleagues in UM and all my dearest friends in NANOCAT. I deeply appreciated their precious ideas and support throughout the entire study.

This research was supported by a grant from the Fundamental Research Grant Scheme (FRGS), University Malaya Research Grant (UMRG) and High Impact Research Grant for the sources of funding through this study. I gratefully acknowledge UM for financial supporting that helping me in this study. Lastly, I would like to take this opportunity to express my deepest gratitude to my beloved parents, siblings and all family members through their encouragement and support me to continue studying.

TABLE OF CONTENTS

Abstract	iii
Abstrak	v
Acknowledgements	vii
Table of contents	viii
List of Figures	xiii
list of table.....	xvi
List of Symbols and Abbreviation	xviii
List of equation	xxii
List of Scheme.....	xxiii
CHAPTER 1: INTRODUCTION	1
1.1 Research Background	1
1.2 Problem Statement.....	4
1.3 Scope of the present work.....	5
1.4 Objectives	6
1.5 Organization of Thesis.....	6
CHAPTER 2: LITERATURE REVIEW.....	9
2.1 Depletion of fossil fuels.....	9
2.2 Biomass as a renewable resources	10
2.3 Glycerol	12
2.4 Production of glycerol	12
2.4.1 Glycerol from fats and oils.....	12
2.4.2 Fats Splitting.....	12
2.4.3 High Pressure Splitting.....	13

2.4.4	Transesterification	13
2.5	Application of glycerol	13
2.6	Converting glycerol to value added chemicals	14
2.6.1	Selective Reduction (Hydrogenolysis and Hydrogenation)	15
2.6.2	Etherification	15
2.6.3	Esterification	16
2.6.4	Dehydration	16
2.6.5	Chlorination.....	17
2.6.6	Reforming.....	17
2.6.7	Selective oxidation of glycerol.....	18
2.7	Heterogeneous Catalyst	18
2.7.1	Catalyst Support	25
2.7.1.1	Carbon Support	25
2.7.1.2	Metal oxides	29
2.8	Preparation method.....	31
2.9	Palladium catalysts for selective oxidation.....	32
2.9.1	Glycerol oxidation to glyeric acid using palladium catalyst.....	34
2.10	Catalyst deactivation.....	36
2.10.1	Oxygen poisoning.....	36
2.10.2	Chemical poisoning.....	37
2.10.3	Leaching	37
2.10.4	Sintering	37

CHAPTER 3: METHODOLOGY	38
3.1 Synthesis of heterogeneous solid supported catalysts	38
3.1.1 Materials and reagents	38
3.1.2 Preparation of catalyst supports	38
3.1.2.1 Pre-treatment of Activated carbon	38
3.1.2.2 Hydrotalcite	39
3.1.3 Preparation of supported catalysts.....	39
3.2 Catalyst characterization.....	40
3.2.1 Nitrogen physisorption measurement.....	40
3.2.2 X-Ray Powder Diffraction (XRD)	44
3.2.3 X-Ray Fluorescence (XRF).....	45
3.2.4 Fourier Transform Infrared Spectroscopy (FTIR).....	47
3.2.5 Temperature-Programmed Reduction (TPR)	49
3.2.6 Temperature Program Desorption CO ₂ (TPD-CO ₂).....	50
3.2.7 Thermal-Gravimetric Analysis- Mass Spectrometry (TGA-MS).....	51
3.2.8 Thermal-Gravimetric Analysis (TGA-Proximate analysis)	52
3.2.9 High Resolution Transmission Electron Microscopy (HR-TEM)	53
3.2.10 Surface acidity determination.....	55
3.3 Catalyst preparation	57
3.3.1 Calcination of catalyst	57
3.3.2 Activation of catalyst.....	58
3.4 Liquid phase oxidation of glycerol	59
3.4.1 Materials	59
3.4.2 Reaction setup	59
3.4.3 Product analysis.....	62
3.4.3.1 High performance liquid chromatography	62

3.4.4	Activity calculation	64
CHAPTER 4: RESULTS AND DISCUSSION FOR CATALYSTS		66
4.1	Catalyst support (Activated Carbon)	66
4.1.1	Surface Acidity Determination (Boehm Titration).....	66
4.1.2	Thermal-Gravimetric Analysis (TGA- Proximate analysis)	69
4.1.3	Fourier Transform Infrared Spectroscopy (FTIR).....	72
4.1.4	Nitrogen Physisorption	74
4.2	Catalyst support (Hydrotalcite).....	78
4.2.1	Thermal-Gravimetric Analysis (TGA-MS).....	78
4.2.2	Temperature Program Desorption CO ₂ (TPD-CO ₂).....	81
4.2.3	X-Ray Powder Diffraction (XRD)	83
4.2.4	Fourier Transform Infrared Spectroscopy	88
4.3	Pd-based supported catalyst.....	89
4.3.1	Thermal-Gravimetric Analysis (TGA)	89
4.3.2	Nitrogen Physisorption (BET).....	94
4.3.3	X-Ray Powder Diffraction (XRD)	97
4.3.4	X-Ray Fluorescence (XRF).....	99
4.3.5	Temperature Program Desorption CO ₂ (TPD-CO ₂).....	101
4.3.6	High-Resolution Transmission Electron Microscopy (HR-TEM)	103
4.3.7	Temperature-Programmed Reduction (TPR)	107
CHAPTER 5: LIQUID PHASE OXIDATION OF GLYCEROL.....		109
5.1	Catalyst screening for glycerol oxidation	109
5.2	Effect of catalyst supports	112
5.3	Effect of reaction condition	113
5.3.1	Influence of partial oxygen pressure	113

5.3.2	Influence of reaction temperature.....	116
5.3.3	Influence of Influence of NaOH/ glycerol molar ratio.....	118
5.3.4	Influence of catalyst amount	121
5.3.5	Influence of stirring rate	123
5.4	Catalyst Stability.....	124
5.4.1	Filtration experiments.....	124
5.4.2	Reusability.....	125
CHAPTER 6: CONCLUSION AND FUTURE WORKS		127
6.1	Conclusion.....	127
6.2	Future works	129
References.....		131
List of Publications and Papers Presented		147
Appendix.....		148

LIST OF FIGURES

Figure 1.1: General scheme of Glycerol Oxidation (Zhou et al., 2008)	2
Figure 2.1: Biodiesel production cycle (Pagliaro et al., 2007).....	13
Figure 2.2: Sabatier principle (Medford et al., 2015)	20
Figure 2.3: Schematic representation of the structure of activated carbon (Toebe et al., 2001).....	27
Figure 2.4: Layer structure of graphite (Toebe et al., 2001)	28
Figure 2.5: Structure of hydrotalcite (Álvarez et al., 2012).....	31
Figure 3.1: Models of two types of physisorption. A, gas-like; B, liquid-like;• before encounter;after encounter, hatched is during encounter (Condon, 2006)	40
Figure 3.2: Type of isotherms	42
Figure 3.3: The excitation energy from inner atom is transferred to one of the outer electrons causing it to be ejected from the atom.	47
Figure 3.4: High resolution transmission electron microscopic principle.	54
Figure 3.5: Calcination procedure for palladium-based supported catalysts	57
Figure 3.6: Reduction procedure for palladium-based supported catalysts	58
Figure 3.7: Experimental set up of the glycerol oxidation.....	61
Figure 3.8: Schematic diagram of experimental set up of the glycerol oxidation	61
Figure 3.9: Calibration of curve of the standards for glycerol oxidation; GLY:glycerol, GLYALD:glyceraldehyde, GLYAC:glyceric acid, DHA:dihydroxyacetone and TARAC:tartronic acid.....	63
Figure 4.1: Acid-base titration profile for of non-treated activated carbon (AC).....	68
Figure 4.2: Acid-base titration profile for treated activated carbon (AC1).....	69
Figure 4.3: Proximate Analysis of non-treated activated carbon (AC).....	71
Figure 4.4: Proximate Analysis of treated activated carbon (AC1).....	71

Figure 4.5: FTIR spectra of (a) non-treated activated carbon (AC) and (b) treated activated carbon	73
Figure 4.6: The schematic representation of an activated carbon granule (Rodrigues-Reinoso, 1998)	76
Figure 4.7: N ₂ adsorption/desorption of non-treated activated carbon (AC); ● desorption ■ adsorption	77
Figure 4.8: N ₂ adsorption/desorption of treated activated carbon (AC1); ● desorption ■ adsorption	77
Figure 4.9 : The thermal evaluation of Mg-Al-CO ₃ LDH as a function of temperature (Yang et al., 2002).....	78
Figure 4.10: TGA analysis of hydrotalcite with Al/(Al+Mg)=0.20.....	80
Figure 4.11: Mass Spectrometric of hydrotalcite with 0.20 ratio	80
Figure 4.12 : Deconstruction of the hydrotalcite structure after calcination (HTc) (Li, 1977)	81
Figure 4.13: Temperature-programmed desorption of CO ₂ profiles of HTc	82
Figure 4.14: XRD pattern of HT 0.20 with pattern list (PDF NO:890460)	85
Figure 4.15: Structure of Hydrotalcite	85
Figure 4.16: XRD pattern of HTc and pattern peak list for MgO (PDF No: 77- 2179) and AlO(OH) (PDF No: 76-1871).....	86
Figure 4.17: Schematic overview of structural and compositional transformation processes during thermal or chemical reaction of Mg-Al hydrotalcite like materials and Mg-Al mixed oxides (Kuśtrowski et al., 2006; Mokhtar et al., 2010)	87
Figure 4.18: FTIR spectra of hydrotalcite and calcined hydrotalcite.....	88
Figure 4.19: TGA curves of 1wt% Pd/AC1, 1wt% Pd/HTc and 1wt% Pd/HTc-AC1 catalysts.....	90
Figure 4.20: TGA-DTA combine with MS curve of 1wt% Pd/AC1	91
Figure 4.21: TGA-DTA combine with MS curve of 1wt% Pd/HTc.....	92
Figure 4.22: TGA-DTA combine with MS curve of 1wt% Pd/HTc-AC1	93

Figure 4.23: N ₂ adsorption/desorption isotherms of 1wt% Pd/AC1 ; ● desorption ■ adsorption	95
Figure 4.24: N ₂ adsorption/desorption isotherms of 1wt% Pd/HTc ; ●desorption ■ adsorption	96
Figure 4.25: N ₂ adsorption/desorption isotherms of 1wt% Pd/HTc-AC1; ●desorption ■ adsorption	96
Figure 4.26: X-Ray Diffraction patterns of various catalysts	98
Figure 4.27: Temperature-programmed desorption of CO ₂ profiles of various catalysts	102
Figure 4.28: The HR-TEM overview image of 1wt% Pd/AC1 and Palladium particles distribution.....	104
Figure 4.29: The HR-TEM overview image of 1wt% Pd/HTc and Palladium particles distribution.....	104
Figure 4.30: The HR-TEM overview image of 1wt% Pd/HTc-AC1 and Palladium particles distribution	105
Figure 4.31: HR-TEM micrographs of a)1wt% Pd/AC1, b) 1wt% Pd/HTc and c)1wt% Pd/HTc-AC1, respectively with magnification of 60,000 times	106
Figure 4.32: Temperature-programmed reduction profiles of palladium catalysts and supports.....	108
Figure 5.1: Effect of the oxygen pressure on the conversion and selectivity to glyceric acid in the liquid-phase glycerol oxidation	115
Figure 5.2: Effect of the reaction temperature on the conversion and selectivity to glyceric acid in the liquid-phase glycerol oxidation	117
Figure 5.3: Effect of the NaOH/Glycerol molar ratio on the conversion and selectivity to glyceric acid in the liquid-phase glycerol oxidation.....	120
Figure 5.4: Glycerol conversion with 1wt% Pd/HTc at different catalyst amounts.	122
Figure 5.5: Glycerol conversion without catalyst at 3h in filtration test with 1wt% Pd/HTc catalyst.....	125
Figure 5.6: Reusability study using 1wt% Pd/HTc catalyst, reaction condition: 0.3M glycerol, glycerol/Pd=3500 mol/mol, Naoh/glycerol=2, 3 hours, 1000rpm at 363 K and 9 bar O ₂	126

LIST OF TABLE

Table 2.1: Overview of glycerol oxidation over supported noble metal catalysts in water using oxidative condition	23
Table 2.2: Iso-electric points of various oxides (Wang & Chen, 2015)	30
Table 2.3: Overview of glycerol oxidation by palladium catalysts	35
Table 3.1: Classification of physical adsorption isotherms	43
Table 3.2: Calcination temperature for various palladium-based supported catalyst.....	57
Table 3.3: Temperature and condition of activation for each catalyst.....	59
Table 3.4: Parameters of HPLC analysis for glycerol oxidation	62
Table 3.5: Response factor and retention time of standards	64
Table 4.1: Oxygen-containing groups of non-treated activated carbon (AC) and treated activated carbon (AC1) pretreated with 5M HNO ₃	68
Table 4.2: Proximate analysis of the activated carbon.....	71
Table 4.3: IR assignments of functional group on Non-treated Activated carbon (AC) and Treated Activated carbon (AC1) (Al-Qodah & Shawabkah, 2009; Barkauskas & Dervinyte, 2003).....	74
Table 4.4: N ₂ physisorption of nontreated activated carbon (AC) and treated activated carbon (AC1)	76
Table 4.5: TGA analysis of hydrotalcite with Al(Mg+Al)=0.20 ratio.....	81
Table 4.6: X-Ray diffraction results of HT 0.20 and HTc 0.20	87
Table 4.7: Summary of TGA-DTA results	90
Table 4.8: Nitrogen Physisorption results of palladium based supported catalysts and catalyst support	97
Table 4.9: Chemical composition of 1wt% Pd/AC1	99
Table 4.10: Chemical composition of 1wt% Pd/HT	100
Table 4.11: Chemical composition of 1wt% Pd/HTc-AC1	100

Table 4.12: CO ₂ adsorption of various catalysts	103
Table 5.1: Glycerol oxidation over various catalyst systems.....	111
Table 5.2: Effect of the oxygen pressure on the conversion and selectivity to glyceric acid in the liquid-phase glycerol oxidation with 1wt%Pd/HTc at different oxygen pressure	115
Table 5.3: Effect of the temperature on the conversion and selectivity to glyceric acid in the liquid-phase glycerol oxidation with 1wt% Pd/HTc at different reaction temperature	117
Table 5.4: Effect of the NaOH/Glycerol mol ratio on the conversion and selectivity to glyceric acid in the liquid-phase glycerol oxidation with 1wt%Pd/HTc at different mol ratio of NaOH.....	119
Table 5.5: Effect of the Glycerol/Pd mol ratio on the conversion and selectivity to glyceric acid in the liquid-phase glycerol oxidation with 1wt%Pd/HTc at different mol ratio of Glycerol/Pd	122
Table 5.6: Effect of the stirring speed on the conversion and selectivity to glyceric acid in the liquid-phase glycerol oxidation with 1wt%Pd/HTc at different stirring speed.....	124

LIST OF SYMBOLS AND ABBREVIATION

1,2-PD	:	1-propanediols
1,3-PD	:	2-propanediols
1wt% Pd/AC1	:	1wt% of palladium metal supported on treated activated carbon
1wt% Pd/HTc	:	1wt% of palladium supported on calcined hydrotalcite
1wt% Pd/HTc-AC1	:	1wt% of palladium supported on composite of treated activated carbon and calcined hydrotalcite
AC	:	Non-treated activated carbon
AC1	:	Treated activated carbon
Apr	:	Aqueous phase reforming
Au/Al ₂ O ₃	:	Gold supported on alumina
Au-Pt/MgO	:	Bimetallic of gold and platinum supported on magnesium oxide
Au/G	:	Gold supported on graphite
Au/PUF	:	Gold supported on poly urea formaldehyde
AgO	:	Silver oxide
Al(NO ₃) ₃ ·9H ₂ O	:	Aluminium nitrate nonahydrate
Al-(OH)-Mg OH	:	Aluminium hydroxide binding with magnesium hydroxide
Al ₂ O ₃	:	Aluminium Oxide
BET	:	Brunauer-Emmett-Teller
Bi/Mo	:	Bismuth supported on molybdenum
Conv.	:	Conversion
CNFP	:	Carbon nanofibers platelet type
CNF-R	:	Carbon nanofiber ribbon type
CNF-F	:	Carbon nanofiber fishbone type
CeO ₂	:	Cerium(IV) Oxide
Cu K α	:	Copper radiation
cm ⁻¹	:	Wavenumber
Cm ³	:	Volume
DAG	:	Diacylglycerol

DHA	:	Dihydroxyacetone
DTA	:	Differential thermal analysis
ECH	:	epichlorohydrin
FTIR	:	Fourier transform infrared
FAME	:	Fatty acid methyl ester
GLY	:	Glycerol
GLYAC	:	Glyceric acid
GLYALD	:	Glyceraldehyde
G	:	Graphite
HNO ₃	:	Nitric acid
HR-TEM	:	High resolution transmission electron microscopy
HYDROXY	:	Hydroxypyruvic
HT	:	Hydrotalcite
HTc	:	Calcined hydrotalcite
HCl	:	Hydrochloric acid
He	:	Helium
H ₂	:	Hydrogen
H ₂ O ₂	:	Hydrogen peroxide
<i>hkl</i>	:	Lattice plane
HPLC	:	High performance liquid chromatography
H ₂ SO ₄	:	Sulphuric acid
HT 0.20	:	Hydrotalcite with ratio 0.20
IR	:	Infrared
KOH	:	Potassium hydroxide
KW	:	Kilo watt
KBr	:	Potassium bromide
KCl	:	Potassium chloride
LiOH	:	Lithium hydroxide
La ₂ O ₃	:	Lanthanum oxide
M	:	Mol/L, molar
Mpa	:	millipascal
MAG	:	Mono acylglycerol
MEXOLA	:	Mesoxalic acid
MWCNT	:	Multi walled carbon nanotube

MnO^2	:	Manganese oxide
MgO	:	Magnesium oxide
Mg(OH)_2	:	Magnesium hydroxide, brucite
M_w	:	Molecular weight
$\text{Mg(NO}_3)_2 \cdot 6\text{H}_2\text{O}$:	Magnesium nitrate tetrahydrate
NaOH	:	Sodium hydroxide
Na_2CO_3	:	Sodium carbonate
N_2	:	Nitrogen gas
NaHCO_3	:	Sodium bicarbonate
O_2	:	Oxygen gas, molecular oxygen
OXALA	:	Oxalic acid
OH	:	Hydroxyl
Pd/ac	:	Palladium supported on activated carbon
PVA	:	Poly vinyl alcohol
PVP	:	Poly vinyl pyrrolidone
PPT	:	polyesterpolypropylene terephthalate
PTT	:	polytrimethylene terephthalate
Pd-Au/G	:	Bimetallic palladium with gold supported on graphite
Pt-Bi/C	:	Bimetallic platinum with bismuth supported on carbon
Pd-Ag/SiO ₂	:	Bimetallic palladium with silver supported on silica
Pt/HT	:	Platinum supported on hydrotalcite
Pt/C	:	Platinum supported on carbon
Pt-Au/MWCNT	:	Bimetallic platinum with gold supported on multi wall carbon nanotube
Pt/CNF	:	Platinum supported on carbon nanofiber
PEG	:	Poly ethylene glycol
Pd/Al ₂ O ₃ :	:	Palladium supported on alumina
PdO	:	Palladium oxide
PO ₂	:	Partial oxygen pressure
RCH ₂ O	:	Alkoxy
Ref.	:	Reference
Rpm	:	Revolution per minutes, stirring

SiO ₂	:	Silicon Dioxide
Sb ₂ O ₃	:	Antimony trioxide
SnO ₂	:	Tin oxide
SS	:	Stainless steel
S _{BET}	:	BET surface area
S _{products}	:	Selectivity of the products
TGA	:	Thermal gravimetric analysis
TPD-CO ₂	:	Temperature programmed desorption of carbon dioxide
TPD	:	Temperature programmed desorption
TGA-MS	:	Thermal gravimetric analysis-mass spectroscopy
TPR	:	Temperature programmed reduction
TARAC	:	Tartronic acid
Temp.	:	Temperature
TiO ₂	:	Titanium Dioxide
TOF	:	Turn over frequency
THPC	:	Tetrakis hydroxymethyl phosphonium chloride
XRD	:	X-ray diffraction
XRF	:	X-ray fluorescence
X _{gly}	:	Conversion of glycerol
Y ₂ O ₃	:	Yttrium oxide
Y _{products}	:	Yield of products
ZPC	:	Zero point of charge
ZrO ₂	:	Zirconium dioxide
ZnO	:	Zinc oxide

LIST OF EQUATION

$\frac{P}{n^a(p_0 - p)} = \frac{1}{n_m^a C} + \left(\frac{C-1}{n_m^a C} \right) \frac{p}{p_0}$	(Equation 3.1).....41
$a_s(BET) = \frac{n_m^a \cdot L \cdot a_m}{m}$	(Equation 3.2)41
$\langle L \rangle = K\lambda\beta\cos\theta$	(Equation 3.3).....45
$X_{GLY} = \frac{y}{x} \times 100$	(Equation 3.4)64
$S_{products} = \frac{\text{area of the product peaks}}{\text{total peak area of the products}} \times 100$	(Equation 3.5).....64
$Y_{products} = X_{GLY} \times S_{products}$	(Equation 3.6).....64
$TOF = \frac{\text{mmol of converted glycerol}}{\text{mmol of total Pd} \times \text{Reaction time (hour)}}$	(Equation 3.7)65
$n\lambda = 2d_{(hkl)} \sin \Theta$	(Equation 4.1).....83
$O_2^* + H_2O^* \rightarrow OOH^* + HO^*$	(Equation 5.1)114
$OOH^* + H_2O^* \rightarrow H_2O_2^* + HO^*$	(Equation 5.2).....114
$HO^* + e^- \leftrightarrow HO^- + ^*$	(Equation 5.3).....114

LIST OF SCHEME

Scheme 2.1: Transesterification of vegetable oil (Triglycerides) and with methanol producing biodiesel and glycerol	11
Scheme 2.2: Overview of converting of glycerol to value added chemicals (Pagliaro & Rossi, 2010).....	15
Scheme 5.1: Liquid phase oxidation of glycerol by palladium catalysts	111
Scheme 6.1: Proposed mechanism of glycerol oxidation to glyceric acid.....	129

University of Malaya

CHAPTER 1: INTRODUCTION

1.1 Research Background

Continuous depletion of fossil fuels as the rapid increase in energy demand has leads to increase of biodiesel production (Behr et al., 2008; Comelli, 2011; Pagliaro et al., 2007). Glycerol is a by-product in the manufacture of biodiesel through the transesterification of fatty acids (vegetable oil). Over 100 kg of glycerol are produced from one tonne of biodiesel (10 wt% of the total product) (Alonso et al., 2012; Behr et al., 2008; Pagliaro & Rossi, 2010). The utilization of glycerol is needed, even though wide application of pure glycerol in food, pharmaceutical, cosmetics, anti-freeze and many others industries exist. To address this problem, synthesis of value-added molecules from crude glycerol is an alternative route instead of disposal via incineration. Some potential uses for glycerol include hydrogen gas production, glycerine acetate as a potential fuel additive, composite additive, cosmetic bonding agent for makeup, including eye drops and conversion to propylene glycol, acrolein, ethanol epichlorohydrin and may be used as an antifreeze agent (Pagliaro & Rossi, 2010). Thus, the ready bio-availability of glycerol makes it a particularly attractive starting point for the synthesis of intermediates and a large number of products which can be obtained from glycerol oxidation (Figure 1.1). Oxidation of glycerol is one option for the utilization of bio-renewable resources. It also offers a promising route for creating specialty chemicals and pharmaceutical intermediates. Organic solvents or inorganic oxidants such as transition metal oxo compounds halogenated compounds and sulfur oxides has been utilized in the traditional methods for glycerol oxidation (Behr et al., 2008) which have less selectivity and leaching problem (Alonso et al., 2012; Zhou et al., 2008). Catalyst has an important role in supporting the selective oxidation reaction in terms of better activity and product selectivity. Since, catalytic oxidation of glycerol has been reported for both mono and bimetallic catalysts, this field has received tremendous attention in recent years. There are two main reaction

pathways for the oxidation of glycerol, i.e. intermediates via primary hydroxyl or secondary hydroxyl group (Figure 1.1). The pathway of the reaction is favoured by the condition of the reaction since glycerol oxidation occurs in acidic or basic pH conditions when using noble metals catalyst. Over supported noble metal catalysts, glyceric acid (Pagliaro et al., 2007) is generally considered to be the primary product of glycerol oxidation with molecular oxygen in liquid water in the presence of added base. Whereas, glycolic acid (C2 acid derived from C–C cleavage) is the secondary product. Tartronic and oxalic acid are produced by the sequential oxidation of glyceric and glycolic acid, respectively.

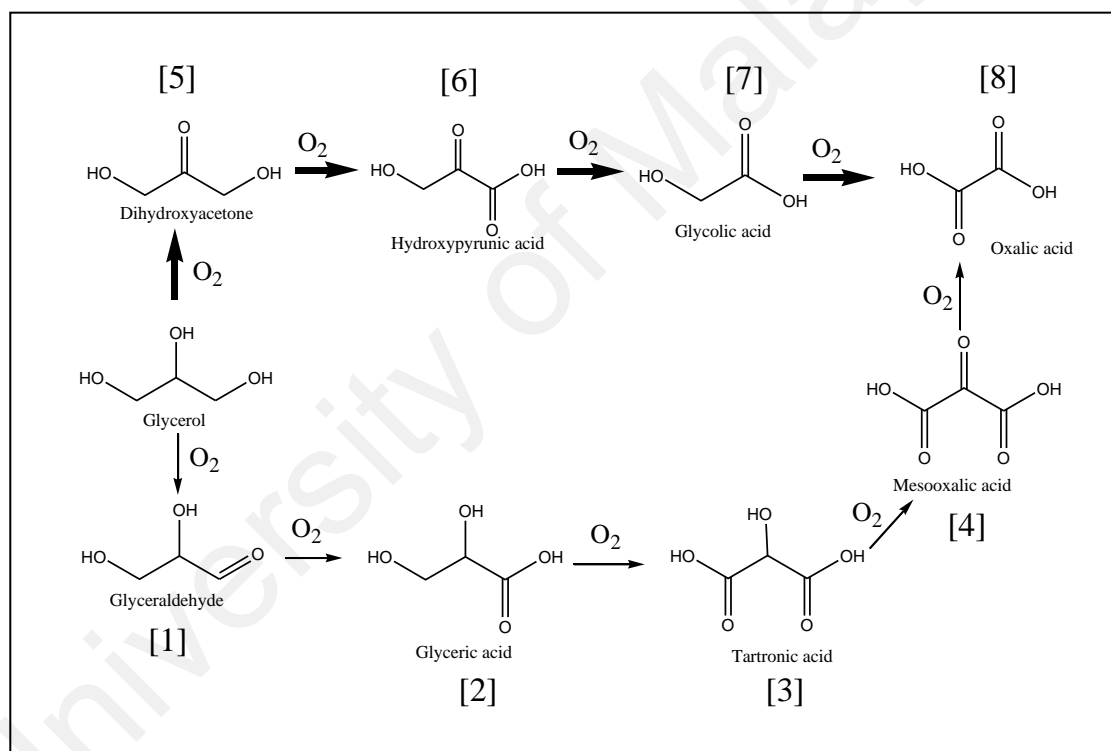


Figure 1.1: General scheme of Glycerol Oxidation (Zhou et al., 2008)

GLYAC is one of the most promising value-added chemicals that can be obtained by selective oxidation of glycerol (primary hydroxyl group). The production of GLYAC by catalytic aerobic oxidation of glycerol has been intensively investigated using heterogeneous catalysts such as monometallic or bimetallic catalysts (Au, Pt, and Pd in a basic medium) (Carrettin et al., 2003; Dimitratos, Lopez-Sanchez, et al., 2006; Dimitratos et al., 2005). Currently, GLYAC is one of the high-demand chemicals because of its

application as intermediate in polymers and in the fine chemicals industry (Behr et al., 2008).

The direct catalytic oxidation of glycerol to GLYAC by supported mono palladium catalyst has been investigated for a few decades. Pd/Ac catalyst has been mentioned as a selective catalyst for GLYAC formation, with a selectivity of 80% at 50% conversion, under reaction condition of 0.3 M glycerol, glycerol/Pd=3000, NaOH/glycerol=4, at 323 K, O₂ pressure 3 bar, but the catalyst is deactivated after half hour (Prati et al., 2007). The use of the base catalyst is crucial for the oxidation reaction. Unfortunately homogeneous catalyst (NaOH, KOH, LiOH) pose potential complexity of the product that can be formed and their subsequent separation. Hence, control of the reaction selectivity by careful design of both catalyst (metal, particles size and support) and the reaction conditions (pressure, temperature, amounts of base and time) are of great importance (Carretin et al., 2003; Chornaja et al., 2012; Hirasawa et al., 2013; Nishimura et al., 2000; Siyo, 2014; Villa, A. et al., 2009; Villa et al., 2012).

In this study, the activity of palladium nanoparticles was supported with various type of catalyst support such as activated carbon, calcined hydrotalcite and composite of calcined hydrotalcite with activated carbon catalysts were demonstrated with selective oxidation of glycerol to glyceric acid. It is expected that these catalysts would be active and, thus will be incredibly useful in the investigation of the heterogeneous catalyst in the oxidation of glycerol. The selected catalyst support has their own properties to help in the reaction. The calcined hydrotalcite has been verified as a good base catalyst and support referring to their chemical and physical properties. The preparation method that has been chosen is immobilization method due to the promising results claimed. The improvements of the catalytic activities have been proposed by doing various testing on different

parameters (temperature, oxygen pressure, molar ratio NaOH/glycerol, mol ratio metal/glycerol and stirring speed).

1.2 Problem Statement

Efficient catalyst that is active and selective to obtain one main product for example glyceric acid from the reaction, is a major problem in glycerol oxidation by dioxygen. Glycerol oxidation products are mostly obtained in mixture. Among all the heterogeneous catalysts, the noble metal catalyst is the most suitable for glycerol oxidation (Pagliaro & Rossi, 2010).

One of the limitations of transition metals catalysts is its susceptibility to oxygen poisoning leads to deactivation (Carrettin et al., 2003). Palladium and platinum-based metal supported catalysts have been investigated as a heterogeneous solid catalyst for the glycerol oxidation reaction (Carrettin et al., 2003; Katryniok et al., 2011). However, these catalysts is easily deactivated, possibly by oxygen poisoning which is directly depended on the oxygen partial pressure. This phenomena will leads to a premature and progressive loss of efficiency of the catalyst at increasing reaction time (Gallezot, 1997). Recently, gold metal catalyst has been chosen as the most suitable catalyst for glycerol oxidation due to its resistance to oxygen poisoning (Carretin et al., 2004).

The reaction conditions typically used for glycerol oxidation by gold catalyst (293–333 K, 1–3 bar O₂ pressure, NaOH:glycerol ratio of 1 to 4 (mol:mol). The need for a base in alcohol oxidation is a serious limitation of gold catalyst system. Unfortunately, the use of an inorganic base such as NaOH produces salts of carboxylic acid products during alcohol oxidation. Neutralization of the product stream and release of the free acid increase the operating cost of the process and produce additional salt by-products, which are of little value and may have a negative environmental impact.

The mechanism of oxidation of glycerol reported in literature is a dehydrogenation mechanism (Behr et al., 2008; Besson & Gallezot, 2000; Gallezot, 1997). The rate determining step in this reaction is the first step, which is adsorption of glycerol on the metal surface and formed metal alkoxide (Davis et al., 2013). Palladium and platinum catalysts with suitable catalyst support are still available for the step, but gold catalyst is not active without the addition of the base (Pagliaro et al., 2007).

Subsequent oxidation occurrence of these primary products to diacid products, such as tartronic and oxalic acid, happened when the reaction is prolonged due to the formation of hydrogen peroxide and hydroxyl group when partial oxygen pressure and molarity of the base is increased (Gil, Marchena, et al., 2011).

1.3 Scope of the present work

Heterogeneous solid supported catalysts were prepared by immobilization method by using polyvinyl alcohol (PVA) as a surfactant. The catalyst supports, activated carbon and hydrotalcite were pre-treated and synthesized before adding to the palladium metal. The activated carbon was pre-treated with HNO_3 to remove the impurities, volatiles components and ash contents. The surface properties and chemical compound of the activated carbon were characterized using Boehm Titration, FTIR, TGA (PROXIMATE ANALYSIS), XRD and BET. The synthesized hydrotalcite was prepared by co-precipitation method at room temperature. The surface properties, such as chemical compound and crystallization structure were characterized using FTIR, TPD- CO_2 , TGA-MS, XRD and BET. Fixed at 1wt% metal loading, three types of heterogeneous catalyst prepared used are 1wt% Pd/AC1, 1wt% Pd/HTc and 1wt% Pd/HTc-AC1. All of these catalysts were analyzed using a number of characterization techniques such as TGA-MS, XRD, XRF, BET, TPD- CO_2 , TPR, and HR-TEM to determine the surface properties, chemical compounds, particles size distribution, crystallization structure and thermal

stability properties. The catalyst supports and nanopalladium supported catalysts were subjected to the oxidation of glycerol at a fixed reaction condition (3 bar O₂, for 180 minutes at 333 K with mol of glycerol/metal is 3500). Among all of these catalysts, only 1wt% Pd/HTc was subjected for further optimization of the reaction conditions. Effect of the partial oxygen pressure, reaction temperature, molar ratio NaOH/glycerol, stirring speed and molar ratio glycerol/metal were evaluated to get the highest conversion and selectivity to glyceric acid. The reaction mechanism of the glycerol oxidation was proposed.

1.4 Objectives

The objectives in this study are:-

1. To design and synthesis supported nano Pd catalysts with control surface properties
2. To demonstrate its catalytic activity toward glycerol oxidation
3. To determine optimization condition of glycerol oxidation towards glycerol conversion and product selectivity

1.5 Organization of Thesis

This thesis has been presented into 6 chapters.

Chapter 1-

- Present a general review of the project including the problem statement
- Research motivation
- Objectives of the study.

Chapter 2-

- Highlight on the literature review and research background of the production and application of glycerol
- Glycerol as a platform chemical to convert to value added chemicals,
- Selective oxidation by heterogeneous solid catalysts and palladium catalysts,
- Production of glyceric acid from selective oxidation by palladium catalysts and catalyst deactivation.

Chapter 3-

- Described the synthesis of heterogeneous solid supported catalysts.
- Details about preparation of catalyst supports followed with preparation of the metal supported catalysts. The catalyst characterization were iterated, and followed by catalyst performance towards glycerol oxidation.

Chapter 4-

- Discussion and presentation on the characterization of synthesized heterogeneous solid supported catalysts
- The catalyst activity toward glycerol oxidation.

Chapter 5-

- Optimization of the reaction condition by varying a few parameters such as:-
 - partial oxygen pressure
 - reaction temperature
 - molar ratio of NaOH/glycerol
 - stirring speed and molar ratio glycerol/metal.
- Discussion of the stability of the catalyst

Chapter 6-

- Summarizes the overall conclusions and recommendation for future research proposal of this study.

University of Malaya

CHAPTER 2: LITERATURE REVIEW

2.1 Depletion of fossil fuels

Recently, majority of world's primary energy needs and chemical commodities are produced from fossil fuel resources, such as coal, petroleum and natural gas (Behr et al., 2008; Sobczak et al., 2010). A non-renewable resource of fossil fuels is the main disadvantage; therefore it is important to find alternative sources for our primary energy supply. The depletion of fossil fuels leads to a significant increase of price of petrochemical products (Corma et al., 2007). Crude oil price has increased nearly by ten-fold in the last decade and similar increase in coal and natural gas prices have also been seen. The continuous use of fossil fuels has also created major environmental problems (Behr et al., 2008). The greenhouse effects (Sobrino & Monroy, 2009), land damage due to the excessive coal mining, acid rains and air pollution which caused human health problems, are some of the environmental problems associated with the excessive use of fossil fuels.

Finding new alternative for fossil fuels has become a trend of research since a few decades ago. There are several potential renewable energy sources, such as biomass, solar, wind, hydropower, ocean thermal, geothermal and tidal energy that are sustainable replacements for fossil fuels. This helps to prevent the environmental problems faced by mankind today (Chiari & Zecca, 2011). Biomass is proven to be the most potential fossil fuels alternative sustainable resources. Biomass consists of 75% carbohydrates, 20% lignins, with remaining fraction consisting of fats, oils, proteins, terpenes and waxes (Corma et al., 2007). These properties makes biomass as the only renewable resources for production of value added chemicals, polymers and fine chemicals.

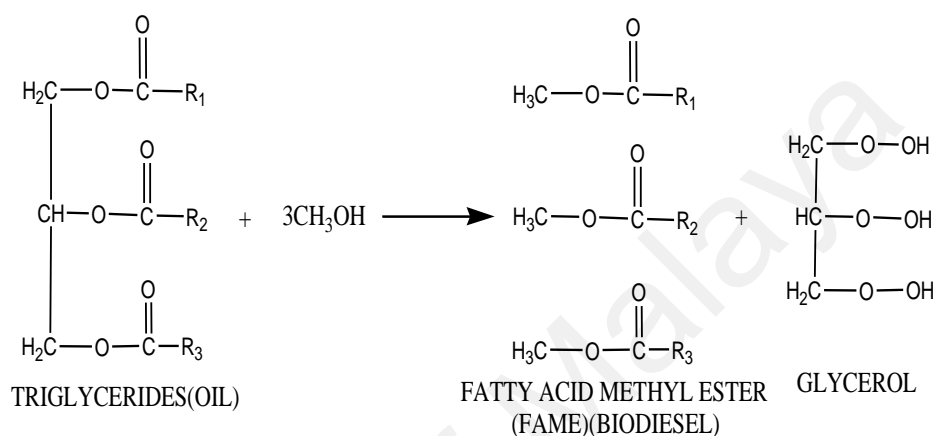
2.2 Biomass as a renewable resource

Biomass is one of the renewable resources which offers great opportunities to replace fossil fuels. A biorefinery is a biomass conversion process that utilizes renewable biomass feeds such as woods, leaves, agricultural residues (e.g. rice and wheat straw, palm shell and palm bunch). The biorefinery process generally consists of two steps. The first step is a separation of the biomass source in its main fractions such as carbohydrates (cellulose, hemicellulose and starch), lignin and plant oils. The subsequent step is converting biomass fractions into heat and power, biofuels, biobased chemicals and biobased materials (Clark et al., 2012).

The subsequent steps that is generally used are extraction, biochemical and thermochemical processes (Clark et al., 2012). Biorefineries may be discriminated according to various classification systems. A popular approach involves by differentiate of feedstocks. Examples are the whole-crop and lignocellulose feedstock. In a whole crop biorefinery, the entire crop is valorized to obtain useful products. Wheat, rye, triticale, and maize based biorefineries are some examples. Typical processing steps are milling, grinding, hydrolysis and extraction giving for example starch, cellulose, oils and proteins. In subsequent steps, these may be converted to food and feed, biofuels and biobased chemicals. For example, starch allows the production of important platform molecules like glucose, bioethanol and sorbitol by chemical or enzymatic conversion (Purushothaman, 2014).

Other than lignocellulose feedstock biorefinery, the production of biodiesel also draw a huge attention in this field. Due to the lack of fossil sources and disadvantage of fossil fuels to the human, animal and environment, the research in biodiesel is proposed. Conventional biodiesel is produced by transesterification of the oil with methanol in the presence of a catalyst to produce fatty acid methyl ester (FAME) and glycerol (Scheme

2.1). Glycerol is a main product (10% by mass feed). The product properties such as lower viscosity and boiling point, is leading to improved engine performance. Besides, the biodiesel oil contains more octane number than diesel (Purushothaman, 2014). Usually, the vegetable oils such as soy bean, palm, canola, castor, peanut, rapeseed and sunflower oils are used for biodiesel production.



Scheme 2.1: Transesterification of vegetable oil (Triglycerides) and with methanol producing biodiesel and glycerol

The use of biodiesel offers several advantages such as renewability, reduced level of harmful emissions, biodegradability and higher lubricity compared to diesel (Comelli, 2011). From 1980 to 2005, the worldwide production of biofuels has increased dramatically from 4.4 to 50.1 billion litres. The manufacture of biodiesel has also risen recently from 11.4 million litres in 1991 to 3.9 billion litres in 2005 (Brett et al., 2011).

Currently, biodiesel companies facing serious issues to identify high added value outlets for the crude glycerol. Crude glycerol typically has a purity of 40-70% and refining is required to produce pharmaceutical grade glycerol (99% purity), to be used in cosmetics, paints, automotive parts, food, tobacco, pharmaceuticals, paper, leather and the textile industry. However, the total market size for these applications is limited and new market trend for glycerol need to be developed (Brett et al., 2011). Recently glycerol has been proposed as a sustainable green solvent of particular interest for example the conversion of glycerol to value-added C3 bulk chemicals.

2.3 Glycerol

Glycerol, also known as glycerine or propanetriol has three hydrophilic alcoholic hydroxyl groups that are responsible for its solubility in water and its hygroscopic nature. It is also an intermediate in the synthesis of a large number of compounds used in industries. Purified glycerol is a highly functionalized chemical compound (Behr et al., 2008). It is widely used in medicines, cosmetics, and sweetening agents. However, the crude glycerol is too costly to handle. To address this problem, synthesis of value-added molecules from crude glycerol is an alternative instead disposal by incineration.

2.4 Production of glycerol

Theoretically, glycerol is a by-product of the conversion of fats and oil to fatty acids or fatty acid methyl esters (Bagheri et al., 2015). These compounds could be obtained by various types of processes.

2.4.1 Glycerol from fats and oils.

Glycerol is obtained as a by-product in the conversion of fats and oils to fatty acids or fatty acid methyl esters. This type of glycerol is known as native or natural glycerol, in contrast to synthetic glycerol from propene.

2.4.2 Fats Splitting

Glycerol does not exist in the free form but as fatty acids esters in plants, animal fats and oils. The fatty acids esters contain all three hydroxyl groups called triglyceride. The glycerol content of fats and oil varies between 8 and 14% depending on the proportion of free acid and the chain length distribution of the fatty acids esters. To obtain glycerol, fats and oils must be split. This is a method for preparing fatty acids, which are then reduced to the corresponding fatty alcohols. The glycerin is then obtained in the sweet water. Crude glycerin recovered from this process, is called as saponification crude (Uprety et al., 2016).

2.4.3 High Pressure Splitting

Splitting under pressure has been known since year 1845. Continuous process reactors are now used. Water and fats are fed into a splitting column in counter current fashion at 5-6 MPa and 523 K, leading to a 15% solution of glycerol in water known as sweet water. This glycerol is marketed as 88% saponification crude or hydrolysis glycerol.

2.4.4 Transesterification

Natural crude glycerol of same quality can be obtained from the continuous transesterification of oils and fats to their methyl esters. One of the most popular transesterification is from biodiesel production, reaction of fatty acid with methanol as presented in Figure 2.1.

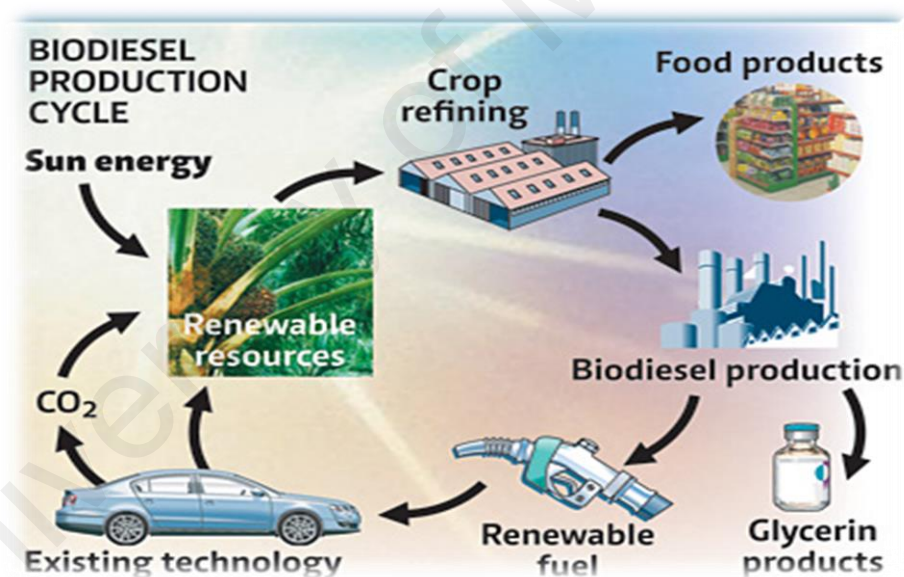


Figure 2.1: Biodiesel production cycle (Pagliaro et al., 2007)

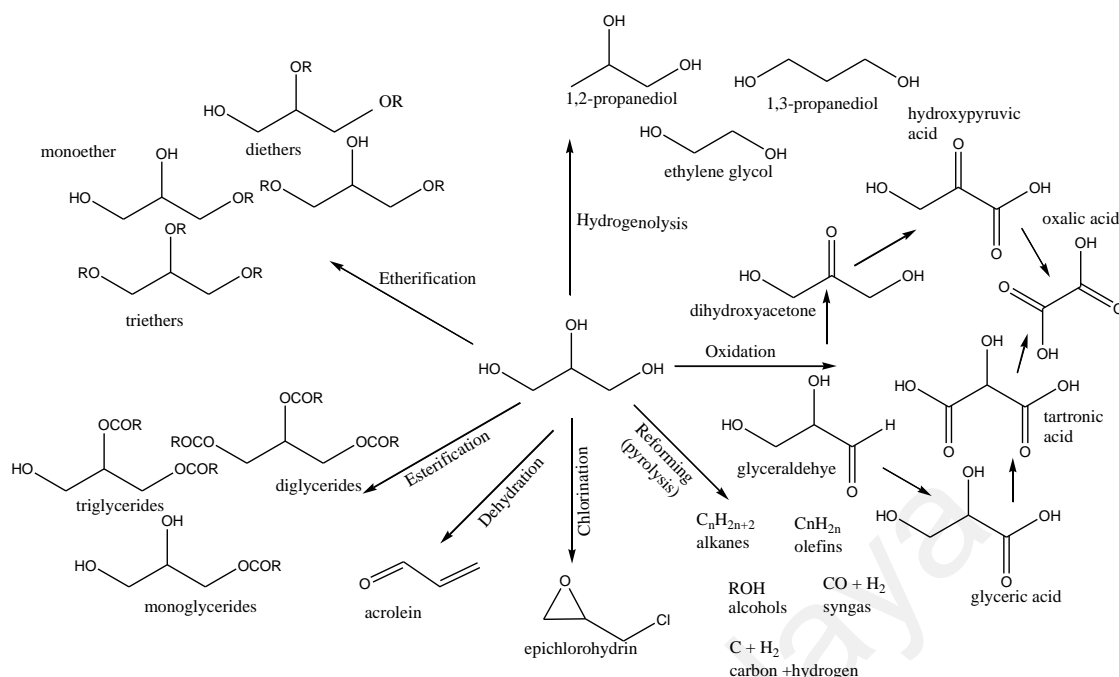
2.5 Application of glycerol

Glycerol is one of the twelve building blocks chemical by US Department of Energy that can be obtained from biomass. Glycerol can undergo various types of reaction to convert to value added chemicals, for example via hydrogenolysis reaction to produce commodity chemicals such as propylene and ethylene glycols. These glycols provide

application in anti-freeze and food industry. Another well-known application is esterification of glycerol to monoacyl and diacyl esters. These esters find application as plasticizers, solvent, emulsifiers in food and cosmetic industries (Behr et al., 2008). Other than that, catalytic oxidation of glycerol leads to the formation of various compounds such as glyceric acid, glyceraldehyde and dihydroxyacetone. One of the direct applications of glycerol is it is used as raw material in the production of dendrimers, hyper-branched polyester that have a high surface area to volume ratio and numerous end groups for functionality (Tan et al., 2013). Some potential uses for glycerol include: hydrogen gas production, glycerine acetate as a potential fuel additive, composite additive, cosmetic bonding agent for makeup, including eye drops and conversion to propylene glycol, acrolein, ethanol epichlorhydrin and may be used as an antifreeze agent.

2.6 Converting glycerol to value added chemicals

Several of publications and review have been reported in the past few years on glycerol conversions using either biochemical or chemo-catalytic methods. This overview will only focus on chemo-catalytic conversions. The conversion of glycerol to value added chemicals by oxidation, etherification, esterification, hydrogenolysis, dehydration, halogenation and reforming (Scheme 2.2) (Behr et al., 2008; Yang, F. et al., 2012). All reaction types will be discussed briefly in the next paragraph, except for oxidation reactions, which will be discussed in more detailed.



Scheme 2.2: Overview of converting of glycerol to value added chemicals (Pagliaro & Rossi, 2010)

2.6.1 Selective Reduction (Hydrogenolysis and Hydrogenation)

Glycerol can be catalytically reduced to propanediols (1, 2-PD and 1, 3-PD) or to ethylene glycol in the presence of hydrogen and metallic catalysts at elevated temperatures (423-523 K) (Comelli, 2011; Pagliaro et al., 2007; Pagliaro & Rossi, 2010). 1,2-Propanediol is used in anti-freeze formulations and as a solvent (Purushothaman, 2014). 1, 3-Propanediol is used as a monomer for polyesterpolypropylene terephthalate (PPT) or polytrimethylene terephthalate (PTT). PPT is a biodegradable polyester and is used in carpets and textile. Currently, 1, 3-Propanediol is produced using two routes: hydration of acrolein to 3-hydroxypropionaldehyde with subsequent hydrogenation (DuPont process) and hydroformylation of ethylene glycol (Shell process). These methods are based on fossil resources and as such, glycerol derived 1, 3-propanediol may be an environmentally friendly alternative (Pagliaro & Rossi, 2010).

2.6.2 Etherification

The etherification of glycerol with isobutylene or tert-butanol has been studied at a temperature range of 323-363 K in the presence of solid acid catalysts such as Amberlyst

(15 and 35), zeolites (HY or H β) or silica supported Hyflon (Lee et al., 2010; Zhou et al., 2008) which leads to alkyl ethers production (ether, diethers and triether). They have applications in surfactant formulations and as fuel additives (Pagliaro & Rossi, 2010).

In industrial application, polyglycerols and oligoglycerols are used as non-ionic surfactants in food products (Pagliaro & Rossi, 2010). Other applications can be found in cosmetics, polymers, antifogging films, pharmaceuticals, biomedical and drug delivery systems. Oligomerisation of glycerol is typically performed in the presence of an acid or base catalyst at moderate temperatures (Pagliaro & Rossi, 2010)

2.6.3 Esterification

Esterification of glycerol can be divided into three types: esterification with carboxylic acid, carboxylation and nitration. Generally, esterification with carboxylic acid produce monoacylglycerols (MAGs) and diacylglycerols (DAGs). DAG and MAG are currently, manufactured industrially either by continuous chemical glycerolysis of fats and oil at high temperature (493-523 K), employing catalyst under a nitrogen atmosphere or by the direct esterification of glycerol with oil (Pagliaro & Rossi, 2010). Both MAGs and DAGs are widely used as food additives in bakery products, margarines, dairy products and sauces. They assist in combining certain ingredients, for example those based on oil or water which would otherwise be difficult to blend. Other than that, they are used as texturing agents for improving the consistency of creams and lotion in cosmetic industrial aspect in the cosmetic industry. In addition, owing to their excellent lubricant and plasticizing properties, MAGs are used in textile processing oils in various types of machinery.

2.6.4 Dehydration

Acrolein and 3-hydroxypropionaldehyde are common target products produced from glycerol dehydration reaction (Pagliaro & Rossi, 2010). Acrolein was produced by an

acid catalyzed dehydration reaction at temperatures between 523-613 K (Alhanash et al., 2010). It is an important intermediate in the chemical industry of commodity chemicals such as acrylic acid, DL-methionine, 3-hydroxypropionaldehyde and 3-hydroxypropionic acid. (Clark et al., 2012). Upon oxidation, acrolein is converted to acrylic acid, an important commercial bulk chemical that may be used as a monomer for the synthesis of superabsorbent polymers (Bagheri et al., 2015). The current commercial production process for acrolein uses propylene oxide as the feed, which is converted over a Bi/Mo mixed oxide catalyst at a temperature range of 450-550 °C (Purushothaman, 2014)

2.6.5 Chlorination

Epichlorohydrin is the most targeted product from the halogenation of glycerol reactions. Traditionally, epichlorohydrin was formed from propene and only one of the four chlorine atoms involved, the remainder formed hydrogen chloride or waste chloride anion (Pagliaro & Rossi, 2010). Epichlorohydrin was formed from glycerol in two steps: hydrochlorination of glycerol with hydrogen chloride to give intermediate products (mixture of 1, 3-dichloropropan-2-ol and 2, 3-dichloropropan-1-ol), followed by reaction with base. Epichlorohydrin is an important precursor for epoxy resins which have application in paints, electronics and construction materials (Pagliaro & Rossi, 2010).

2.6.6 Reforming

Glycerol can be reformed as a gas and liquid chemicals by reforming process. Aqueous Phase reforming (APR) is one of the major achievements in glycerol reforming reactions. Glycerol was converted to hydrogen and carbon dioxide (syngas) under relatively mild conditions (temperature between 498-573 K) using metal catalyst in a single reactor in aqueous phase (Wen et al., 2008). Syngas produced from glycerol reforming has been used for the synthesis of methanol at temperatures between 468 and 518 K and pressures between 20 and 27 MPa in the presence of a catalyst (Purushothaman, 2014).

Furthermore, the syngas is important in biorefinery because the gas can be used as a source of fuels and chemicals using the Fischer–Tropsch (or methanol) synthesis, offering an energy-efficient alternative to liquid transportation fuels derived from petroleum (Schwengber et al., 2016; Srirangan et al., 2012).

2.6.7 Selective oxidation of glycerol

Selective oxidation of glycerol are currently receiving a lot of attention. Possible oxidation products are dihydroxyacetone, glyceraldehyde, glyceric acid, tartronic acid, mesoxalic acid and oxidative degradation products such as glycolic acid, oxalic acid and formic acid. The reaction has two pathways: primary and secondary hydroxyl group. Particularly, the oxidation products are not commercially available in large quantities, yet. Clearly, there is an economic incentive to identify technology to produce these products starting from glycerol. Glycerol oxidation by heterogeneous catalysts will be discussed further in the next subtopic.

2.7 Heterogeneous Catalyst

A heterogeneous catalyst is when catalyst is in separate phase from reactant, another substance added to a reaction system to improve the rate of chemical reaction approaching a chemical equilibrium. Heterogeneous catalysts are materials with the capability of adsorbing molecules of gases or liquids onto their surfaces. An example of heterogeneous catalysis is the use of finely divided platinum to catalyze the reaction of carbon monoxide with oxygen to form carbon dioxide. This reaction is used in catalytic converters mounted in automobiles to eliminate carbon monoxide from the exhaust gases. The heterogeneous catalyst consists of active sites, promoter and catalyst support prepared by various type of preparation method. Sabatier principle (Figure 2.2) explain that good catalyst should have weak interaction between reacting molecules and metal surfaces that is enough for the product molecules to desorb but strong enough for reactant molecules to adsorb and

rearrange upon chemisorption. It also explain when the graph rates against the heat of adsorption plotted is a volcano-shaped curves from observation of reaction in Figure 2.2 (Medford et al., 2015). The strength of heat of adsorption catalyst is not an interest for catalytic activity because it is depended on the application. For example, if the catalyst is used for oxidation, the surface of the working catalyst may be an oxidized state. Silver is an ethylene epoxidation catalyst and is most selective, if the surface has a high coverage of oxygen approximating an AgO surface rather than the metallic silver. Selective catalysis is only found at O₂ pressure high enough for AgO patches to be formed on the metal surface ($p \geq 1-10\text{mbar}$) (Ozbek et al., 2011). Catalytic phenomenon consists of elementary reaction on the catalyst surface. Chemical bonds were formed between the surface atoms and the adsorbing molecule. The bonding between the reactant with adsorbate molecule was rearranged to chemisorbed reaction occurrence and is usually accompanied by a change in a formal valence of the surface atom to which the reaction intermediated is coordinated. Particle size also play an important role in reactivity of the catalyst. By increasing the particles size, the decreasing in reactivity will be experienced (Dimitratos, Lopez-Sanchez, et al., 2006). This properties relate to changes in electronic structure, smaller metal particles, as well as changes in exposed surface geometry. It confirmed that, reaction (dissociation) happened when the adsorbate coordinate to a surface site with a minimum number of neighboring reactive surface metal atoms. The addition of promoter or additives may be needed to stabilize the particles or to poison non-selective sites.

Recently, the selective oxidation of glycerol using molecular oxygen as an oxidant has become of great interest. Glycerol oxidation can be divided into two pathways, they are via 1) primary hydroxyl group, and 2) secondary hydroxyl group. It was found that mechanism of alcohol liquid phase oxidation on metal surfaces started via dehydrogenation mechanism pursued by the oxidation of the adsorbed oxygen (Namdeo

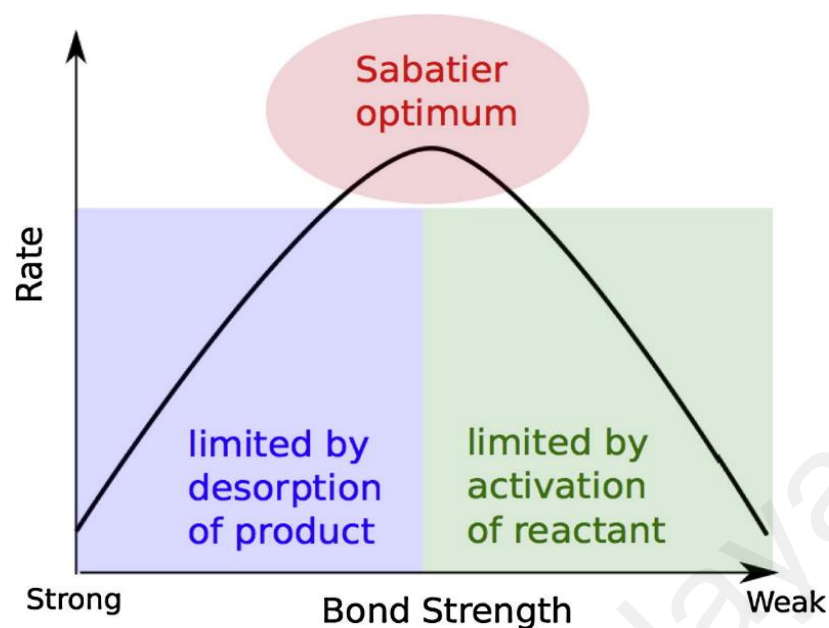


Figure 2.2: Sabatier principle (Medford et al., 2015)

et al., 2016). The surface chemistry of the oxidative dehydrogenation mechanism was also proposed (Gallezot, 1997). The first step for surface reaction is dehydrogenation, which is giving the alkoxide (RCH_2O), subsequently dehydrogenated into the corresponding aldehyde. The second step is the adsorbed hydrogen atoms which are removed from the surface by reaction with oxygen dissociatively adsorbed on the metal (Gallezot, 1997). The presence of water in the reaction media will hydrate aldehyde to form a geminal diol, which is further dehydrogenated to form identical acid. In the presence of organic solvents, alcohol oxidation stops at the aldehyde stage because the geminal diol could not be formed. However, this is a limited practical importance for safety reasons. Most of the organic solvents could not be used in the presence of oxygen and metal catalysts.

Numerous products could be obtained via the oxidation of glycerol, and some of these products, such as glyceric acid (GLYAC), glyceraldehyde (GLYALD), tartronic acid (TARAC), mesooxalic acid (MEXOLA), oxalic acid (OXALA), hydroxypyruvic acid (HYDROXY) and dihydroxyacetone (DHA) as shown in Scheme 2.2. An overview of the supported noble metal catalysis are able to catalyze the oxidation of glycerol, and the

selectivity is controlled by nature of the catalysts. By carefully controlling the condition of either primary or the secondary hydroxyl group could selectively be oxidized which eventually leads to different oxidation products.

An overview of supported noble metal catalysts is given in Table 2.1. Typically, the reactions are carried out between 333 K – 363 K, with molecular oxygen as the oxidant (1-11 bar) and in either acidic, basic or neutral conditions. Both batch and continuous set-up have been investigated.

In Table 2.1, the important role of base catalyst in oxidation of glycerol to glyceric acid is shown. In 2005, Diminitratos et.al reported that bimetallic catalyst Pd-Au/G is active for oxidation of glycerol to glyceric acid (39.1% yield at 100% conversion) in basic medium (Table 2.1, No 1). They reported that, as the reaction is pro-longed the selectivity of glyceric acid is decreased. Gold catalyst have received a lot of attention in this studies, hence monometallic gold catalysts supported by various type of the catalyst have been proposed by a some researchers (Table 2.1, No 2,3,4) (Brett et al., 2011; Gil, Muñoz, et al., 2011; Sobczak et al., 2010). Sobczak et al reported by using Au/Al₂O₃ with 6 bar O₂ at 333 K the conversion is 78% with 30% glyceric acid selectivity. Gil et al has also reported 100% glycerol conversion but with 24.8% selectivity of the product to glyceric acid using the same active metal precursor (gold) with different type of support which is graphene. These two researches, showed good result for the activity of gold catalyst but the selectivity is still low (<50%) and the formation of by product increased as the time of the reaction is being extended. Some of the researchers believe that this phenomenon is due to the formation of hydrogen peroxide from the splitting of molecular oxygen or formation of sodium glycerate (Zope et al., 2012).

Due to the low selectivity in glyceric acid production from glycerol oxidation, a bimetallic catalyst with base-free condition have been introduced in this field. In 2011,

Brett L. Gemma and the group has reported the activation of Au-Pt/MgO in glycerol oxidation with mild condition (333 K) (Table 2.1, No 3). The outcomes of this experiment is quite interesting. Even though the conversion is slightly low from the previous research but the selectivity increased (42.9% conversion, 72.2% selectivity to glyceric acid) (Brett et al., 2011).

Uses of platinum too, get good responds in oxidation of glycerol either monometallic or bimetallic. This metal showed good catalytic activity result for this application. The activity of platinum metal supported on carbon materials (Ac) and metal oxides (hydrotalcite, HT) has been investigated under continuous mode (atmospheric pressure) at 333 K for oxidation of glycerol. Tongsakul et. al, 2012 and Zhang et al, 2012 showed good results for activation and selectivity (Table 2.1, No 7 &8). Rodrigues et al, 2013 have reported on bimetallic of platinum with gold supported on MWCNT support (Table 2.1, No 11).

In contrast with glyceric acid production, dihydroxyacetone (DHA) is stable in acidic condition (Katryniok et al., 2011). Hu et. al, 2010 used Pt-Bi/C as a catalyst and HCl to tune condition to acidic medium (pH about at 2) (Hu et al., 2010). Their report showed that DHA is stable in acidic medium, and can undergo further reaction to hydroxypyruvic acid. The reaction of DHA to hydroxypyruvic acid is reversible, thus an acidic solution slowed the DHA consumption and thus increase its yield (Hu et al., 2010). Other than that, Pd-Ag/SiO₂ catalyst showed selectivity to DHA too where the reaction is done in neutral medium. Hirasawa et. al, 2013 reported that Pd seems to contribute to activity for alcohol oxidation and silver seems to contribute to the selectivity of the ketone (Hirasawa et al., 2013). The main drawback of using noble metal catalysts for the oxidation of glycerol is their tendency to deactivate at longer reaction times. This is ascribed to the

oxygen poisoning, supported by the observation that the rate of deactivation is directly proportional to the oxygen partial pressure

Table 2.1: Overview of glycerol oxidation over supported noble metal catalysts in water using oxidative condition

No	Catalysts	Oxidant	Reaction condition	Glycerol conv. (%)	Selectivity (%)	Yield (%)	ref.
1	Pd-Au/G	O ₂ (3bar)	Glycerol/metal: 500 mol/mol, NaOH/glycerol: 4 mol/mol, Time :2 h, Temp :363 K	100.0	39.10 (GLYAC)	39.10	(Dimitratos et al., 2005)
2	Au/Al ₂ O ₃	O ₂ (6 bar)	Glycerol/metal: 980 mol/mol, NaOH/glycerol: 2 mol/mol, Time :5 h, Temp:333 K	78.0	30.00 (GLYAC)	23.10	(Sobczak et al., 2010)
3	Au-Pt/MgO	O ₂ (3 bar)	Glycerol/metal: 1000mol/mol, NaOH/glycerol: 0 Time:4 h, Temp :333 K	42.9	72.20 (GLYAC)	30.97	(Brett et al., 2011)
4	Au/G	O ₂ (5 bar)	Glycerol/metal: 3500 mol/mol, NaOH/glycerol: 2 mol/mol, Time:7 h, Temp :333 K	100.0	24.80 (GLYAC)	24.80	(Gil, Marchena, et al., 2011)
5	Pt/HT	O ₂ (1 bar)	Glycerol/metal: 800 mol/mol, NaOH/glycerol: 0 Time:6 h, Temp :333 K	55.0	75.00 (GLYAC)	41.30	(Tsuji et al., 2011)

Table 2.1 continued: Overview of glycerol oxidation over supported noble metal catalysts in water using oxidative condition

No	Catalysts	Oxidant	Reaction condition	Glycerol conv.(%)	Selectivity (%)	Yield (%)	ref.
6	Pt-Bi/C	O ₂ (2 bar)	Glycerol/metal: 1000 mol/mol, acidic medium Time:7 h, Temp :358 K	80.0	60.00 (DHA)	48.00	(Hu et al., 2010)
7	Pt/HT	O ₂ (1bar)	Glycerol/metal: 1000 mol/mol, base-free medium Time:6 h, Temp :323 K	80.0	40 (GLYAC)	32.00	(Tongsakul, D. et al., 2012)
8	Pt/C	O ₂ (atmosph eric) (continu ous ;150 mLmin ⁻¹)	Glycerol/metal: 1000 mol/mol, base-free medium Time:6 h, Temp :333 K	70.3	66.4 (GLYAC)	46.7	(Zhang et al., 2012)
9	Pd- Ag/SiO ₂	O ₂ (3 bar)	Glycerol/metal: 2500 mol/mol, base-free medium Time: 4 h, Temp :353 K	4.0	91.6 (DHA)	3.66	(Hirasawa et al., 2013)
10	Pt- Au/MW CNT	O ₂ (3 bar)	Glycerol/metal: 2500mol/mol, NaOH/glycerol : 2 mol/mol Time:3 h, Temp :333 K	98.0	47.0 (GLYAC)	46.1	(Rodrigues et al., 2013)
11	Au/PU F	O ₂ (5 bar)	Glycerol/met al: 3500 mol/mol, NaOH/glyce rol: 2 mol/mol Time: 1 h, Temp : 333 K	40.0	36.9 (GLYAC)	14.8	(Gil et al., 2014)
12	Pt/CNF	O ₂ (4 bar)	Catalyst ; 0.5g base-free medium Time: 6 h, Temp :333 K	89.9	83.2 (GLYAC)	74.8	(Zhang, Q. et al., 2015)

2.7.1 Catalyst Support

The supported catalysts generally were prepared by contacting a (porous) pre-shaped support with an aqueous solution of suitable precursor of the active component. The good distribution and high dispersion of the active component on the support is a main procedure in heterogeneous catalysts. The selection of the support is based on the series of desirable characteristics; inertness, stability under reaction and regeneration conditions, adequate mechanical properties, appropriate physical form for the given reactor and high surface area (which is usually, but not always desirable), which are the suitable and frequently used support materials are alumina, silica and carbon. The interaction between the solvated precursors and the support surface as modified by the solvent is generally of an electrostatic nature (Costa & Rossi, 2012).

2.7.1.1 Carbon Support

Carbon materials are often used because of their high surface area and chemical inertness, in particular in strong basic and acid environments. Sometimes, the chemical inertness of carbon can be a disadvantage. The low reactivity of the surface makes it difficult to deposit metals, hence, the pre-treatment of the carbon in oxidizing environment (nitric acid pre-treatment) is used to introduce oxygen containing surface group, therefore enhancing the interaction with the metal (Li et al., 2005). Besides, carbon is a suitable support material due to the reclaim of the metal by burning off the carbon for precious metal catalysts.

Activated carbon is often used as catalyst support due to their high surface area (500-1200 m².g⁻¹), chemical inertness and high thermability stable (El-Shafey et al., 2016). Activated carbon is produced by pyrolysis of natural or synthetic organic polymer materials. Most common natural polymers that have been used are wood, coconut shells or fruit pits. The carbon material is activated in pyrolysis process by an air or steam

treatment to increase the accessibility of the carbon surface (Yu et al., 2016). After activation, carbon still holds a large range of elements for example, oxygen, hydrogen, sulfur and others. Textural of activated carbon is complicated since it involves macropores, mesopores and micropores as well (Rashidi et al., 2012). Generally, the activated carbon average structure consisting of aromatic sheets and strips, with variable slits of molecular dimensions and these being micropores as in Figure 2.3 (Yu et al., 2016). The micropores maybe considered, locally at least, as slit-shaped. The extent of activation will condition the reduction of the number of the aromatic sheets in the original char, leaving in some cases single and, in general, nonplanar layers. During the pyrolysis of the precursor, heteroatoms such as oxygen, hydrogen and nitrogen are eliminated as volatile gaseous products. The residual elementary carbon atoms are then grouped into stacks of flat aromatic sheets crosslinked in random manner. Since the arrangement of these sheets is irregular, it leaves free interstices among them, which may become filled or partially blocked with the tars and other decomposition products which become disorganized carbon. This disorganized carbon is the first to react with the gases in the activation process, clearing the porosity which makes activated carbon such an excellent adsorbent. The appropriate control of the activation process is important to obtain activated carbon for specific application such as catalyst supports. The adsorptive properties of activated carbon are defined not only by its porous structure but also by its chemical composition. The presence of heteroatoms such as oxygen and hydrogen on the activated carbon surface (derived either from raw material or chemically bonded to the structure during preparation) has a big impact on the adsorptive properties of the activated carbon. Among all the heteroatoms, the oxygen surface group is most important in activated carbon chemisorption. Carbon-oxygen surface groups are not completely formed by reaction with oxygen gas but they can also react with other oxidizing gases (ozone, nitrous oxide, nitric oxide, carbon dioxide, etc.) and with oxidizing solution

(nitric acid, sodium hypochlorite, hydrogen peroxide, etc.). Other than oxidizing agent, nature and amount of oxygen surface complexes are also affected by its surface area, particle size, ash content, temperature and degree of carbonization. Carbon-oxygen surface is formed in different types. The presence of these groups gives activated carbon acid-base properties which depend on the pretreatment conditions (Kalijadis et al., 2011).

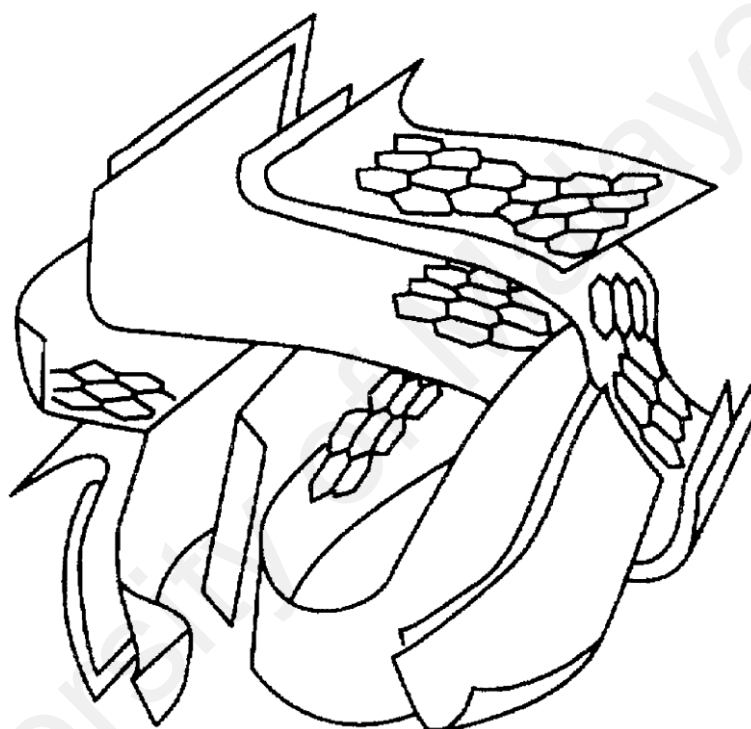


Figure 2.3: Schematic representation of the structure of activated carbon (Toebes et al., 2001)

In contrast to activated carbon, graphite is a non-porous material with highly crystalline material composed of stacked planes of aromatic rings (Figure 2.4) which is produced from high temperature treated carbon (Meryemoglu et al., 2016; Toebes et al., 2001). Intercalation process in graphite happened due to the electronic character of the stacked aromatic system. Intercalation process is a process where atoms or molecules slip between the layer, either accepting or donating electrons to bond with the carbon system (Assouik et al., 2016). Non-treated graphite is not suitable for catalyst support due to its non-porous structure. However after oxidation treatment, the surface of the planar

containing acidic functional group enable adsorption of the precursor. The modified graphite can be used to adsorb cations from neutral or basic medium.

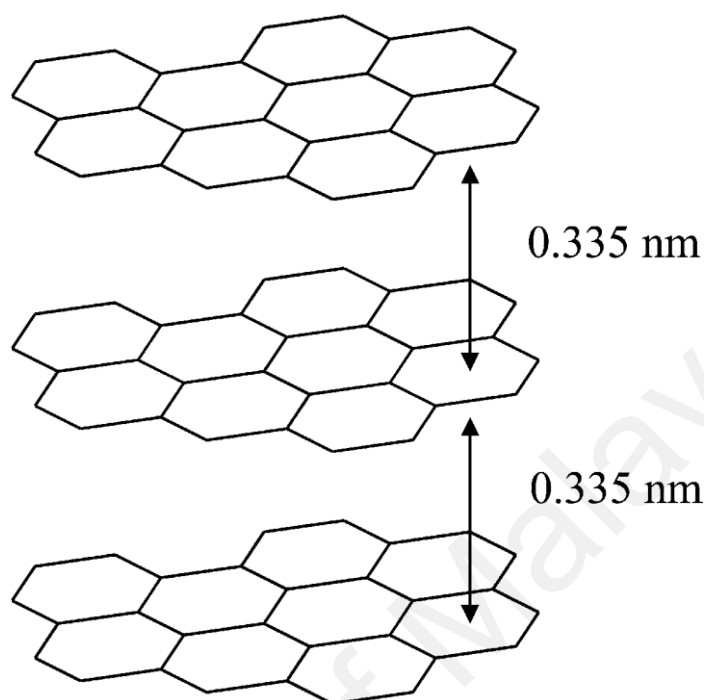


Figure 2.4: Layer structure of graphite (Toebes et al., 2001)

Recently, other than activated carbon and graphite, carbon nanostructures such as carbon nanofibers and carbon nanotubes have been discovered as catalyst support based on carbon materials (Gil, Muñoz, et al., 2011). Carbon nanofiber are categorized by high aspect ratio bodies with enhanced mechanical strength and surface areas in the range 100–1000 $\text{m}^2\cdot\text{g}^{-1}$ (Kim, 2014). They present a large amount of edges in the lattice and basal regions, providing increased metal–support interactions (Kim, 2014), and lower mass transfer constraints associated with their mesoporous character, in comparison with microporous activated carbons. The morphology of the carbon nanofiber filaments can be controlled by a proper selection of the growth conditions (fiber width, alignment of the graphene layers or amount of lattice defects are strongly influenced by growth temperature, catalytic metal, type of carbon source (CO , C_2H_4 , etc.) or carbon source to carrier (He , H_2 , etc.) ratio (Kim, 2014). Thus, carbon nanofibers are usually classified into three types depending on how the graphene sheets line up with respect to the fiber

axis: in platelet type (CNFP), the graphene sheets are lined up perpendicular to the fiber axis, ribbon type (CNF-R); in CNF, graphene sheets are parallel to the axis; and, finally, in fishbone type (CNF-F), the graphene sheets are inclined with respect to the fiber axis (Gil, Muñoz, et al., 2011).

2.7.1.2 Metal oxides

Most of metal oxide surfaces consist of hydroxylated group or become hydroxylated when contact with liquid or water vapor (Lee & Yoo, 2014). Common metal used as catalyst support are TiO_2 , $\gamma\text{-Al}_2\text{O}_3$, SiO_2 and recently, aluminosilicate (zeolites) has been introduced (Aznárez et al., 2015; Moteki et al., 2011; Musialska et al., 2010). The hydroxyl functional group of the metal oxide is identified by IR spectroscopy, and the OH stretch region show several bands corresponding to different types of surface group (Lee & Yoo, 2014). These hydroxyl group can be classified as acid, neutral and basic, also called Bronsted-sites. Metal oxides surface will be charged when they are dispersed in the aqueous solutions. The charged surface in combination with the charged layer around the particle is called the electrical double layer. The pH value at which the net surface charge is zero is referred to as the zero point of charge (ZPC) or often loosely referred to as the iso-electric point (IEP) (Lee & Yoo, 2014). In contrast with carbon materials, metal oxides adsorptive character is determined by the isoelectric point of the metal oxides as accumulated in Table 2.2. At pH values below its IEP an oxide particle tends to adsorb compensating anions like PdCl_4^{2-} . At pH values above its IEP, the surface becomes negatively charged and cations like $\text{Pd}(\text{NH}_3)_4^{2+}$ can be adsorbed (Lee & Yoo, 2014; Toebes et al., 2001; Wang & Chen, 2015)

Table 2.2: Iso-electric points of various oxides (Wang & Chen, 2015)

Type	Oxide	IEP	Adsorption
Acidic	Sb ₂ O ₃	<0.4	Cations
	WO ₃	<0.5	
	SiO ₂	1.0-2.0	
Amphoteric	MnO ₂	3.9-4.5	Cations or anions
	SnO ₂	~5.5	
	TiO ₂	~6	
	γ-Fe ₂ O ₃	6.5-6.9	
	ZrO ₂	~6.7	
	CeO ₂	~6.75	
	α,γ-Al ₂ O ₃	7.0-9.0	
Basic	Y ₂ O ₃	~8.9	Anions
	α-Fe ₂ O ₃	8.4-9.0	
	ZnO	8.7-9.7	
	La ₂ O ₃	~10.4	
	MgO	12.1-12.7	

Currently, hydrotalcite has been discovered as a new catalyst support in metal oxides group (Omonmhenle & Shannon, 2016; Wang & Chen, 2015). Hydrotalcites (HT) is a Mg-Al hydroxyl carbonates with the formula Mg₆Al₂(OH)₁₆CO₃.4H₂O, also known as anionic clays (Wang & Chen, 2015). These anionic clays resembles cationic brucite (Mg(OH)₂) where the magnesium cations are octahedrally coordinated by hydroxyl ions, resulting in stacks of edge-shared layers of the octahedral layers where for hydrotalcites, part of the Mg²⁺ ions are replaced by Al³⁺ ions forming positively charged layers. Charge-balancing anions (usually CO₃²⁻) and water molecules are situated in the interlayers as shown in Figure 2.5. (Xie et al., 2006). After the heat treatment, hydrotalcite decompose into interactive, high surface area, and well dispersed Mg-Al oxides which presents basic sites that are associated to structural hydroxyl groups as well as strong Lewis basic sites associated to O²⁻ Mⁿ⁺ acid-base pairs (Álvarez et al., 2012; Corma et al., 2005). Hence, calcined hydrotalcites are able to catalyze variety of base-catalyzed reaction and also exhibit attractive properties as precursors for redox catalyst with metal function (Naresh et al., 2014; Pendem et al., 2012). The general formula of hydrotalcite-like compounds

('layered double hydroxides') is $[M^{II}_{1-x}M^{III}_x(OH)_2] A^{n-}_{x/n} \cdot mH_2O$, where A is an anion and can be varied, two and three valence cations can be introduced into brucite layer.

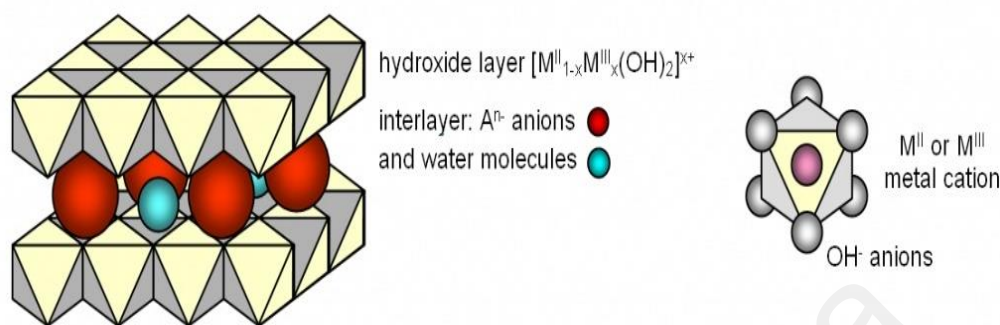


Figure 2.5: Structure of hydrotalcite (Álvarez et al., 2012)

2.8 Preparation method

A good catalyst not only depends on the type of precursor and support, but the preparation method also plays a crucial role in the catalysts synthesis. The particle size and distribution of the metal particles are influenced by the preparation method (Astruc et al., 2005; Dimitratos et al., 2005; Tsuji et al., 2011). The simplest preparation method is the impregnation method in which a metal particles is simply stirred with the chosen support, filling the void spaces and then calcined (Sudarsanam et al., 2013; Toebes et al., 2001). This preparation method leads to a bimodal distribution of particles, small (2-10 nm) and larger particles (>20 nm) (Behr et al., 2008).

Deposition precipitation is another type of preparation method. This method allows good control in particles size distribution. The metal precursor solution is stirred in a slurry of support. The pH of the solution is varied by the addition of base. The structure of the catalysts produced by this method is dependent on a number of variables including concentrations of precursors solutions, pH, stirring time and calcination conditions (Costa & Rossi, 2012; Ma et al., 2011). Another preparation method which leads to the formation of small nanoparticles on metal oxides is co-precipitation. In this method the support is

produced during the catalyst preparation. Sodium carbonate is added to a mixture of gold precursor and metal nitrate (Brett, 2012). This leads to a good dispersion of gold. The rate of precipitation determines the metal particles sizes .

The chemical vapour deposition, involves the reaction of a volatile organo metal compound with a support. The substrate is activated by heating, radiation or plasma process. Then, deposition consists of either homogeneous gas phase reactions take place in the gas phase or heterogeneous chemical reactions which take place on/in close proximity of a hot surface resulting in the formation of powders or coatings respectively.

The sol immobilisation technique is relatively a new technique for the preparation of supported catalysts. This involves forming a metal colloid and immobilising polymer stabilized particles on support. Before the immobilization step the metal is chemically reduced from a number of oxidation state to 0. By using this method a narrow particle distribution is achieved (Costa & Rossi, 2012). These supported catalysts were found to be active for CO oxidation without calcination, unlike catalysts prepared by impregnation and deposition precipitation, which leads to sintering of the gold particles (Liu et al., 2014). Another method is to create a gold colloid with small particle size using a polymer, such as polyvinyl alcohol (PVA) (Dimitratos, Villa, et al., 2006), as a stabilising agent and sodium borohydride (NaBH_4) as the reducing agent (Corma et al., 2007). Catalysts prepared by this method have been shown to be more active than those prepared by impregnation and have been shown to be effective for a number of alcohol oxidations.

2.9 Palladium catalysts for selective oxidation

Palladium nanoparticles play an important role in the chemical synthesis and pollution deduction. Palladium is widely used as heterogeneous and homogeneous catalysts in many industrial applications, e.g. the synthesis of vinyl acetate, hydrogenation of acetylene and in the cleaning of automobile exhaust (Yang et al., 2014). It was reported,

that the first successful example of palladium catalyzed the aerobic oxidation of secondary alcohols to ketone was reported by Blackburn et al in 1977 (Blackburn & Schwartz, 1977). Further successful oxidations of alcohols with palladium nanoparticles were also reported. For example benzyl alcohol (Villa et al., 2010), aromatic alcohols (Wu et al., 2013), glycerol (Hirasawa et al., 2013) and linear and unsaturated alcohol (Hirasawa et al., 2013).

Palladium nanoparticles can be prepared using different methods as described before (Nguyen et al., 2010) applying different palladium salt precursors, reducing agents, and stabilizers (Nguyen et al., 2010). Sawoo et al. synthesized palladium nanoparticles by reduction of a palladium precursor (K_2PdCl_4) in water with a Fischer carbene complex using polyethylene glycol (PEG) as a stabilizer agent. They stated that the size of palladium nanoparticles decreased as the molar ratio of the PEG to palladium increased in the synthesis solution (Sawoo et al., 2009).

James Cookson (Cookson, 2012) stated that controlling the particle sizes is the key to producing a more effective and efficient catalyst. Nanomaterials range (1-100 nm) are seen as a bridge between atomic and bulk materials, and have been shown to exhibit a variety of unique chemical, physical and electronic properties. One of the key properties for a good catalyst performance is high surface area to volume ratio.

The size and morphology of the resulting palladium nanoparticles are sensitive to different parameter conditions, such as surfactant used, reducing agent employed, reaction time, the nature of stabilizing ligand and the ratio of the palladium precursor to the other reagents (Cookson, 2012).

2.9.1 Glycerol oxidation to glyceric acid using palladium catalyst

Oxidation reactions of glycerol in water using supported monometallic and bimetallic palladium catalysts obtain glyceric acid have been intensively explored by various research groups. An overview is given in Table 2.3. Typically, the reactions are carried out between 303-333 K, with air or oxygen as the oxidant (1-10 bar) and under basic conditions. Reactions are performed in a batch reactor set-up.

University of Malaya

Table 2.3: Overview of glycerol oxidation by palladium catalysts

No	Catalysts	Oxidant	Reaction condition	Glycerol conv.(%)	Sel.(%)	Yield (%)	ref.
1	Pd/C	O ₂ (1 bar) (100 mL.min ⁻¹)	Catalyst: 0.320g pH: 11 Time:21 h, temp: 333 K	73.5	62.0 (GLYAC)	45.60	(Carrettin et al., 2003)
2	Pd/G	O ₂ (3 bar)	Glycerol/metal: 500 mol/mol, NaOH/glycerol: 4 mol/mol, Time:5 h Temp :323 K	90.0	62.4 (GLYAC)	23.10	(Dimitratos et al., 2005)
3	Pd/Al ₂ O ₃	O ₂ (1 bar) Slurry bubble reactor	Glycerol/metal: 500 mol/mol, pH 11, Time:10 h, Temp :333 K	100.0	74 (GLYAC)	74.00	(Chornaja et al., 2012)
4	Pd-Au/C	O ₂ (atmospheric) 120 mLmin ⁻¹	Catalyst :0.2g, NaOH/glycerol: 4mol/mol, Time:3 h Temp :333K	99.4	40 (GLYAC)	39.76	(Zhao et al., 2014)

Carrettin et al showed that Pd/C catalyst is active for the selective oxidation of glycerol to glyceric acid, with 73.5 % conversion and 62 % selectivity (Table 2.3, No 1). The catalyst was prepared by impregnation method and formaldehyde as reducing agent. They reported that the addition of OH⁻ e.g NaOH, increases the conversion of glycerol, They proposed that in the absence of a base, the first step in the reaction which is dehydrogenation is slow for palladium catalyst (Carrettin et al., 2003). A Pd/Graphite which was prepared by immobilization method by Dimitratos et al, 2005 reported a different results (Table 2.3, No 2). They said that glyceric acid is more stable on gold catalyst compared than palladium catalyst (Dimitratos et al., 2005). Other than carbon materials, metal oxides, for example, alumina have also been studied. Chornaja et al, 2012 reported that the extractive pyrolytic method can be used for the preparation of palladium catalyst supported on alumina (Table 2.3, No 3). They also reported that the glycerol conversion is increased when the palladium size decreased. So the theory on the influence

of the palladium particle size on the glycerol conversion on alumina is confirmed (Chornaja et al., 2012). The activation of bimetallic catalyst had been discussed further in this reaction, Zhao et al, 2014 reported that bimetallic catalyst Pd-Au is more active than monometallic (Zhao et al., 2014). The conversion value (99.4%) is high but the selectivity to glyceric acid is still low (40%) (Table 2.3, No 4). They suggested that bimetallic catalyst has lower adsorption energy. Thus, lower 'true' activation energy, reflect different reactivity of the surface active sites. The surface of active sites became susceptible to deactivation. The other products resulted from C-C cleavage is either catalyzed directly at the Pd-on-Au particle surface or promoted by reaction with in situ formed H_2O_2 (Zhao et al., 2014).

The palladium-based catalyst application in oxidation reaction is still new and not as extensive as gold-based catalysts. The improvement in designing the palladium catalyst either monometallic or bimetallic still remain insufficiently detailed.

2.10 Catalyst deactivation

The serious issue in industrial catalytic processes is the loss of the catalytic performance (activity and/or selectivity) during the reaction. Several studies were focused on the reasons of catalyst deactivation. Generally, in the case of liquid-phase oxidation of alcohols, four major reasons were found to be responsible for the deactivation of the catalyst.

2.10.1 Oxygen poisoning

This phenomenon happened when oxygen is strongly adsorbed on the surface (called blocking). This could happen when a high amount of oxygen is being introduced. This effect is also known as "over-oxidation" and could be classified as irreversible deactivation (Butt, 2012).

2.10.2 Chemical poisoning

The catalyst could be poisoned or deactivated by the adsorption of the substrate, reaction intermediates and/or by-products which could be formed during the reaction on the active sites of the catalyst. Chemical poisoning is classified as reversible deactivation because the adsorbed products on the catalyst might be removed via washing of the catalyst (Butt, 2012).

2.10.3 Leaching

The term leaching refers to the loss of the active metal species by migration into a liquid phase. Leaching is an irreversible deactivation. Different factors could affect the amount of metal leaching e.g. high pH values. Noteworthy, metal leaching could be avoided or at least minimized by adding a second metal as promoter (Butt, 2012)

2.10.4 Sintering

The term sintering refers to a loss of the active surface resulting from agglomeration and coalescence of small particles. Sintering is classified as irreversible deactivation and could occur for supported and unsupported metal catalysts. Different factors could lead to an acceleration of this phenomenon e.g. high temperature (Butt, 2012).

CHAPTER 3: METHODOLOGY

3.1 Synthesis of heterogeneous solid supported catalysts

The method of catalysts preparation consists of two different stages. They are:

- 1) Preparation of support
- 2) Preparation of the supported catalysts

3.1.1 Materials and reagents

Sodium tetrachloropalladate (II) (Na_2PdCl_4 , 99.995%), poly(vinyl alcohol) (PVA) $M_w = 13,000-23,000$, sodium borohydride (NaBH_4 , 98%) were purchased from Aldrich. Stock activated carbon was purchased from United Chem (surface area = $1100-1250 \text{ m}^2 \cdot \text{g}^{-1}$ and pH $\sim 9-10$). The other reagents used in this work are magnesium nitrate hexahydrate ($\text{Mg}(\text{NO}_3)_2 \cdot 6\text{H}_2\text{O}$) (Merck, 99%), aluminium nitrate nonahydrate ($\text{Al}(\text{NO}_3)_3 \cdot 9\text{H}_2\text{O}$) (Merck, 98.5%), sodium hydroxide (NaOH) (Merck, 99%), sodium carbonate (Na_2CO_3) (Sigma-Aldrich, 98%), hydrochloric acid (HCL) (Sigma-Aldrich, 37%) and nitric acid (HNO_3) (Sigma-Aldrich, 70%).

3.1.2 Preparation of catalyst supports

3.1.2.1 Pre-treatment of Activated carbon

The crude activated carbon was treated with 5 M nitric acid (70%, Sigma–Aldrich) under vigorous magnetic stirring at room temperature for 24 h. The treatment was performed at the ratio of nitric acid to carbon sample set to 500 mL for 10 g respectively. This ratio was expected to be sufficient to avoid changes in the nitric acid concentration due to consumption. After treatment, it was then filtered and the carbon sample was thoroughly rinsed with distilled water until pH of the solution reached pH neutral. The sample was dried at 333 K for 12 h.

3.1.2.2 Hydrotalcite

The hydrotalcite (Mg/Al ratio = 4) was prepared using a co-precipitation method (Corma et al., 2005). In brief, the required amounts of 2.40 mol $\text{Mg}(\text{NO}_3)_2 \cdot 6\text{H}_2\text{O}$ and 0.6 mol $\text{Al}(\text{NO}_3)_3 \cdot 9\text{H}_2\text{O}$ were dissolved in 227.5 mL distilled water (solution A). Solution A was then added drop wise to another (solution B), which contained 250.9 mL aqueous solution of Na_2CO_3 (2 mol) and NaOH (6 mol) under vigorous stirring at room temperature. The suspension was left for 12 h at 300 K and the pH range of the sol-gel solution was 12-13. The sample was then filtered off and washed with distilled water until the pH of the solution reach to ~ 7 . The resultant gel was dried at 333 K overnight and calcined at 723 K in N_2 for 5 h to obtain its oxide form.

3.1.3 Preparation of supported catalysts

The supported Pd catalysts with 1wt% Pd loading were prepared using an immobilization method with polyvinyl alcohol. The Pd precursor was pre-reduced with NaBH_4 with 2:1 molar ratio of NaBH_4 :Pd (formation of dark brown sol). Within a few minutes of sol generation, the colloids (acidified at pH 2, by chloric acid) were immobilized by adding support (activated carbon, hydrotalcite, and composite of hydrotalcite and activate carbon) under vigorous stirring. The activated carbon and hydrotalcite were mixed by taking a 1:1 weight ratio to obtain the composite of activated carbon-hydrotalcite (AC1-HTc). The slurry was stirred until all the palladium has been deposited on the support. Next, the sample was filtered off and dried at 333 K overnight. The catalyst was then calcined at different temperature for each types of catalysts under N_2 flow ($50 \text{ mL} \cdot \text{min}^{-1}$) and reduced in a stream of H_2 at $50 \text{ mL} \cdot \text{min}^{-1}$ flow rate for 4 h at different temperature which respect to the types of catalysts and will discussed further in Section 3.3.

3.2 Catalyst characterization

3.2.1 Nitrogen physisorption measurement

Theoretically, the rate of product formation over a catalyst is a function of the accessibility of the reactant to the active site on the surface area of the catalyst. Thus, it is important to be able to quantify the surface area of this phase, and the adsorption of inert gas makes this measurement possible (Zhang & Yang, 2013).

The surface area and porosity properties of the catalyst can be determined from nitrogen physisorption measurement (Serwicka, 2000). Physisorption or physical adsorption is a phenomenon of gas molecules adhering on the surface of the solids at a pressure less than vapor pressure (Condon, 2006). The bond between adsorbed gas molecules and surface are relatively weak and not covalent or ionic bond. There are two types of physisorption, gas-like physisorption and liquid-like physisorption as illustrated in Figure 3.1. Measurement of the amount absorbed versus adsorptive pressure at constant temperature is called the adsorption isotherm.

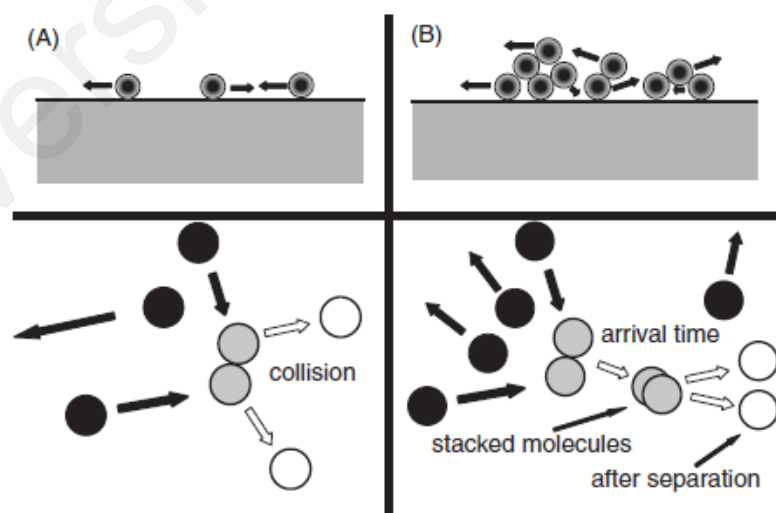


Figure 3.1: Models of two types of physisorption. A, gas-like; B, liquid-like; ● before encounter; ○ after encounter, hatched is during encounter (Condon, 2006)

Despite the oversimplification of the model on which the theory is based, the B.E.T. method is the most widely used. It is the standard procedure for the determination of surface area of finely divided and porous material (Bond, 1998). The BET equation applicable at low p/p_0 range is customarily written in linear form as:

$$\frac{P}{n^a(p_0 - p)} = \frac{1}{n_m^a C} + \left(\frac{C-1}{n_m^a C} \right) \frac{p}{p_0} \quad \text{(Equation 3.1)}$$

Where n^a is the amount of gas adsorbed at the relative pressure p/p_0 , n_m^a is the monolayer capacity and C is the so-called BET constant. According to the BET theory, it is related to the enthalpy of adsorption in the first adsorbed layer and gives information about the magnitude of adsorbent-adsorbate interaction energy (Rouquerol et al., 1994). If the information is applicable, a plot of $p/[n^a(p_0-p)]$ vs p/p_0 should yield a straight line with intercept $1/n_m^a C$ and slope $(C-1)/n_m^a C$. The value of n_m^a and C may then be obtained from a plot of a single line, or regression line, through the points (Rouquerol et al., 1994). The volume of the monolayer having been ascertained, allows the surface area of the sample to be determined by a single adsorbate molecule, a value derived from the assumption of close packing at the surface by the formula (Bond, 1998):

$$a_s(BET) = \frac{n_m^a \cdot L \cdot a_m}{m} \quad \text{(Equation 3.2)}$$

Where a_s is the specific surface area, L is Avogadro's number ($6.023 \times 10^{23} \text{ mol}^{-1}$), m is the mass of the adsorbent and a_m is the cross sectional area of the adsorbate molecule, for which a value of $0.162 \text{ nm}^2 \text{ molecule}^{-1}$ for N_2 is widely accepted. The assumptions in the BET equation break down if the BET plot is not linear, and the plot is usually restricted to the linear part of the isotherm over the p/p_0 range of 0.05-0.3 (Gallezot, 1997).

There are six different types of isotherms as shown in Figure 3.2, and isotherm interpretation at Table 3.1. For the possible isotherm to be amenable to BET analysis, the value of C should be neither too low nor too high, i.e. $20 < C < 200$, and the BET plot must be linear for the p/p_0 region taken for calculations.

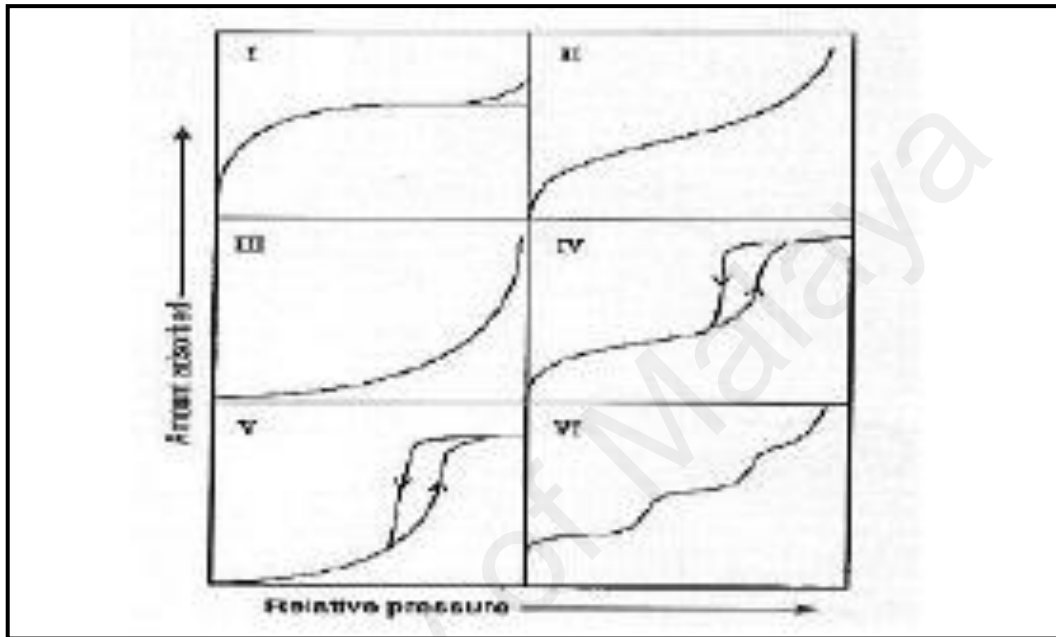


Figure 3.2: Type of isotherms

Table 3.1: Classification of physical adsorption isotherms

Type	Interpretation
I	Physisorption on a material that has extremely fine pores (micropores)
II	This is the characteristics of a material, which is not porous, or possibly macroporous and high energy of adsorption
III	This is the characteristics of a material, which is not porous, or possibly macroporous and has low energy of adsorption
IV	This is the characteristics of a material, which contains mesoporosity and has a high energy of adsorption. These often contain hysteresis attributed to the mesoporosity
V	This is the characteristics of a material, which contains mesoporosity and has a low energy of adsorption. These often contain hysteresis attributed to the mesoporosity
VI	This type of isotherm is attributed to several possibilities. Most likely if the temperature is below the adsorptive triple point, the adsorbate is more like a solid forming a structured layer. Other possible explanations include multiple pore size.

Technique:

Before the analysis was carried out, about 200 to 400 mg of catalysts powder was degassed at 363 K for 1 h and 4 h at 573 K. Then, the specific surface area, pore volume, and average pore size of the catalysts were measured by N₂ adsorption-desorption technique using Micromeritics Tristar ASAP 3020 at 77 K.

3.2.2 X-Ray Powder Diffraction (XRD)

XRD is one of the most frequently applied techniques in catalyst characterization. This technique is used to identify bulk phase and estimate particle sizes (Stefenelli et al., 2013). X-rays with wavelengths in the Å range, are sufficiently energetic to penetrate solids and are well suited to probe their internal structures.

An X-ray source consists of a target, which is bombarded with high-energy electrons. The emitted X-rays arise from two processes. Electron slowed down by the target emits a continuous background spectrum of Bremsstrahlung. Superimposed on this are characteristic narrow lines. The Cu K_α line arises when a primary electron creates a core hole in the K shell, which is filled by an electron from the L shell (K_β: the K-hole is filled from the M-shell, etc) under emission of an X-ray quantum (Conesa et al., 1990).

XRD is an elastic scattering of x-ray photons by atoms in a periodic lattice. The scattered monochromatic X-rays that are in phase give constructive interference. The XRD pattern of powdered sample is measured with a stationary X-ray source (usually Cu K_α) and a movable detector, which scan the intensity of the diffracted beams radiation as a function of the angle 2θ between the incoming and the diffracted beams. When working with a powdered sample, an image of diffraction lines occurs because a small fraction of the powder particle will be oriented such that by chance a certain crystal plane (hkl) is at the right angle with the incident beams for constructive interference.

The width of diffraction peaks carries information on the dimensions of the reflecting planes. Diffraction lines from perfect crystals are very narrow. For crystallite sizes below 100 nm, however line broadening occurs due to incomplete destructive interference in scattering directions where the X-ray is out phase. The crystallite size $\langle L \rangle$ can be determined from Scherrer equation.

Equation 3.3: Scherrer equation

$$\langle L \rangle = \frac{K\lambda}{\beta \cos\theta} \quad \text{(Equation 3.3)}$$

Where β line width λ is the wavelength of the X-rays, θ is the angle between incident X-rays and the normal plane, and K is a constant, usually 1.

Technique:

X-ray diffraction measurements were carried out using a Bruker X-ray Diffraction model D8 Advance Powder X-ray diffractometer (θ - 2θ mode, Cu- K_{α} radiation at $\lambda = 1.54019 \text{ \AA}$, scintillation detector) equipped with EVA diffract software for data acquisition and analysis. The diffractogram was recorded over 2θ values ranging from 2 - 60° with a scanning rate of 0.04 s/step at ambient temperature. Analysis of the spectra was carried out using X'Pert HighScore Plus software for the full pattern analysis. The crystal phases of the sample were identified by overlaying the standard JCPDF diffraction pattern matching for both peak positions and relative intensity.

3.2.3 X-Ray Fluorescence (XRF)

XRF is a nondestructive analytical technique used to identify and determine the concentrations of elements present in solid, powdered and liquid samples. This technique is capable of measuring all elements from beryllium to uranium at trace levels often

below one part per million, and up to 100 % (Titiladunayo & Fapetu, 2011). The sample is irradiated by intense X-rays, which cause the emission of fluorescent X-rays. The spectrum of emitted rays is detected either by an energy-dispersive or wavelength-dispersive detector. The elements in the sample are detected by characteristic wavelengths of emitted x-rays and concentration is determined by the intensity of the X-rays.

During this process, the primary X-ray, which has sufficient energy, ejected the inner orbital electrons and creating vacancies. These vacancies present an unstable condition for the atom. As the atom returns to its stable condition, electron from the outer shells are transferred to the inner orbital, and in this process it gives off a characteristic X-ray whose energy is the difference between the two binding energies of corresponding shells (Figure 3.3). Because each element has a unique set of energy levels, each element produces X-rays at a unique set of energies, allowing one to non-destructively measure the elemental composition of a sample. The process of emissions of characteristic X-rays is called "X-ray Fluorescence" or XRF ("X-ray Fluorescence (XRF) and Particle-Induced X-ray Emission (PIXE)," 2007). The atom absorbs the X-ray by transferring all of its energy to an innermost electron.

For a particular energy (wavelength) of fluorescent light emitted by an element, the number of photons per unit time (generally referred to as peak intensity or count rate) is related to the amount of that analyte in the sample. The counting rates for all detectable elements within a sample are usually calculated by counting, for a set time, the number of photons that are detected for the various analytes "characteristic" X-ray energy lines. Therefore, by determining the energy of the X-ray peaks in a sample's spectrum, and by calculating the count rate of the various elemental peaks, it is possible to qualitatively

establish the elemental composition of the sample and to quantitatively measure the concentration of these elements.

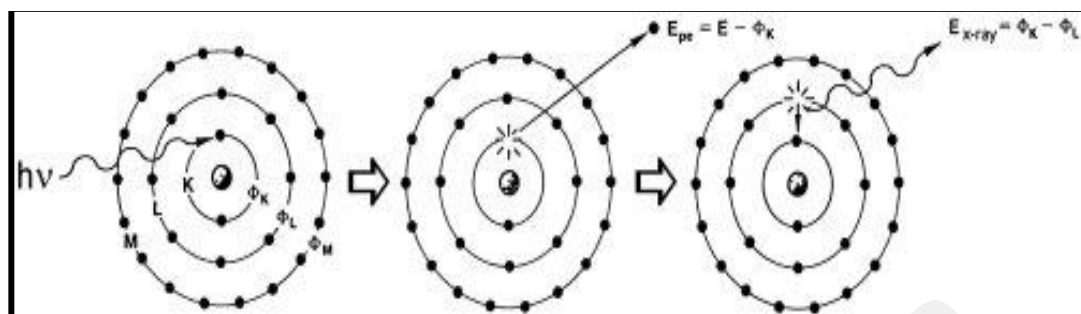


Figure 3.3: The excitation energy from inner atom is transferred to one of the outer electrons causing it to be ejected from the atom.

Technique:

The XRF analysis was performed using a Bruker X-ray Fluorescence model S4 Explorer (made from Germany) equipped with Spectra plus software for data acquisition and analysis. Data were acquired by using X-ray generator, using source operating at 1 KW at ambient temperature. The analysis was performed using semi-quantitative method. Samples were finely grinded using mortar and placed in the sample cup (40 mm diameter) installed with 6 μm mylar film at the bottom.

3.2.4 Fourier Transform Infrared Spectroscopy (FTIR)

Infrared (IR) spectroscopy is one of the chemical analytical techniques used by organic and inorganic chemists. It is the absorption measurement of different IR frequencies by a sample positioned in the path of an IR beam. IR spectroscopic analysis is to determine the chemical functional groups in the sample. Different functional groups absorb characteristic frequencies of IR radiation.

The IR region is commonly divided into three small areas; near IR, middle IR and far IR. The range from 12000 cm^{-1} to 4000 cm^{-1} is called near infrared, that from 4000 cm^{-1} to 400 cm^{-1} middle infrared (most frequently used) and the range below 400 cm^{-1} is the far infrared region. IR absorption information is generally presented in the form of a spectrum with wavelength or wavenumber as the x-axis and absorption intensity or percent transmittance as the y-axis.

IR spectroscopy allows an identification of various sorts of functional groups via their characteristic vibrations viz. the stretching and bending vibrations. Molecular bonds vibrate at various frequencies depending on the elements and the type of bonds. For any given bond, there are several specific frequencies at which it can vibrate. As a result, a chemical functional group tends to adsorb infrared radiation in a specific wavenumber range regardless of the structure of the rest of the molecule.

For example, the C=O stretch of a carbonyl group appears at around 1700 cm^{-1} in a variety of molecules. Hence, the correlation of the band wavenumber position with the chemical structure is used to identify a functional group in a sample. The wavenumber positions where functional groups adsorb are consistent, despite the effect of temperature, pressure, sampling, or change in the molecule structure in other parts of the molecules. Thus, the presence of specific functional groups can be monitored by this spectroscopy (Yang et al., 2007). FTIR spectrometer obtains infrared spectra by first collecting an interferogram of a sample signal with an interferometer, which measures all of infrared frequencies simultaneously. A FTIR spectrometer acquires and digitizes the interferogram, performs the FT function, and outputs the spectrum.

Technique:

IR spectra were recorded in the transmission mode using Bruker IFS66V/S spectrometer. The catalysts were grounded well with potassium bromide (KBr) into uniform fine particle size and were then compressed into a KBr pellet of 12 mm diameter at 20000 psi. IR spectra of 400-4000 cm^{-1} range was recorded by a 32 scan data accumulation at a resolution of 4.0 cm^{-1} under ambient temperature and pressure. For acidity measurements, the catalysts were out-gassed overnight at 673 K and 10^{-3} Pa dynamic vacuum using self-supported wafers of 10 $\text{mg}\cdot\text{cm}^{-1}$, then pyridine was admitted into the cell at room temperature. After saturation, the samples were outgassed at different temperatures (523 and 623 K) for 1 h under vacuum, cooled to room temperature, and the spectra were recorded.

3.2.5 Temperature-Programmed Reduction (TPR)

TPR techniques permit to find the most efficient reduction/oxidation conditions. Besides, the interaction between the supported precursor phases and the support can be identified by these methods. These experiments are particularly useful in case of multi-metallic systems, for the evaluation of the role of the added compounds or doping agents (alloy formations or promotion effects). In the TPR technique an oxidized catalyst precursor is submitted to a programmed temperature rise while a reducing gas mixture flows over it (usually, hydrogen diluted in some inert gas like argon).

The reduction rates are continuously measured by monitoring the change in composition of the reactive mixture after the reactor. The decrease in H_2 concentration in the effluent gas with respect to the initial percentage monitors the reaction progress. An interesting application of this technique is that the TPR analysis may be used to determine the surface properties of the metal based supported catalysts (Malleham et al., 2016).

Technique:

TPR was carried out to determine the oxidation state and the chemical nature of metal species of the supported catalysts. The measurement was carried out in a Thermofinnigan TPDRO 1100 instrument. The sample was first calcined ex-situ in a furnace at 723 K for 4 h. Then, about 50 mg of the catalyst was pre-treated in a tubular quartz reactor, by heating material from room temperature to 383 K at $10 \text{ K}\cdot\text{min}^{-1}$ under $10 \text{ cm}^3\cdot\text{min}^{-1}$ N_2 for 20 minutes. This step is crucial in eliminating any possible contaminants and moisture present on the surface of the catalyst. The material was cooled to room temperature again after pre-treatment. TPR measurement was carried out in flow of $10 \text{ cm}^3\cdot\text{min}^{-1}$ 5% H_2 in nitrogen, from room temperature to 873 K at a heating rate of $10 \text{ K}\cdot\text{min}^{-1}$ and was hold for 60 minutes . The reduction was measured by monitoring the hydrogen consumption with TCD detector. The water produced during the reduction was trapped in 5 Å molecular sieve column.

3.2.6 Temperature Program Desorption CO₂ (TPD-CO₂)

TPD-CO₂ is one of the technique used to determine the basicity of the heterogeneous catalysts (Prinetto et al., 2004). The sample will be saturated with the chosen adsorbate (CO₂) by flowing the reactive gas. Then, the sample is submitted at an increasing temperature at constant rate, and it was swept by an inert gas (helium, argon, and nitrogen).

In TPD studies, the sample system is equilibrated until saturation occurs with a probe molecule in isothermal conditions and at given partial pressure. The Langmuir adsorption model may be used as well for TPD spectra interpretation as it describes both gas adsorption and desorption in the two cases of associatives and dissociatives (Fadoni & Lucarelli, 1999).

Technique:

TPD-CO₂ was carried out to determine the basicity of the catalyst supports and palladium based supported catalysts. The measurement was carried out in a Thermofinnigan TPDRO 1100 instrument. The sample was first calcined ex-situ in a furnace at 723 K for 4 h and in a stream of N₂ and H₂ (90:10) flowing at 150 mL.min⁻¹ for 3 h at different temperatures for different types of supported palladium catalysts; 1wt% Pd/AC1 at 600 K, 1wt% Pd/HTc at 773 K and 1wt% Pd/HTc-AC1 at 750 K. The catalyst (50 mg) was placed in a tubular quartz sample tube and the sample was pre-treated at ambient condition under N₂ flow 10 mL.min⁻¹ for 30 minutes. The sample was exposed to CO₂ at room temperature to the 393 K (10 K.min⁻¹). Desorption was carried out from room temperature to 873 K at a heating rate of 10 K.min⁻¹.

3.2.7 Thermal-Gravimetric Analysis- Mass Spectrometry (TGA-MS)

TGA-MS basic principle is a measuring the mass of a sample as a function of temperature and mass spectrometry that allows to characterize and quantify compounds in the off-gas in real time along with mass loss. It is a very useful technique to study a solid-gas system. This technique is used in the chemistry of solids to characterize phase transformations and, if necessary, to dose them with selected probe to see the weight loss more clearly (Becker, 1965; Keattch & Dollimore, 1975). The method for example can be used to determine water of crystallization, follow degradation of materials, determine reaction kinetics, study oxidation and reduction, or to know the principles of stoichiometry, formulae and analysis (Kloprogge et al., 2001).

As the main parameter used in this instrument is often temperature, thus the common name of thermogravimetry is used. The measuring instrument is therefore a weighing device. It has no memory that changes in the mass of the sample clearly imply evaluation or uptake of matter by the sample. In weighing the sample, it assumes that it can be

connected to the weighing device. The method only works well if the sample is in compact form. Generally this is a solid or powder; sometimes a liquid placed in an open crucible or even fixed on a solid phase.

Technique:

To investigate the thermal stability of the catalyst used, the measurement was done using Thermogravimetric Analysis (TGA). The analysis was carried out using Mettler Toledo TGA/SDTA851^e thermobalance. An alumina crucible of 100 μl was used for all measurements. About 10 to 50 mg of catalysts were used to characterize the weight loss of the samples. The TGA temperature program was run dynamically from ambient to 973 K at a heating rate of 5 $\text{K}\cdot\text{min}^{-1}$ under nitrogen with flow rate of 50 $\text{mL}\cdot\text{min}^{-1}$.

3.2.8 Thermal-Gravimetric Analysis (TGA-Proximate analysis)

Proximate analysis is one of the thermal analysis techniques. It is mostly, it is used to determine the content of: a) moisture; b) volatile matter; c) fixed carbon; and d) ash of the carbonaceous materials (Vermani, 2003). The analysis is usually carried out in an automated thermogravimetric system. Moisture matter mostly water, which refer to the matter that volatilized until near 373 K in an inert atmosphere (N_2 , He, and etc.). Volatile matter content is determined in an inert atmosphere at temperature range of 373 to 1223 K. Fixed carbon matter is the material burned in air at 1223 K. Other than that, fixed carbon content is determined by subtracting the sum of percentage compositions of moisture content, volatile content and ash content from 100%. Lastly, the non-combustible matter is the ash. Generally, the composition of ash, fixed carbon, and volatile matter are given on a dry basis. The representation of weight versus temperature (or time) also gives information about the thermal stability of the activated carbon (Durán-Valle, 2012; Nwabanne & Igbokwe, 2011).

$$\% \text{ fixed carbon} = 100 - (\% \text{ash tent} + \% \text{volatile matter content})$$

Technique:

To investigate the proximate analysis and thermal stability of the activated carbon, the measurement was done using Thermogravimetric Analysis (TGA). The analysis was carried out using Mettler Toledo TGA/SDTA851^e thermobalance. An alumina crucible of 100 μl was used for all measurements. About 10 to 50 mg of catalysts were used to characterize the weight loss of the activated carbon sample. The TGA temperature program was run at different temperature programmed. Firstly, from 298 to 383 K at a heating rate of 278 $\text{K}\cdot\text{min}^{-1}$ under nitrogen with flow rate of 50 $\text{mL}\cdot\text{min}^{-1}$ and hold at 383 K for 5 minutes. Then, heat from 383 K to 1193 K heating rate of 278 $\text{K}\cdot\text{min}^{-1}$ under nitrogen with flow rate of 50 $\text{mL}\cdot\text{min}^{-1}$ and hold at 1193 K for 20 minutes. Lastly, the gas was changed to O_2 and the temperature range is 1193 K to 1093 K with heating rate of 278 $\text{K}\cdot\text{min}^{-1}$ and was hold for 20 minutes.

3.2.9 High Resolution Transmission Electron Microscopy (HR-TEM)

HR-TEM is a widely used techniques for structural and morphological studies in catalysts field. HR-TEM has been extensively and successfully used for analyzing crystal structures and lattice imperfections in various kind of advanced materials on an atomic resolution scale. HR-TEM image is an interference pattern between forward-scattered and diffracted electron waves from samples (Williams & Carter, 1996). The highest magnification of HR-TEM can be 10^6 or even higher (Ernst & Ruhle, 2003).

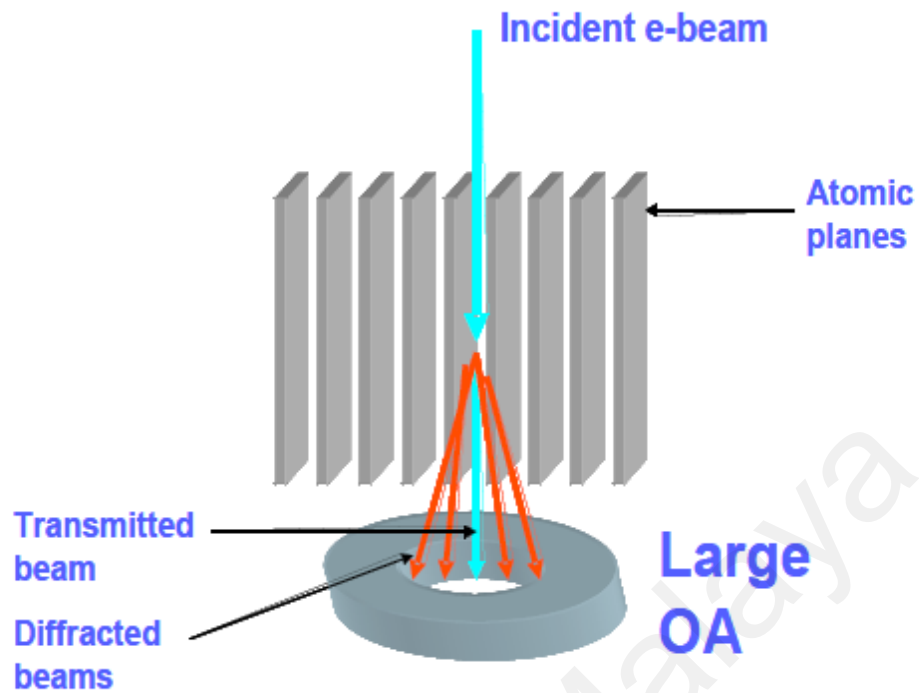


Figure 3.4: High resolution transmission electron microscopic principle.

The atomic planes are oriented parallel to the incident electron beam in the microscope as demonstrated in Figure 3.4. Strong transmitted beam and a multitude of diffracted beams from the different sets of atomic planes will produce from this parallel oriented with incident beam. Sometimes, HR-TEM technique is counter intuitive to researchers, who are mainly involved with XRD analysis. The requirement for diffraction is the X-ray beam be oriented at a Bragg angle to the diffracting planes. Differently with XRD, due to the high electron energy and the resulting very short wavelength of the electrons, appreciable diffraction results even from atomic planes that are not oriented at a Bragg angle to the incident beam. This is gives tremendous advantage because it allows reconstructions of the crystal lattice to be obtained almost instantaneously and from a single sample orientation.

Technique:

HR-TEM analysis was conducted using the JEM-2100F instrument at an accelerating voltage of 200 kV. The nanoparticles sample was prepared by titrating the dispersed samples on a 300 mesh copper grids. The samples were prepared and left overnight to dry. The samples were then placed into the HR-TEM sample holder prior to being placed into the HR-TEM. Images of nanoparticles sample was selected and taken at 50,000, 100,000, and 500,000 \times magnification. The size and lattice-fringe spacing was measured using image-J. The particle size distribution was plotted after particles of nanoparticles sample was measured, and the lattice-fringe spacing was used to support the results from XRD analysis.

3.2.10 Surface acidity determination

Most properties of the carbon materials are influenced by the functional group on the surface of the carbon materials (Boehm, 2002). Oxides group are the main group of this carbon materials. Oxygen in the surface oxides are bound in the form of various functional group and this functional group is linked to the high surface area properties (Kalijadis et al., 2011). At high temperature, the surface oxides will decompose to CO_2 and CO . Alternatively, the surface oxides functional group of carbon materials can be created by thermal or chemical treatment for example liquid oxidant e.g HNO_3 (J.L. Figueiredo et al., 1999).

The surface oxides can have either acidic or basic properties and successfully determined by titration method (Barkauskas & Dervinyte, 2003). Usually, the acidic and basic surface are coexist, but the concentration of the acidic sites will increase when the concentration of basic sites is decreased.

The acidic surface properties are caused by the presence of carboxyl group, lactones or lactol and hydroxyl groups of phenolic characters (Teng et al., 2000). All of these groups have different acidity value and can be determined by titrating with base solution (NaOH, NaHCO₃ and Na₂CO₃) (Rodrigues-Reinoso, 1998).

Contrast to the acidic surface properties, the origin of the basic surface properties is still under discussion (Boehm, 2002). The chemisorption of oxygen during the surface treatments suggest that the basicity may be due to oxygen functional group, existence of pyrone-type structures on the edge of polyaromatic layers (Voll & Boehm, 1971).

Technique:

The amount of acidic sites in the activated carbon was determined by direct titration with 0.01 M NaOH solution. Accurately 0.1 g of activated carbon was transferred into 100 mL round bottom flask. 50 mL of the solution of 10⁻⁴ M KCl was introduced into the flask. The flask was stirred vigorously at 400 rpm for 24 h under vigorous magnetic stringing to ensure equilibrium was reached. The solution was then directly titrated with 0.01 M NaOH solution. The titration was carried out using Mettler DL25 Autotitrator. This equipment is equipped with titrator DL25, automatic burette 20 mL, and was connected to a computer, which controlled the equilibrium condition and titrant delivery. The dynamic dosing of the titrant in increments of 0.1 mL to the suspension samples and the pH of the solution was measured every 10 second.

3.3 Catalyst preparation

3.3.1 Calcination of catalyst

All palladium-based supported catalysts were calcined under N_2 at different temperature for each catalysts (Table 3.2). The diagram (Figure 3.5) below illustrates the calcination procedure used:

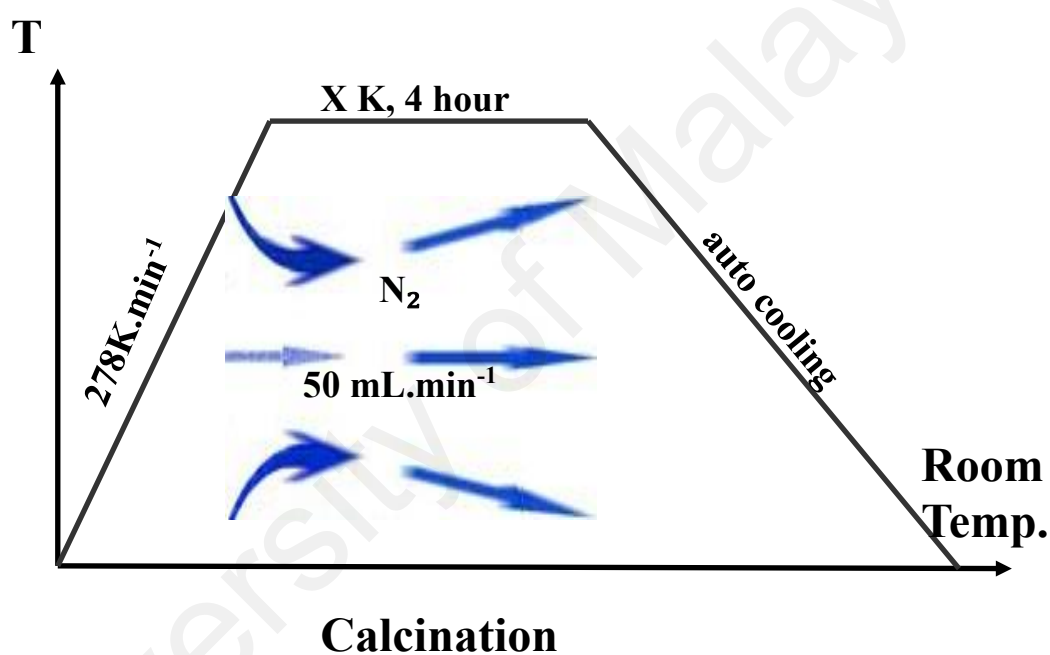


Table 3.2: Calcination temperature for various palladium-based supported catalyst

No	Catalysts	Calcination temperature (X K)
1	1wt% Pd/AC1	673
2	1wt% Pd/HTc	783
3	1wt% Pd/HTc-AC1	673

3.3.2 Activation of catalyst

All catalysts were activated under hydrogen flow before subjected to glycerol oxidation reaction. All palladium-based supported catalysts were reduced under H_2 at different temperature for each catalysts (Table 3.3). The diagram (Figure 3.6) below illustrates the calcination procedure used. After activation, the quartz reactor was purged with N_2 to remove excess H_2 gas. After a few minutes, the catalyst was transferred to a 200 mL stainless steel autoclave for glycerol oxidation

Calcination and reduction process were carried out using quartz reactor Carbolite tubular furnace.

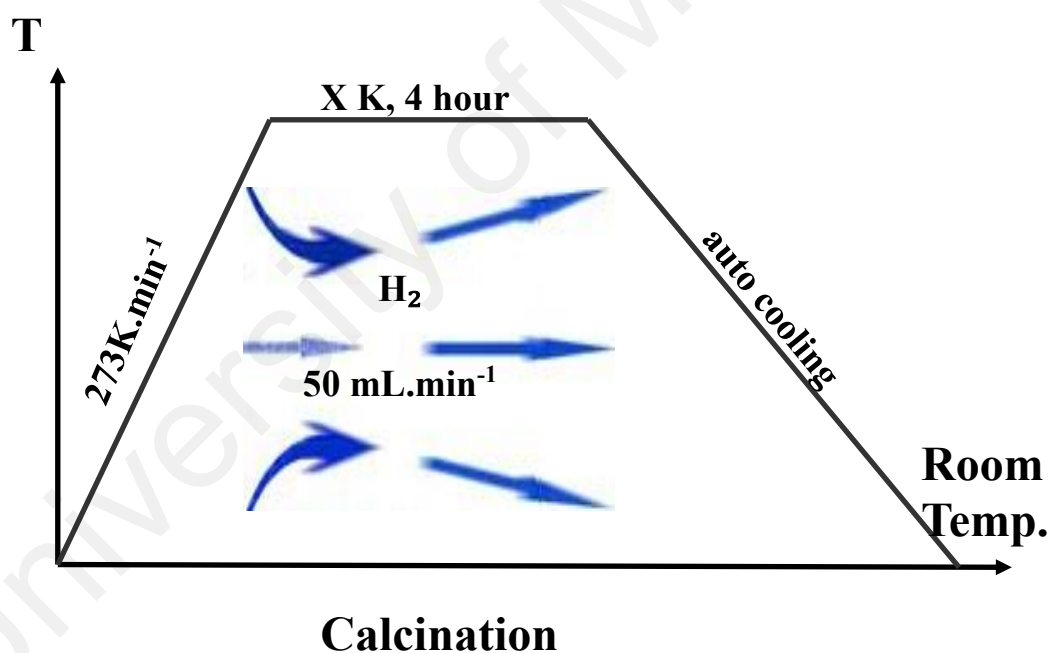


Figure 3.6: Reduction procedure for palladium-based supported catalysts

Table 3.3: Temperature and condition of activation for each catalyst

No	Catalysts	Reduction temperature (K)
1	1wt% Pd/AC1	600
2	1wt% Pd/HTc	773
3	1wt% Pd/HTc-AC1	750

3.4 Liquid phase oxidation of glycerol

3.4.1 Materials

Glycerol (GLY, >99%) was purchased from Friendemann Schmidt, sodium hydroxide (NaOH) (Merck, 99%), D-Glyceric acid (GLYAC, 99%) and Dihydroxyacetone (DHA, 97%) were purchased from Aldrich, DL-Glyceraldehyde (GLYALD, > 90%) was purchased from Sigma, Tartronic acid (TARAC > 97%) were purchased from Fluka, The purified O₂, purified H₂ and nitrogen were obtained from Mox-Linde. All chemicals and solvent were used as received.

3.4.2 Reaction setup

Liquid phase glycerol oxidation was carried out in a 200 mL stainless steel autoclave by Top Industries. The reactor was charged with 50 mL of 0.3 M glycerol, 0.1261 g of catalyst (molar ratio Gly: Pd = 3500) and aqueous NaOH (0.6 M). After sealing the pressure was pressurized with N₂ to 3 bar and then heated to the reaction temperature (333 K). After the reaction temperature is achieved, the gas was switch to O₂ until 3 bar. During the experiment, the stirring rate was adjusted to 750 rpm (magnetic stirrer). The reaction parameters were changed appropriately in order to study the effect of reaction conditions. Details of the reaction condition is described in each result (Chapter 5). Figure 3.7 shows experimental set up glycerol oxidation.

The sample was taken every 30 minutes and after reaction finished (3 h) the sample was collected and was analyzed offline. Every 30 min, about 1 mL sample was taken from sampling port by open the needle valve slowly (to avoid any pressure gas release).

University of Malaya

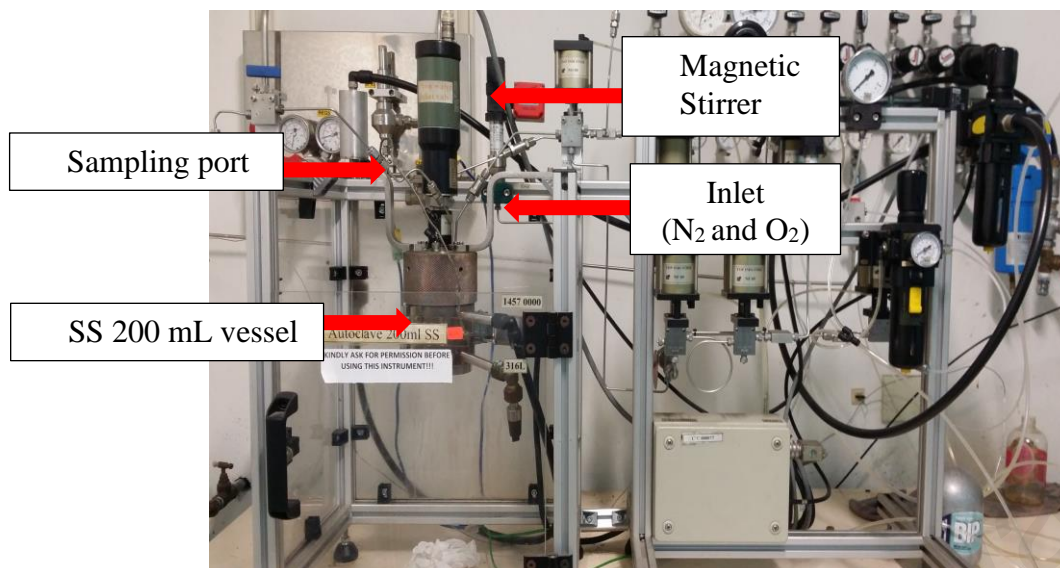


Figure 3.7: Experimental set up of the glycerol oxidation

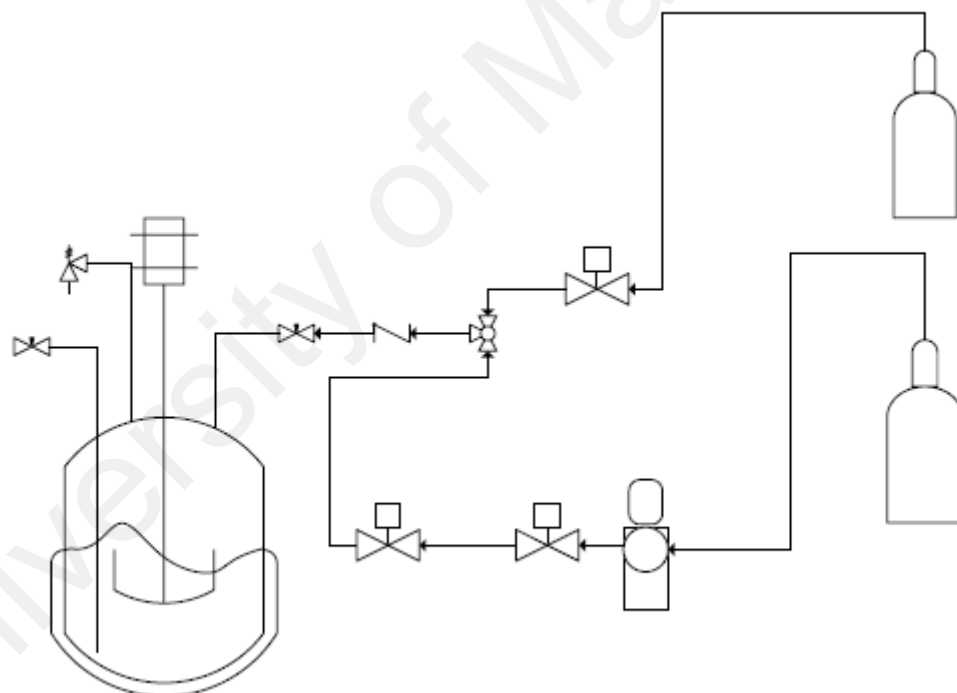


Figure 3.8: Schematic diagram of experimental set up of the glycerol oxidation

3.4.3 Product analysis

3.4.3.1 High performance liquid chromatography

The products were analyzed by using HPLC (Shimadzu). After an appropriate reaction time, the reactor was cooled down, the product was taken out and filtered. Before injected to HPLC, the samples were filtered with nylon syringe filter (0.2 micron). Table 3.4 summarizes the parameters of HPLC analysis.

Table 3.4: Parameters of HPLC analysis for glycerol oxidation

<i>Column</i>	<i>Agilent Hi-Plex H, 7.7 × 300 mm, 8 μm</i>
<i>Mobile phase</i>	0.0085 M H ₂ SO ₄
<i>Temperature</i>	338 K
<i>Flow rate</i>	0.55 mL.min ⁻¹
<i>Detector</i>	Refractive index
<i>Duration</i>	30 min

Standards calibration was carried out for glycerol, glyceric acid, glyeraldehyde, dihydroxyacetone, and tartronic acid Figure 3.9. The response factor and retention time of each standard are summarizes in Table 3.5

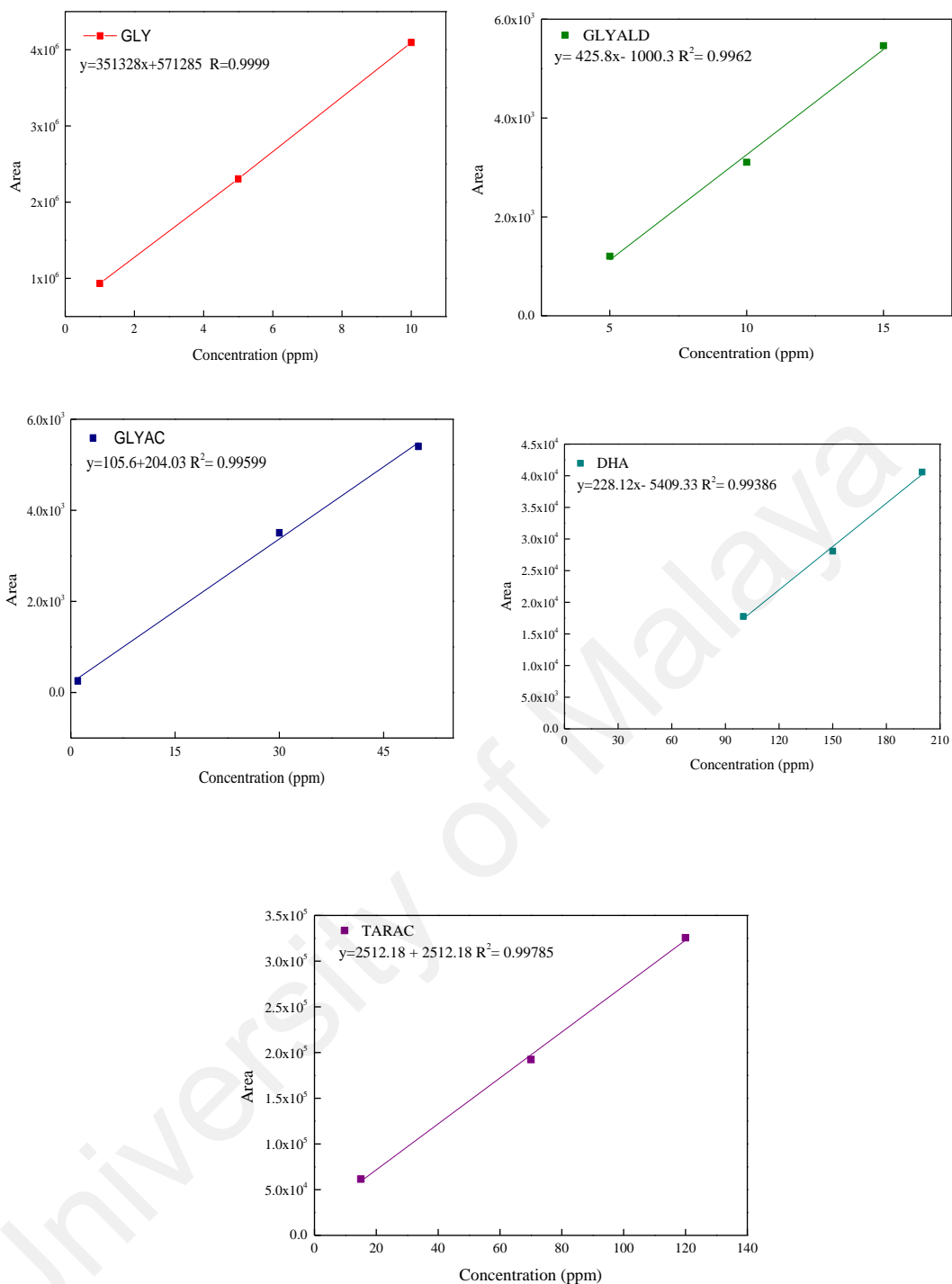


Figure 3.9: Calibration of curve of the standards for glycerol oxidation; GLY:glycerol, GLYALD:glyceraldehyde, GLYAC:glyceric acid, DHA:dihydroxyacetone and TARAC:tartronic acid

Table 3.5: Response factor and retention time of standards

Standards	Response factor	Retention time (min)
Glycerol	2.8463×10^{-6}	13.39
Glyceraldehyde	2.349×10^{-3}	11.59
Glyceric acid	9.47×10^{-3}	11.01
Dihydroxyacetone	4.28×10^{-3}	13.19
Tartronic acid	3.98×10^{-4}	10.02

3.4.4 Activity calculation

The conversion, selectivity and yield of the product are calculated using the following equations based on the HPLC results refer Appendix:

Conversion of glycerol (X_{GLY}):

$$X_{GLY} = \frac{y}{x} \times 100 \quad \text{(Equation 3.4)}$$

x = Total area of the peaks — area of the solvent peak

y = x — area of starting material peaks

Selectivity of products ($S_{products}$):

$$S_{products} = \frac{\text{area of the product peaks}}{\text{total peak area of the products}} \times 100 \quad \text{(Equation 3.5)}$$

Yield of products ($Y_{products}$):

$$Y_{products} = X_{GLY} \times S_{products} \quad \text{(Equation 3.6)}$$

Where S_{products} = selectivity of the glyceric acid, glyceraldehyde, dihydroxyacetone and tartronic acid.

Turnover frequency (TOF) refers to the molar ratio of converted substrate to catalyst per hours. Thus, TOF is expressed by:

$$\text{TOF} = \frac{\text{mmol of converted glycerol}}{\text{mmol of total Pd} \times \text{Reaction time (hour)}} \quad (\text{Equation 3.7})$$

University of Malaya

CHAPTER 4: RESULTS AND DISCUSSION FOR CATALYSTS

Physicochemical properties of catalyst supports (activated carbon and hydrotalcite) and supported palladium catalysts were characterized and evaluated by TGA-MS, XRD, XRF, FTIR, TPD-CO₂, TPR, BET, HR-TEM and surface acidity determination. The results of the characterization are discussed briefly in this chapter.

4.1 Catalyst support (Activated Carbon)

The type of carbon support that used in this studies is activated carbon. The raw activated carbon was purchased commercially from local supplier. Before used in preparation of supported palladium catalyst, the raw activated carbon was pre-treated with HNO₃ treatment. The properties of raw activated carbon and treated activated carbon were evaluated. The coding used for raw activated carbon is AC and treated activated carbon is AC1.

4.1.1 Surface Acidity Determination (Boehm Titration)

Activated carbons have the advantages of catalyst support such as relatively inexpensive materials, possess high surface area, easily recover of supported metals by simple combustion of the support and chemically inert in both acidic and basic conditions. The raw activated carbon consist of impurities, ash content and low iodine number (Li et al., 2005). Raw activated carbons are low in reactivity and efficiency. The oxides surface functional group is responsible for the catalyst application. These surface functional group can be introduced to the activated carbon by pre-treatment method (Kalijadis et al., 2011). The concentration of acid used does affect the formation of the oxygen-containing surface functional group. Li Jiayun and groups have reported that the pretreatment with high concentrations of HNO₃ will produce a great amount of oxygen-containing groups assembling densely on the activated carbon. As a result an interaction between oxygen-

containing groups and palladium metal precursor became too strong to disperse the palladium particles as well as will formed bigger particles (Li et al., 2005).

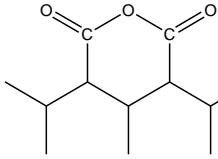
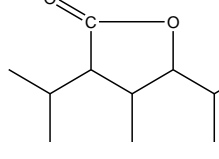
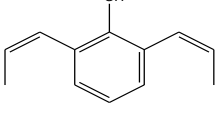
The surface oxide on a carbon can adjust as acidic or basic surface, and can be conveniently determined by acid-base titration technique. In this research, the raw activated carbon is pre-treated with nitric acid. Theoretically, the surface of treated carbon is acidic, hence to confirm this property, the Boehm Titration was carried out to check this property. The surface functional group were divided into three groups. They are carboxyl ($pK_a = 2.0- 4.0$), lactone ($pK_a = 4.0 - 7.0$) and phenol ($pK_a = 7.0 - 10.0$) (Barkauskas & Dervinyte, 2003).

The results presented in Figure 4.1 and Figure 4.2 show titration profiles of the raw and treated activated carbon. Figure 4.1 contains one distinct peak that is detected in NaOH filtrate. The acid dissociation (pK_a) has a value of 7.70 which can be assigned as phenolic groups (Shen et al., 2007). Meaning, the carbon surface of non-treated activated carbon (AC) contained phenolic group, and consumed low volume of NaOH to neutralize the surface (Kalijadis et al., 2011). The number of acidic sites of the sample were determined from the equivalent point value. Equivalent point value was reached when the moles of the based added is equivalent to the mole of acid sites in the sample (Kalijadis et al., 2011). The number of acidic sites for AC is 0.33 mmol.g^{-1} (Table 4.1).

The treated activated carbon (AC1) showed two distinct peaks (Figure 4.2) which are referred to the presence of two different functional groups on the carbon surfaces. The oxidative treatment of activated carbon leads to erosion of their structure. The first pK_a value, 2.51 is assigned to dicarboxylic acid, and the second peak to lactone group. The total amount of acidic sites for AC1 is 5.51 mol.g^{-1} . This is higher than AC due to the acid pre-treatment and implying higher number of functional groups is created after the pre-

treatment on the surfaces. Thus, stronger acidic groups need a higher volume of the base to neutralize the surfaces.

Table 4.1: Oxygen-containing groups of non-treated activated carbon (AC) and treated activated carbon (AC1) pretreated with 5M HNO₃

Activated carbon	 carboxyl group mmol.g ⁻¹	 lactonic group mmol.g ⁻¹	 phenol group mmol.g ⁻¹	total acidity mmol.g ⁻¹
AC	ND	ND	0.33	0.33
AC1	1.91	3.60	ND	5.51

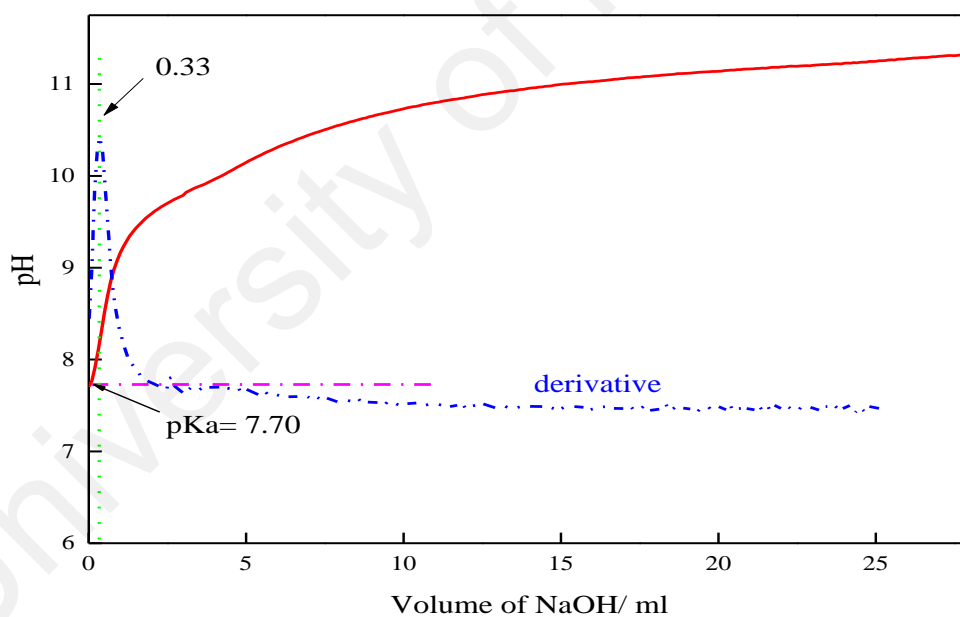


Figure 4.1: Acid-base titration profile for of non-treated activated carbon (AC)

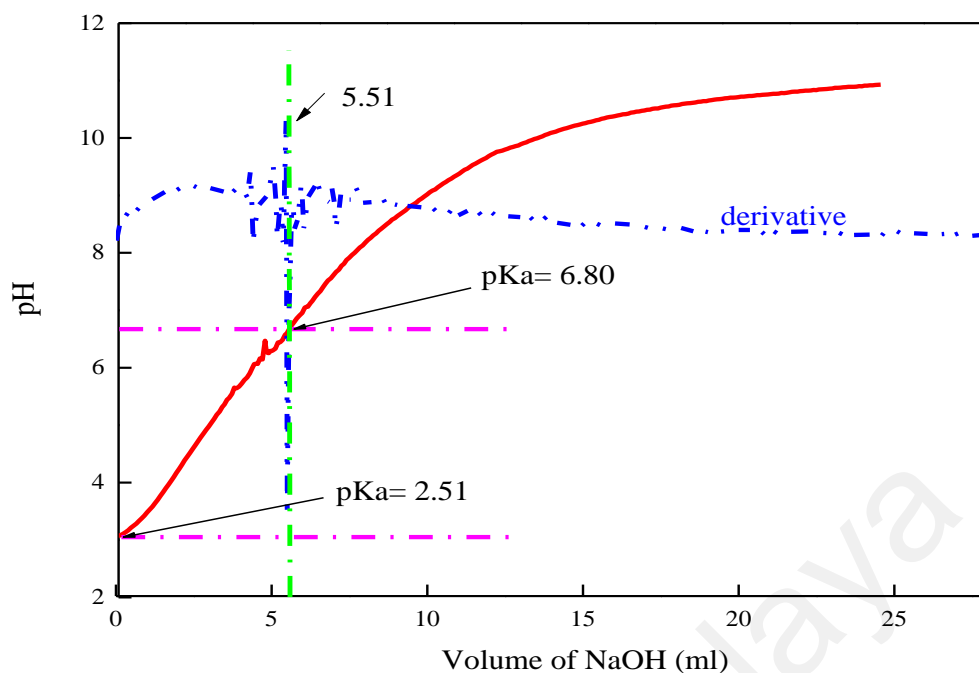


Figure 4.2: Acid-base titration profile for treated activated carbon (AC1)

4.1.2 Thermal-Gravimetric Analysis (TGA- Proximate analysis)

Proximate analysis of activated carbon is one of the ways to measure the chemical properties of activated carbon. It classifies carbonaceous materials in terms of moisture content, volatile matter, fixed carbon and ash content (Rashidi et al., 2012). The analysis was performed by using a thermogravimetric analysis. The proximate analysis was recorded by measuring the weight loss as a function of temperature and time.

The thermogram of the TGA analysis of AC and AC1 were shown in Figure 4.3 and Figure 4.4. The initial part of the thermograms for both samples showed the release of moisture content and volatile compounds related to physically bound water only. There are two basic types of moisture available, intrinsic and extrinsic moisture. The extrinsic moisture is influenced by the weather condition while intrinsic moisture is the moisture content of the materials itself. Based on Table 4.2, the moisture content value of AC1 (15.539%) is higher than AC (14.478%).

The second stage of the process involves the release of the volatile matters and organic matters. The degradation of organic volatiles compounds gradually decomposed until 1173 K. The biomass compounds for examples hemicellulose, cellulose and lignin are degraded at this range. Yang and the group had reported that the hemicellulose starts to degrade at 493 K, cellulose decomposes at a temperature greater than 573 K while lignin decomposes slowly under the room temperature ambient to 1173 K (Yang et al., 2007). After pretreatment, the value of volatile compounds of activated carbon increased from 10.0461% to 14.8508 %. This phenomenon happened due to the solubilization of hemicellulose and lignin under neutral or alkaline condition. The pretreated biomass undergoes oxidative delignification due to the reaction of the aromatic ring of lignin with the oxidizing agents leading to improvements digestibility compared to alkaline pretreatment only (Bensah & Mensah, 2013).

Besides that, the ash contents of the remaining inorganic materials left after the combustion process and the fixed carbon was calculated. Other than to increase the functionality of the activated carbon by adding the surface oxides functional group to the activated carbon surface, the purpose to do acid pre-treatment is to decrease the value of ash content. The ash content will reduce overall activities of activated carbon, for example, the metal can leach out from the activated carbon (Itodo et al., 2010). The residue of AC is 8.1128%, 1.3638 mg, and residue for AC1 is 3.869%, 0.6360 mg. Thus, it is shown that after the pre-treatment the ash content decreased.

Table 4.2: Proximate analysis of the activated carbon

Component	Non-treated Activated Carbon (AC)	Treated Activated Carbon (AC1)
Moisture content (%)	14.4780	15.5390
Volatile matter (%)	10.0461	14.8508
Fixed carbon (%)	67.3084	65.7439
Ash content (%)	8.1128	3.8639

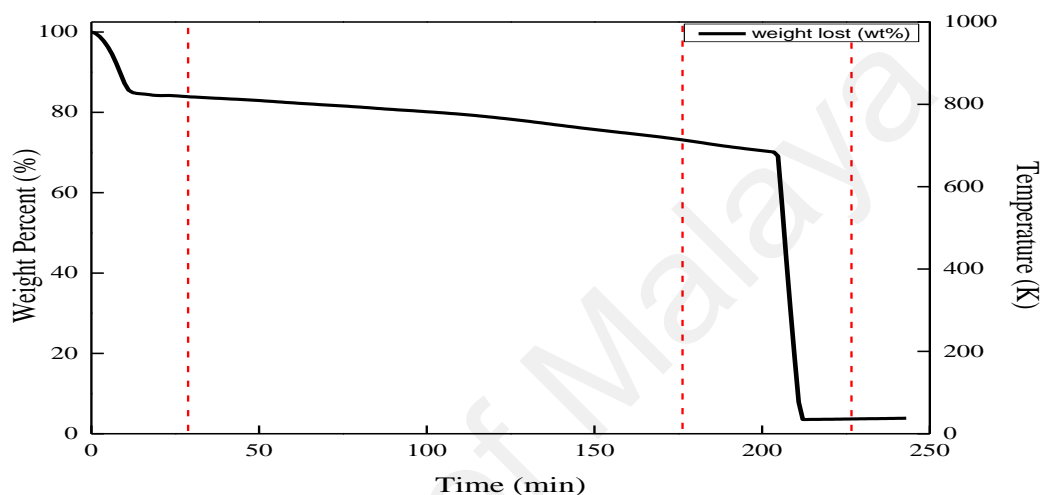


Figure 4.3: Proximate Analysis of non-treated activated carbon (AC)

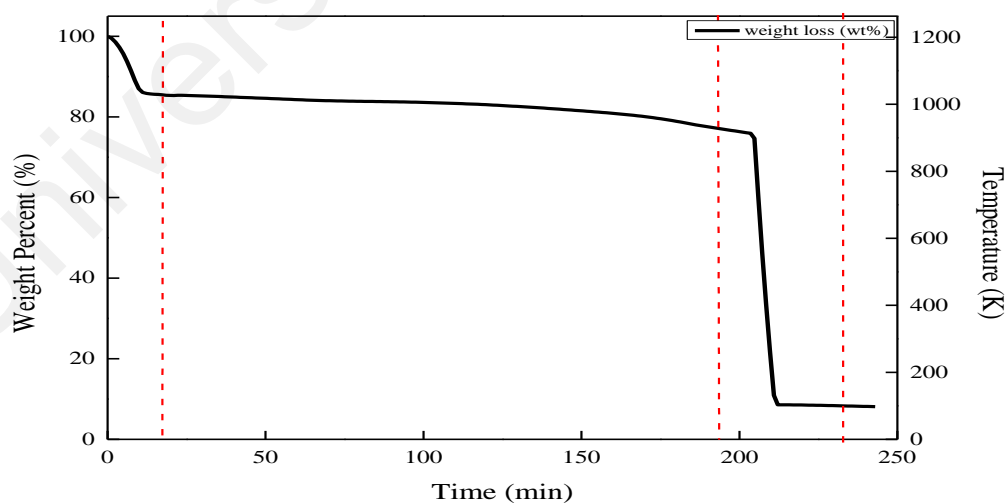


Figure 4.4: Proximate Analysis of treated activated carbon (AC1)

4.1.3 Fourier Transform Infrared Spectroscopy (FTIR)

The surface functional group of activated carbon was characterized by FTIR. The IR transmission spectra had absorption peaks where the specific chemical bonds existed as summarized in Table 4.3. Hence, it was possible to know the type of surface oxide functional group that was created on the activated carbon surface by comparing the locations and intensity of peak lines. The FTIR spectra of AC and AC1 were shown in Figure 4.5.

The AC exhibited absorption bands at 3853.19, 3445.54, 2356.40, 1552.83 and 1212.51 cm^{-1} as shown in Figure 4.5(a). The absorption bands at 3853.19 and 3445.54 cm^{-1} are represented by O-H stretching vibration of hydroxyl functional group in phenol group (J.L. Figueiredo et al., 1999). The strong peak was located at 2356.40 cm^{-1} indicated the $\text{C}\equiv\text{C}$ stretching vibration in alkyne groups (Shaarani & Hameed, 2011). FTIR peaks at 1552.83 cm^{-1} may be referred to the $\text{C}=\text{C}$ vibration in aromatic rings of the activated carbon (Anisuzzaman et al., 2015). The small peak at 1212.51 cm^{-1} is attributed to C–O–C of group stretching mode of lactone group (Shaarani & Hameed, 2011)

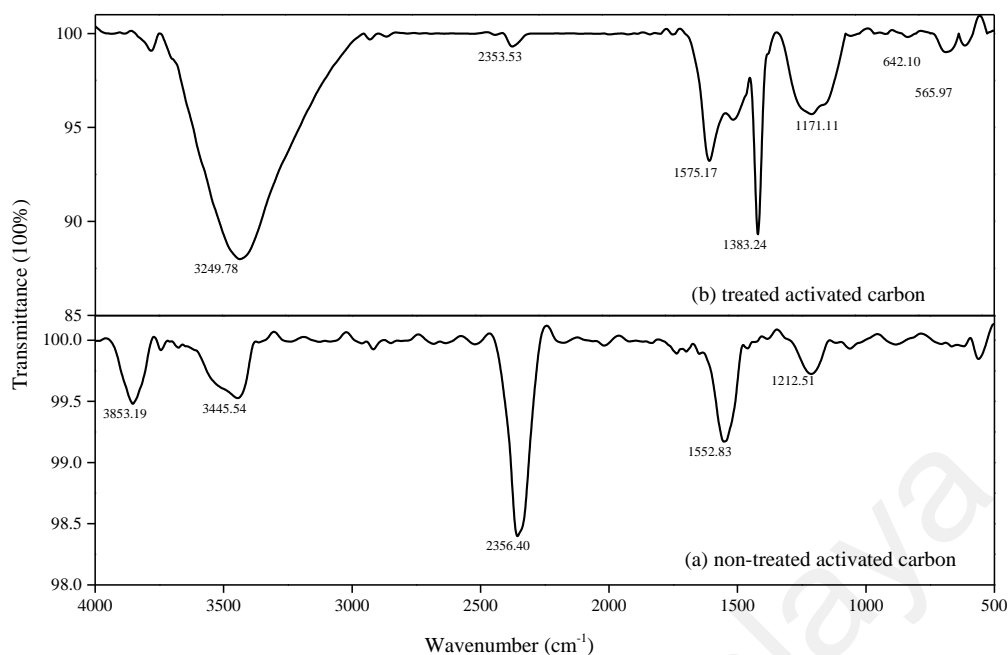


Figure 4.5: FTIR spectra of (a) non-treated activated carbon (AC) and (b) treated activated carbon

There is more functional group formed on the surface of AC1 as compared to AC due to pretreatment. The formation of new surface functional group exhibited at absorption bands at 1481.58, 1383.24, 1171.11, 642.10, 565.97 and 477.75 cm^{-1} as presented in Figure 4.5(b). The absorption peak at 1481.58 cm^{-1} is attributed carbonates-carboxyl group (J.L. Figueiredo et al., 1999). After pre-treatment, the lactone group is formed (referring to Surface acidity group Section 4.1.1). The peak 1383.24 cm^{-1} is assigned to the formation of lactone group (Shen et al., 2007). Other than lactone, the formation of carboxylic group is also formed on the surface of activated carbon after pretreatment supported by peak at 1171.11 cm^{-1} . (Shaarani & Hameed, 2011). The region 450-750 cm^{-1} showed two bands at 642.10 and 565.97 cm^{-1} which are associated with the in-plane and out-plane aromatic ring deformation vibrations (Al-Qodah & Shawabkah, 2009).

Table 4.3: IR assignments of functional group on Non-treated Activated carbon (AC) and Treated Activated carbon (AC1) (Al-Qodah & Shawabkiah, 2009; Barkauskas & Dervinyte, 2003)

Group or functionality	Assignment regions (cm ⁻¹)	Non-treated Activated carbon (AC) (cm ⁻¹)	Treated Activated carbon (AC1) (cm ⁻¹)
Carbonates; carboxyl-carbonates	1100-1500, 1590-1600	1552.83	1481.58
Alcohol/ O-H stretching	3500-3200	3445.54	3249.78
Lactones	1160-1370, 1675-1790	1212.51	1383.24
Carboxylic anhydrides	980-1300, 1740-1880	-	1171.11

The FTIR analysis was mainly used as a qualitative analysis as for the evaluation of the functional groups of carbon materials. It is not easy to get good FTIR spectra of activated carbon because carbons are black materials that absorbed almost all of radiation in the visible spectrum, and the peaks detected were usually the sum of the interactions of different types of group (Shen et al., 2007).

4.1.4 Nitrogen Physisorption

The textural studies of activated carbon were determined by nitrogen physisorption. AC showed high BET specific surface area of 1062.78 m².g⁻¹ (Table 4.4). The result corroborates well with the previously reported study (Gil, Muñoz, et al., 2011), the activated carbon has high surface area. The textural properties of activated carbon is complicated since it involves macropores, mesopores and micropores as well (Rashidi et al., 2012). Generally, the activated carbon structure consisting of aromatic sheets and strips, with variable slits of molecular dimensions and these being micropores (Teng et al., 2000). The micropores maybe considered, locally at least, as slit-shaped.

The BET specific surface area of AC1 is 917.87 m²/g (Table 4.4) which is lower compared to AC. This is due to partial blockage of micropores entrance, which led to the formation of oxygen-containing group during the HNO₃ pretreatment (Farooq et al., 2009; Li et al., 2005).

The N₂ sorption isotherm of activated carbon can be observed as a combination of Type I and Type IV isotherms according to IUPAC (Figure 4.7 and Figure 4.8). The high adsorption volume at low partial pressure ($P/P_0 \leq 0.1$) is consistent with Type I isotherms, expressive of a microporous structure (Gil, Muñoz, et al., 2011; Lu et al., 2005). The hysteresis loop due to the capillary condensation at higher partial pressures matches with Type IV isotherm and is associated with mesoporosity for carbon materials (Tessonier et al., 2009).

The average pore diameter of AC is 5.36 nm. Meanwhile, after pretreatment the average pore diameter of activated carbon decreased to 3.59 nm. Considering that, types of pores that was developed during the pretreatment mainly are micropores as described in Figure 4.6 (Y. Zhang et al., 2003). It was found that the pore distribution changed from mesopore to micropore after the HNO₃ pretreatment as shown in Table 4.4, the mesopore area value is decreasing after acid pretreatment. Moreover, the pore size of the carbonaceous materials depended on how much the content of volatile matter and ash since the volatile matter remains clogging in the carbon pores (Aji et al., 2015). The volatile matter value increased after acid pretreatment due to the decomposition of the organic materials (Aji et al., 2015).

Table 4.4: N₂ physisorption of nontreated activated carbon (AC) and treated activated carbon (AC1)

	AC	AC1
BET surface area (m².g⁻¹)	1062.78	917.87
Micropore area (m².g⁻¹)	822.08	710.38
Mesopore area (m².g⁻¹)	240.7	207.49
Total pore volume (cm³.g⁻¹)	0.49	0.46
Micropore volume (cm³.g⁻¹)	0.33	0.33
Mesopore volume (cm³.g⁻¹)	0.16	0.13
Mean pore diameter (nm)	5.36	3.59

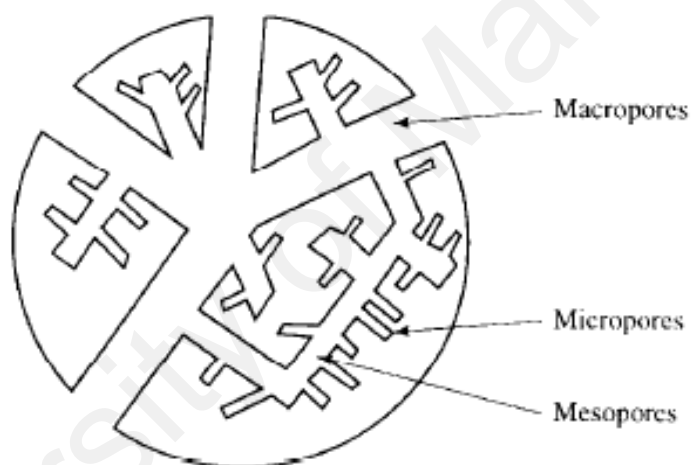


Figure 4.6: The schematic representation of an activated carbon granule (Rodrigues-Reinoso, 1998)

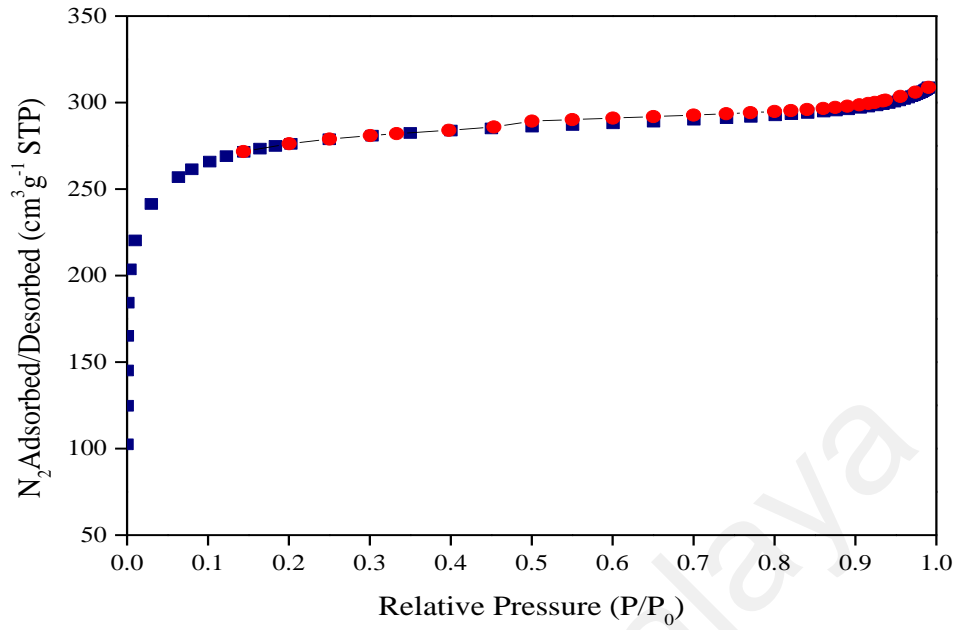


Figure 4.7: N₂ adsorption/desorption of non-treated activated carbon (AC); ● desorption ■ adsorption

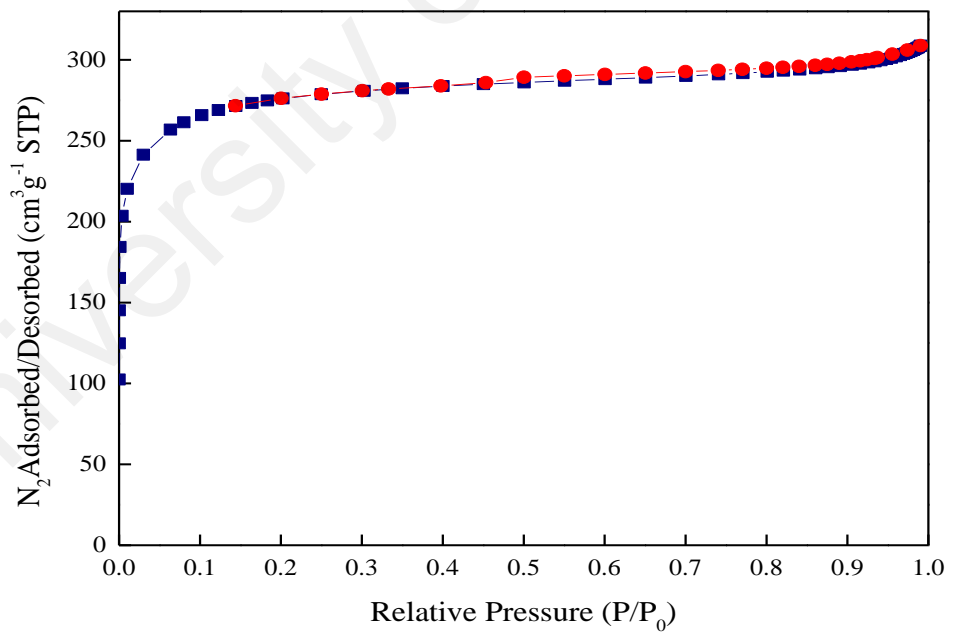


Figure 4.8: N₂ adsorption/desorption of treated activated carbon (AC1); ● desorption ■ adsorption

4.2 Catalyst support (Hydrotalcite)

4.2.1 Thermal-Gravimetric Analysis (TGA-MS)

Generally, TGA of hydrotalcite exhibit three main regions due to loss of molecular water, dehydroxylation, loss of CO₂ and loss of organic material at four different temperature ranges (see Figure 4.9) (Cavani et al., 1991; Xie et al., 2006). General chemical structure of the hydrotalcite is Mg₆Al₂CO₃(OH)_{16.4}(H₂O) (Cavani et al., 1991). The mass spectrometry will allow to identify and calculate the compounds in the off-gas in real time with mass loss.

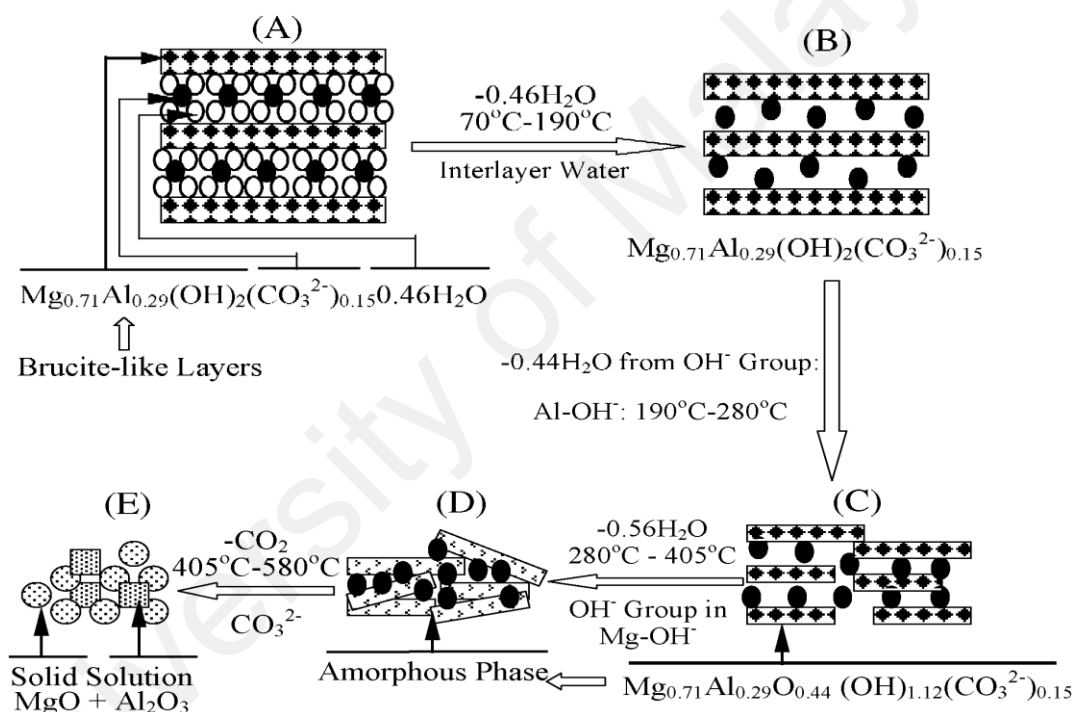


Figure 4.9 : The thermal evaluation of Mg-Al-CO₃ LDH as a function of temperature (Yang et al., 2002)

The TGA analysis of synthesized hydrotalcite with Al/(Mg+Al) = 0.20 (Figure 4.10), and (Table 4.5) showed that synthesized hydrotalcite exhibit losses in three consecutive endothermic stages; the first weight loss, about 6.01 wt% in the temperature range of 303 K to 383 K is described mostly due to removal of molecular water from the interlayer,

together with the relatively smaller amounts of CO₂ is confirmed with MS result (Figure 4.13) (Reyero et al., 2013). At 364 K, both interlayer water and smaller amounts of CO₂ are removed. Further, at 395 K only small amount of CO₂ is removed.

The second weight loss region of 6.10 wt% (Figure 4.10) is in the temperature range of 383 K to 475 K. There is one small DTA-peak which corresponds to the evaluation of CO₂ from interlayer carbonate and loss of OH⁻ groups in the brucite layers. The mass spectrometric (Figure 4.11) indicate the evaluation of CO₂ and H₂O in this region. This supported that dehydroxylation happens leading to the removal OH⁻ from hydrotalcite structure.

The third weight loss region 15.54 wt% (see Figure 4.10) is in the temperature range of 475 K to 694 K. There are two DTA peak which corresponds to the evaluation of CO₂ from interlayer carbonate which indicates that OH⁻ and CO₃²⁻ are exchange in this range (Yang et al., 2002). In this temperature range, there are also two characteristics endothermic peaks from DTA, one centered at ~564 K and the other at ~618 K. The mass spectrometric showed peaks at CO₂ and H₂O were detected. Theoretically, the H₂O formed from the two molecules of OH⁻ groups of Al-(OH)-Mg OH⁻ groups. Assuming that hydroxyl group from Al³⁺ and Mg²⁺ (Yang et al., 2002). The total weight loss from 618 K to 673 K is 4.33%, which can be attributed to the removal CO₂ from CO₃²⁻ in the Mg-Al-CO₃ LDH, because almost no water was detected in this temperature range by in situ MS. The total weight loss observed for HT 0.20 is about 31.97 % (Reyero et al., 2013).

Thermally treating hydrotalcites induces dehydration, dehydroxylation and loss of compensation anions will be forming the Mg-Al mixed oxides with basic properties as shown in Figure 4.12 (Cavani et al., 1991).

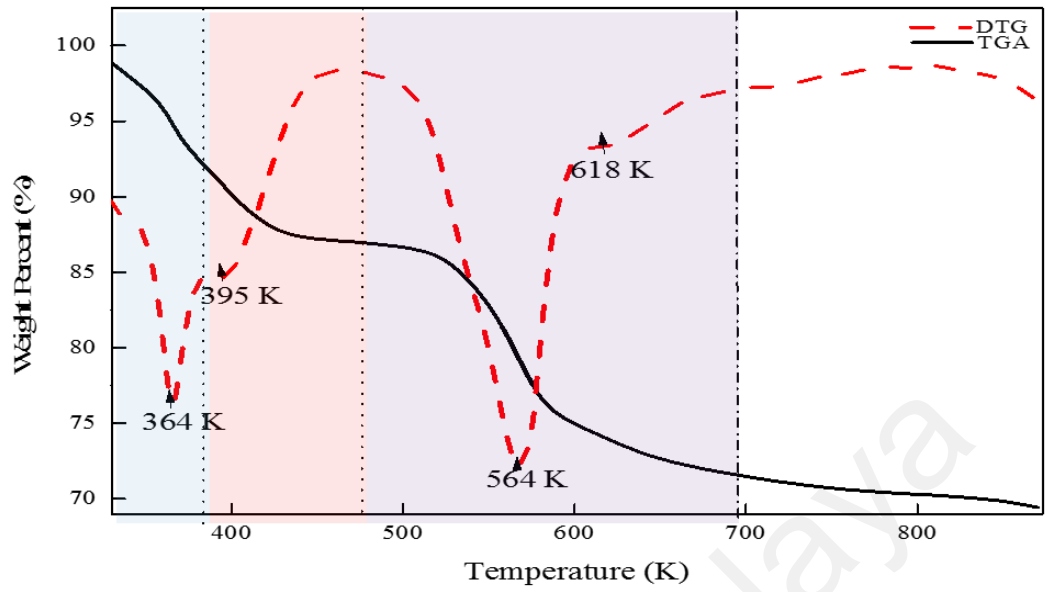


Figure 4.10: TGA analysis of hydrotalcite with Al/(Al+Mg)=0.20

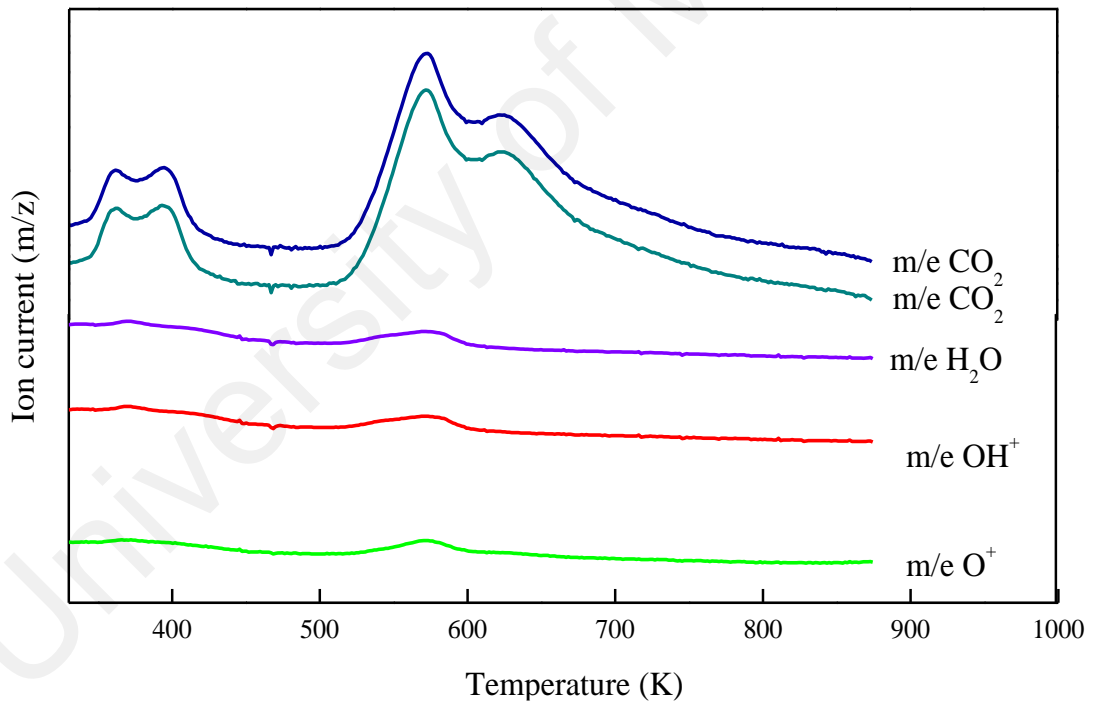


Figure 4.11: Mass Spectrometric of hydrotalcite with 0.20 ratio

Table 4.5: TGA analysis of hydrotalcite with Al(Mg+Al)=0.20 ratio

Temperature (K)	Weight Loss (%)	Remarks
303-383	6.01	1)removal of water (dehydration) $\text{H}_2\text{O}_{(\text{HT})} \rightarrow \text{H}_2\text{O}_{(\text{g})}$ 2)small amount of decarbonisation
383-475	6.10	1)removal of water from OH^- in the hydrotalcite structure 2) decarbonisation
475-694	15.54	1)dehydroxylation from $\text{Al}(\text{OH})\text{-Mg}(\text{OH})^-$ $2\text{OH}^- \rightarrow \text{H}_2\text{O}$ 2) decarbonisation $\text{CO}_3^{2-} \rightarrow \text{CO}_2 + \text{O}^{2-}$

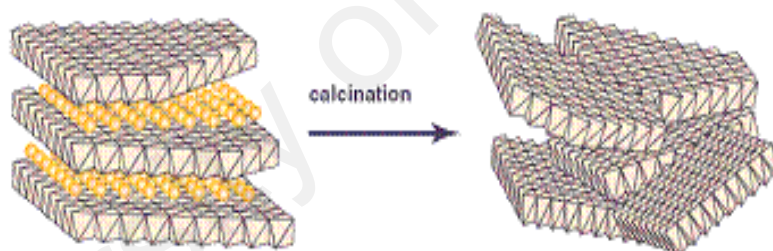


Figure 4.12 : Deconstruction of the hydrotalcite structure after calcination (HTc) (Li, 1977)

4.2.2 Temperature Program Desorption CO_2 (TPD- CO_2)

Hydrotalcites are basic clays with a structure consisting of positively-charged brucite-like (Magnesium Hydroxide) layers and interlayer containing charged compensation anion and water molecules (Hutson & Attwood, 2008). After thermally heating, the Mg-Al-mixed oxides with basic properties, large surface area, and poorly crystallized Mg-O type structure. These properties are potentially useful as adsorbents and as heterogeneous base catalyst and catalytic support (Pérez et al., 2009).

The basic properties of the hydrotalcites were studied by TPD using CO₂. The thermogram corresponding to CO₂ desorption of calcined hydrotalcite (HTc) is shown in Figure 4.13. The complex desorption profile is clearly related to the presence of basic sites with different basic strength.

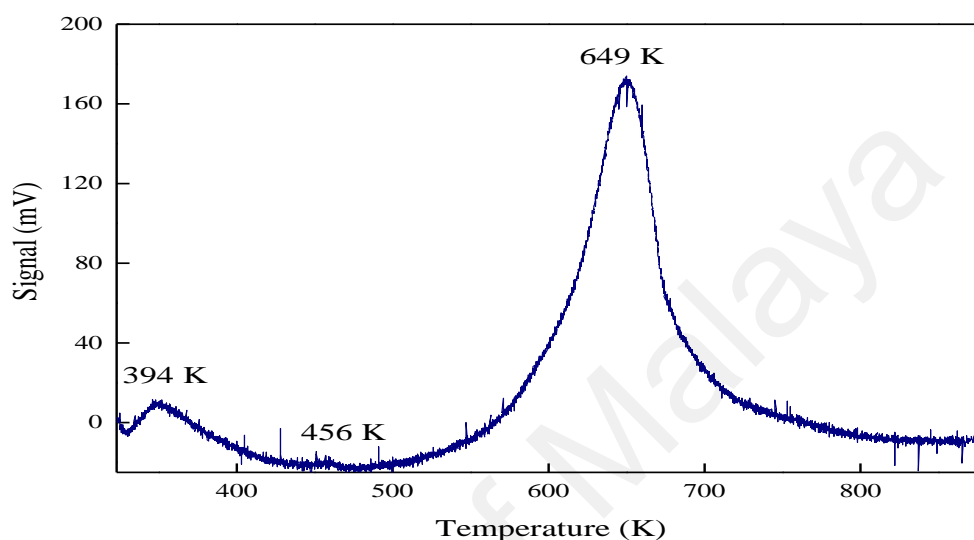


Figure 4.13: Temperature-programmed desorption of CO₂ profiles of HTc

Generally, the TPD-CO₂ of hydrotalcites were deconvoluted into three desorption peaks range. Firstly, low-temperature peak, with a maximum of desorption at range temperature 390-411 K which is attributed to weak basic strength. Secondly, medium-temperature peak, with a maximum of desorption at range temperature 443-463 K corresponds to medium basic strength. Last range peak which contributed to the strong basic strength is in the range of 533-553 K (Bastiani et al., 2004; Pérez et al., 2009).

TPD-CO₂ of HTc has three peaks (see Figure 4.13). The first peak is at 394 K with CO₂ desorbed value of 40 $\mu\text{mol.g}^{-1}$, imply to the range of low-temperature peak and attributed to the weak basic strength of hydrotalcite site. It has been proposed that the weak basic sites in calcined hydrotalcite regarding to the surface OH⁻ groups. At this

temperature range, the type of adsorbed CO₂ species is bicarbonate. Bicarbonate formed when the proton from the OH⁻ transfer to the carbonate ion (Palmer et al., 2009). Other than that, the bicarbonate species disappeared above 373 K (Di Cosimo et al., 1998).

There is a small peak observed from TPD-CO₂ profiles (see Figure 4.13) for medium basic strength at 456 K. The types of CO₂ adsorbed species is a bidentate bicarbonate, related to the oxygen in both Mg²⁺-O²⁻ and Al³⁺-O²⁻ pairs. The presence of these sites is favored in Mg/Al mixed oxides due to the higher electronegativity of Al³⁺ compared to Mg²⁺.

The major peak in TPD-CO₂ profiles of HTc belongs to the strong basic strength sites. The peak was detected at 649 K with 882.91 μmol/g of CO₂ desorbed value. This type of CO₂ adsorbed species is a unidentate bicarbonate, which forms strongly on basic surface O²⁻ and remained adsorbed even after evacuation at 673 K (Di Cosimo et al., 1998)

4.2.3 X-Ray Powder Diffraction (XRD)

Crystallinity and the phase purity of hydrotalcite were determine by X-ray diffraction technique. In polycrystalline materials each reflection was observed at a given 2Θ in a powder X-ray diffraction pattern. Measured at wavelength λ, it is related to lattice planes with a distance d and an orientation by the Millers indices hkl as described by Bragg's law (Jauncey, 1924):

$$n\lambda = 2d_{(hkl)} \sin \Theta \quad \text{(Equation 4.1)}$$

XRD is not only the current method in structural investigations of hydrotalcite, but it is also widely used for the identification, quantitative determination and characterization of hydrotalcite phases. Since a typical XRD pattern is obtained for each crystalline phase, the pattern may be regarded as a “fingerprint” of the respective material (Jauncey, 1924).

The ex-situ XRD measurements revealed that the preparation of the Mg-Al hydrotalcite was successful and the samples with high crystallinity were obtained. Powder XRD diffraction pattern for hydrotalcite samples dried at 333 K was presented in Figure 4.14. The pattern showed sharp and symmetrical reflections for (003) at 11.23° with 100% intensity, (006) at 22.77° , (015) at 38.87° and (0012) at 48.17° planes (Chmielarz et al., 2013). All these peaks are characteristics of well crystalline single phase PDF File no. 89-0460. The average crystallite size of HT was calculated and tabulated in Table 4.6. This is done by using the Scherrer equation, which utilizes the XRD data.

The basal spacing is 7.86 \AA , meaning that hydrotalcite is well synthesized (Kanezaki, 1998). The basal spacing is approximately equal to the sum of the thickness of one layer of Mg-Al-CO₃ LDH ($4:8 \text{ \AA}$) and the interlayer distance of Mg-Al-CO₃ LDH ($\sim 3:0 \text{ \AA}$) as reported (Kanezaki, 1998). The structure of hydrotalcite is presented in Figure 4.15 (Zhao et al., 2012).

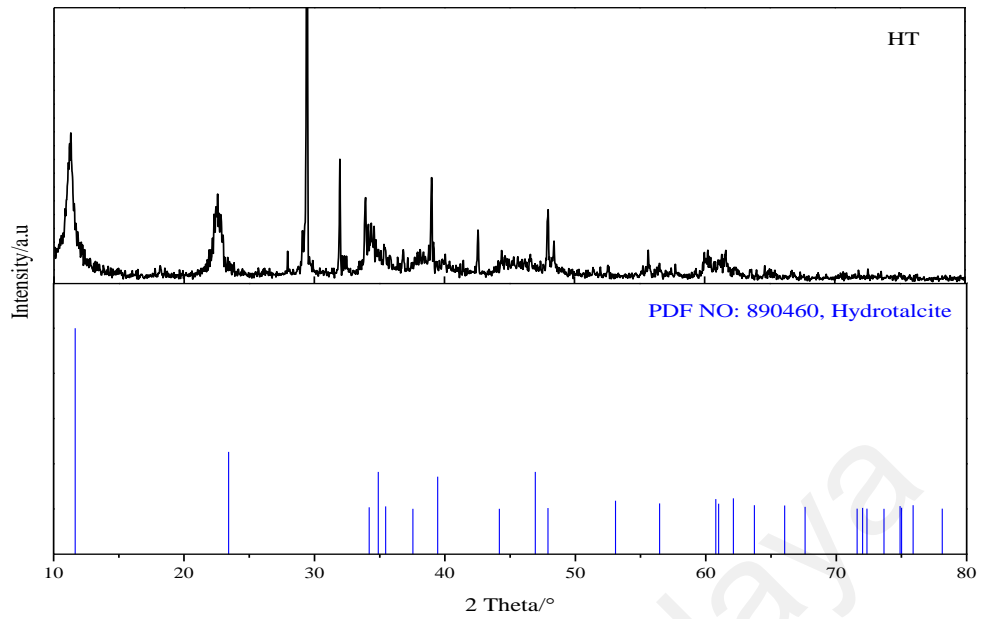


Figure 4.14: XRD pattern of HT 0.20 with pattern list (PDF NO: 890460)

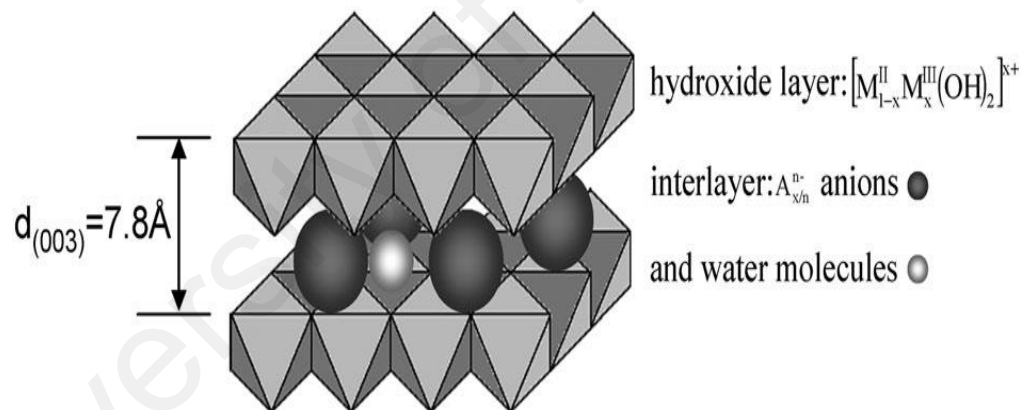


Figure 4.15: Structure of Hydrotalcite

XRD pattern of calcined hydrotalcite (HTc) was presented in Figure 4.16. Calcination of the hydrotalcite results in the destruction of the hydrotalcite-like structure and the peak at 11.23° (003) plane disappeared. This means that the layered structure of hydrotalcite had collapsed, consistent with the observation from TGA analysis (Figure 4.12). This behavior could be attributed to the dehydroxylation of the brucite-like layers and the

removal of the interlayer anions (CO_3^{2-}) as observed during the thermogravimetric measurement. It was confirmed that after 673 K, the OH^- and CO_3^{2-} are leaving the compound from MS spectra (Figure 4.12). The formation peaks at 28° and 45° in (Figure 4.16) can be assigned to aluminum oxide hydroxide (PDF No. 01-1305). Aluminum oxides hydroxide and magnesium oxide were formed too. The MgO peaks (at about 43° and 63°) have higher peak 2 values. This is caused by the incorporation of smaller Al^{3+} cations in the bulk lattice which respect to PDF No 77-2179 (Cavani et al., 1991; Reyero et al., 2013; Tongsakul, Duangta et al., 2012; Xie et al., 2006). Some researchers have reported that the calcined hydrotalcite (mixed oxides) is able to transform to the hydrotalcite by reacting with carbonate containing water. This process is called reconstruction as described in Figure 4.17 (Kuśtrowski et al., 2006; Mokhtar et al., 2010; Yang et al., 2002).

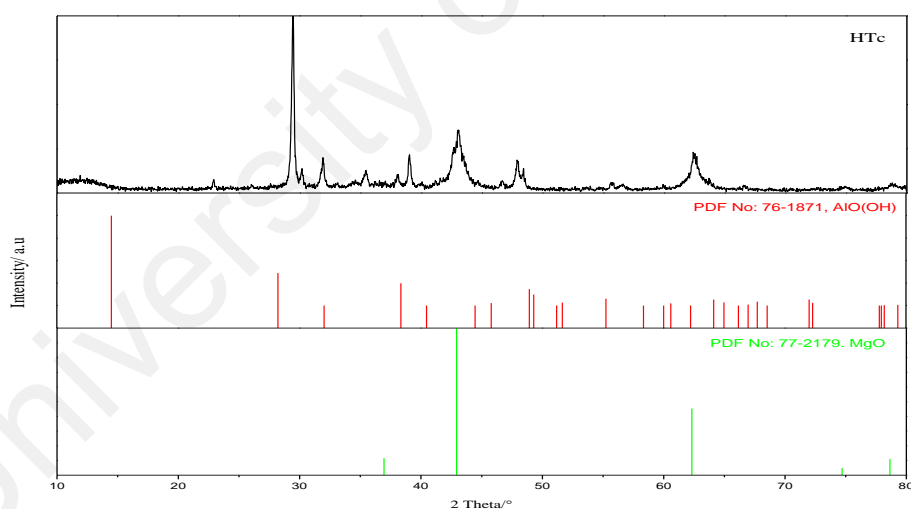


Figure 4.16: XRD pattern of HTc and pattern peak list for MgO (PDF No: 77-2179) and AlO(OH) (PDF No: 76-1871)

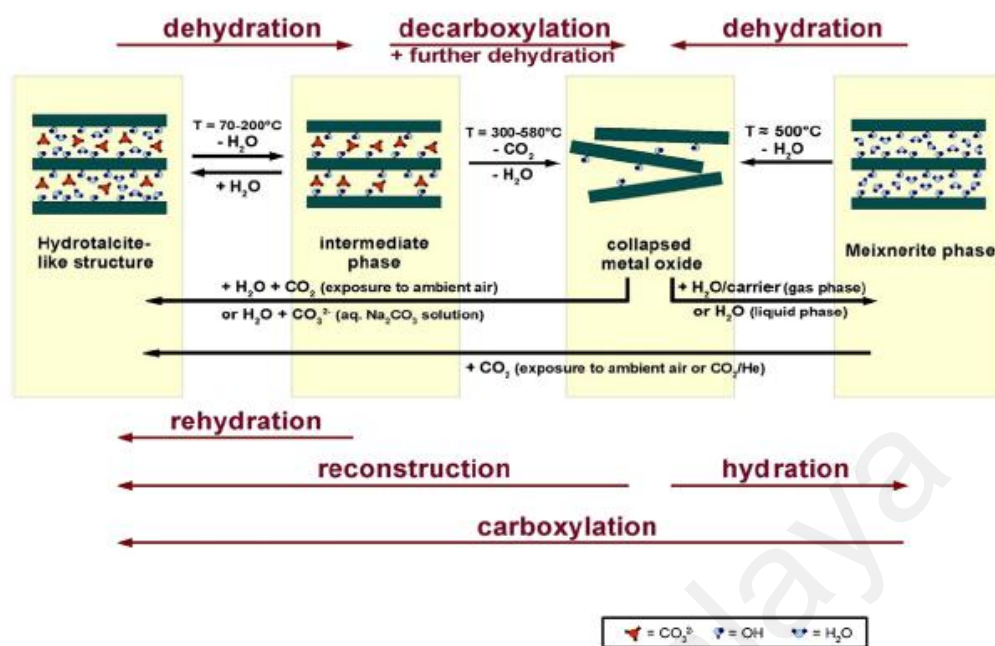


Figure 4.17: Schematic overview of structural and compositional transformation processes during thermal or chemical reaction of Mg-Al hydrotalcite like materials and Mg-Al mixed oxides (Kuśtrowski et al., 2006; Mokhtar et al., 2010)

Table 4.6: X-Ray diffraction results of HT 0.20 and HTc 0.20

Entry	$2\Theta(^{\circ})$	Intensity sample/%	h k l	Compound name	Crystallite size(nm)
HT 0.20	11.23	100	0 0 3	Hydrotalcite	10.40
	22.77	53.22	0 0 6		
	38.87	14.27	0 1 5		
	48.17	17.64	0 0 1 2		
HTc 0.20	29.44	100	1 2 0	Aluminium Oxide Hydroxide	12.10
	48.32	3.67	1 3 1		
	43.07	25.34	2 0 0	Magnesium Oxide	19.7
	62.43	14.02	2 2 0		

4.2.4 Fourier Transform Infrared Spectroscopy

FTIR analysis was used to identify the types of functional groups in hydrotalcites compounds (Kloprogge et al., 2001). Besides, the information about the types of the bond formed by functional group and about their orientations can also be obtained. The FTIR of hydrotalcite and calcined hydrotalcite were presented in Figure 4.18

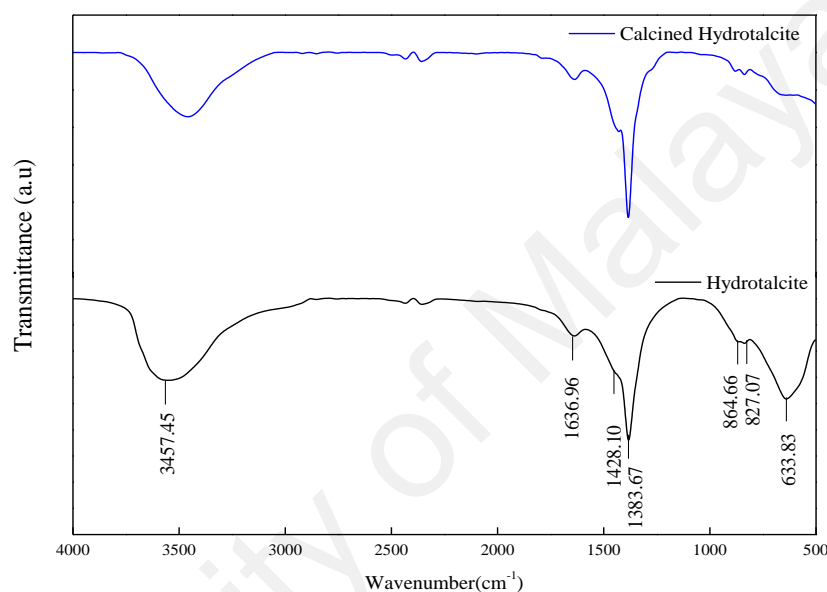


Figure 4.18: FTIR spectra of hydrotalcite and calcined hydrotalcite

Generally, there are three types of IR-active vibrations that distinguished hydrotalcite components: molecular vibrations of the hydroxyl groups, lattice vibrations of the octahedral layers and vibrations of interlayer species. The FTIR spectra of hydrotalcite and calcined hydrotalcite are as presented in Figure 4.18. The result shows a very broad band at 3457.45 cm⁻¹ corresponding to the stretching vibration of hydroxyl group in the brucite-like sheets and water content in samples. The absorption peak at 1636.96 cm⁻¹ is attributed to bending vibration of water molecules in the interlayer space (Cavani et al., 1991; Kovanda et al., 2005).

The presence of foreign anions in the interlayer space of hydrotalcites can be identified by absorption bands observed below 1500 cm^{-1} (Yang et al., 2002). The absorption peak at 1383.67 cm^{-1} with shoulder peak at 1428.10 cm^{-1} is described as presence of carbonates, which means at this area it is attributed to the vibration of CO_3^{2-} . Peaks at 864.66 cm^{-1} and 827.07 cm^{-1} are respectively to the stretching modes of carbonates ion. The absorption peak was observed at 633.83 cm^{-1} can be assigned to the stretch hydroxyl mode of Mg-OH.

After calcination at 673 K , the samples exhibits significant peaks relatively to the hydrotalcite sample. The intensity at 3457.45 cm^{-1} and 1383.67 cm^{-1} decreased due to the collapse of hydrotalcite structure after calcination (Yang et al., 2002).

4.3 Pd-based supported catalyst

The palladium based supported catalysts were prepared by immobilization method using PVA as a surfactant. The metal loading was fixed at 1wt%. Three types of catalyst were synthesized. They are 1wt% Pd/AC1, 1wt% Pd/HTc and 1wt% Pd/HTc-AC1.

4.3.1 Thermal-Gravimetric Analysis (TGA)

The properties of the catalyst affect to the catalyst activity and selectivity of the product. Impurities from the metal salt and ligands groups from preparation method are the example of the impurities that affect the catalytic activity of the heterogeneous catalyst. For example, in immobilization method, the stabilizer (PVA, PVP and THPC) used in the preparation method to encapsulate the active metal and prevent it from agglomerate before adding to the catalyst support (Goel & Rani, 2012). Unfortunately, the stabilizer needs to be removed before the catalytic testing. The stabilizer can form a protective layer, which in many cases limits the accessibility of the active site for the reactants in both liquid and gas phase reaction (Villa, Alberto et al., 2009; Zhao et al., 2013). The thermal stability of palladium based supported catalysts with different catalyst

support were determined through TGA as shown in Figure 4.19. Generally, all the catalysts exhibited three main regions peak over the temperature ranges.

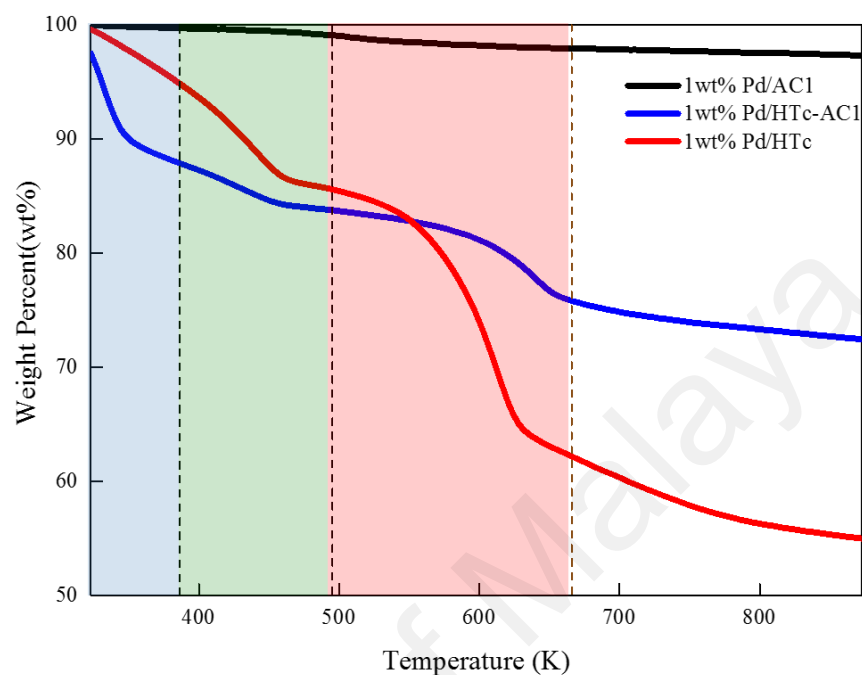


Figure 4.19: TGA curves of 1wt% Pd/AC1, 1wt% Pd/HTc and 1wt% Pd/HTc-AC1 catalysts

Table 4.7: Summary of TGA-DTA results

Sample	Temperature (K)	Weight Loss (%)	Related gas product according to MS
1wt% Pd/AC1	303-373	0.5	H ₂ O
	373-673	1.7	H ₂ O, CO ₂
	673-973	1.8	acetone, alcohol
1wt% Pd/HTc	303-485	15	H ₂ O
	485-640	23	H ₂ O, CO ₂
	640-783	7	CO ₂
1wt% Pd/HTc-AC1	303-400	13	H ₂ O
	400-550	4	CO ₂ , alcohol
	550-750	10.43	Alcohol

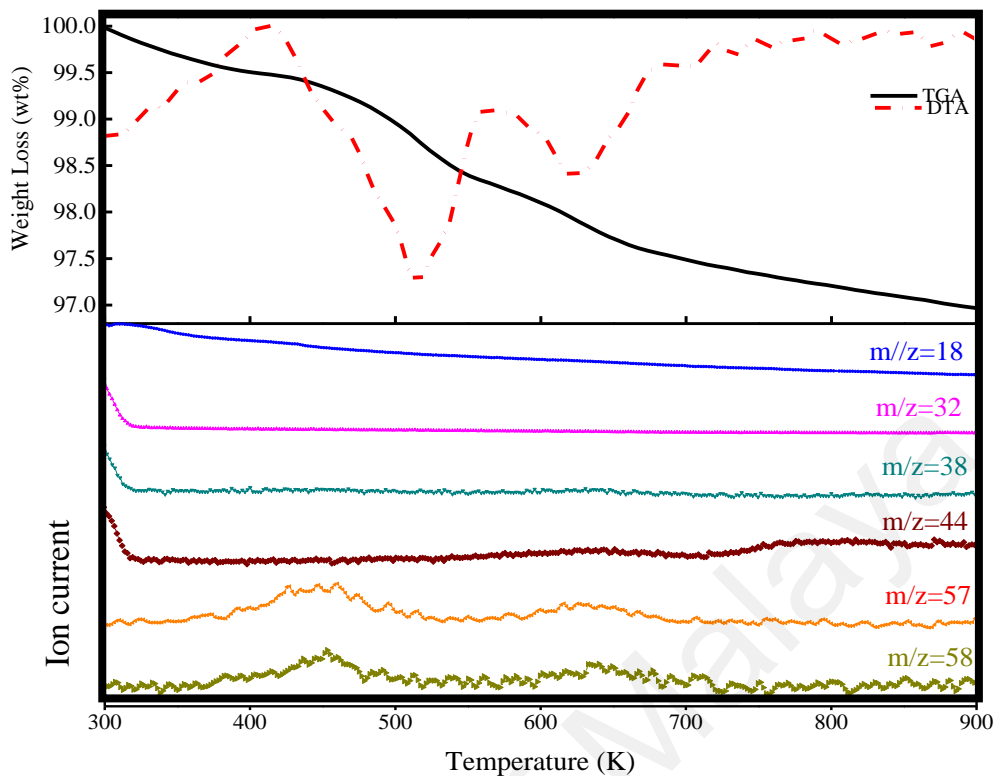


Figure 4.20: TGA-DTA combine with MS curve of 1wt% Pd/AC1

Figure 4.20 showed TGA-DTA combine with mass spectrometric results of the 1wt% Pd/AC1. Table 4.7 summarizes the results in terms of peak position and weight loss. First weight loss is exhibited below 373 K, due to the removal of H₂O from samples confirmed with MS at m/z=18 describe formation H₂O (Cavani et al., 1991). O₂ is also detected at m/z=32 and formation of HCl that is confirmed from MS results at m/z=34. The HCl formation was due to the usage of HCl in catalyst preparation (Zhao et al., 2013). Second region of weight loss in the range of 373-673 K was due to the breakage of the crystalline water bond from catalyst surface and also decomposition of surface oxygen-containing functional groups from carbon supports e.g carboxylic acid and lactone (agreed with surface acidity determination above at section 4.1.1). At 973 K, Pd/Ac loss about 4.9% and the weight loss is continuous due to carbon burning (Sariođlan, 2013). From this curve, the calcination temperature is determined at 673 K.

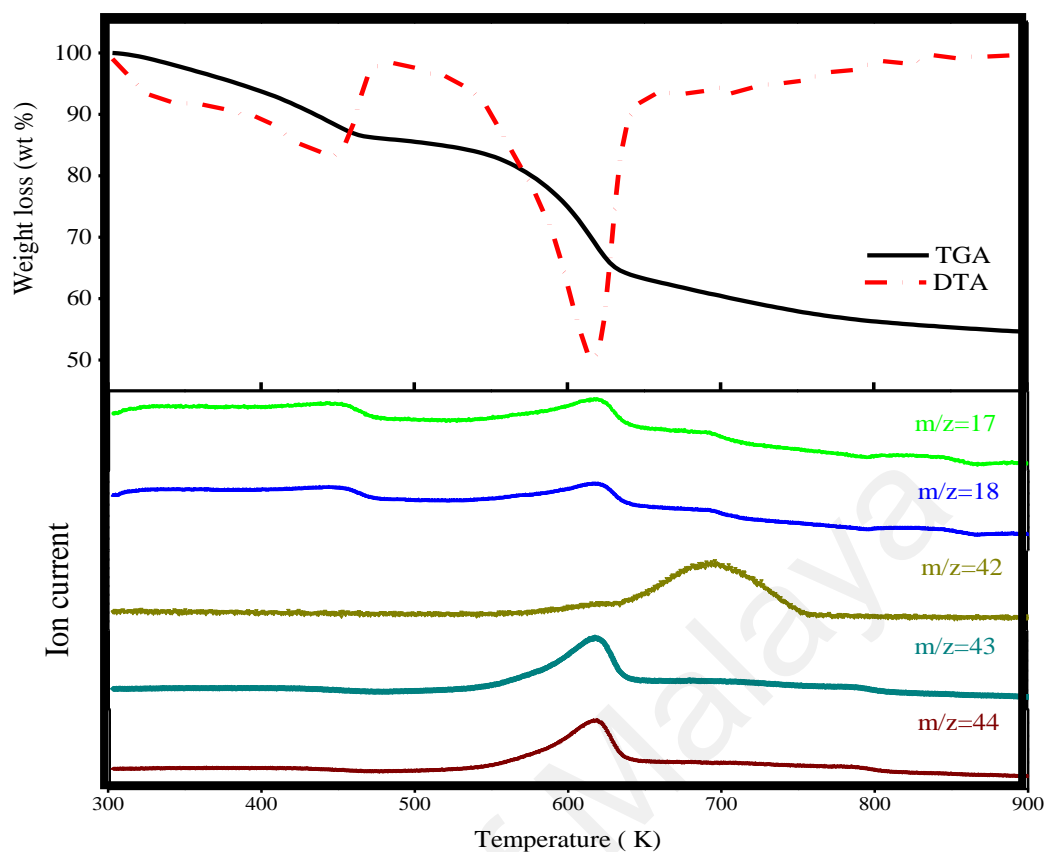


Figure 4.21: TGA-DTA combine with MS curve of 1wt% Pd/HTc

Figure 4.21 showed TGA-DTA combine with MS spectra of 1wt% Pd/HTc. The first weight loss is below 485 K which is explained about removal of H₂O from sample. From MS spectra, there are two types of ion current that were detected, m/z=17 and m/z=18 attributed to the H₂O. There are two types of water that were removed in this region. First type of H₂O is moisture which is probably occurred from preparation method (below 373 K). The second type of water is a crystalline water from hydrotalcite supports (Yang et al., 2002). The second region was due to the hydrotalcite composition. From 485 K to 640 K due to the dehydroxylation of hydrotalcite. Last but not least, the third one corresponds to the evaluation of CO₂ from interlayer carbonate in the brucite layers (Corma et al., 2005; Kovanda et al., 2005). 1wt% Pd/HTc lost about 45 wt% and calcined temperature for this catalyst was picked at 783 K.

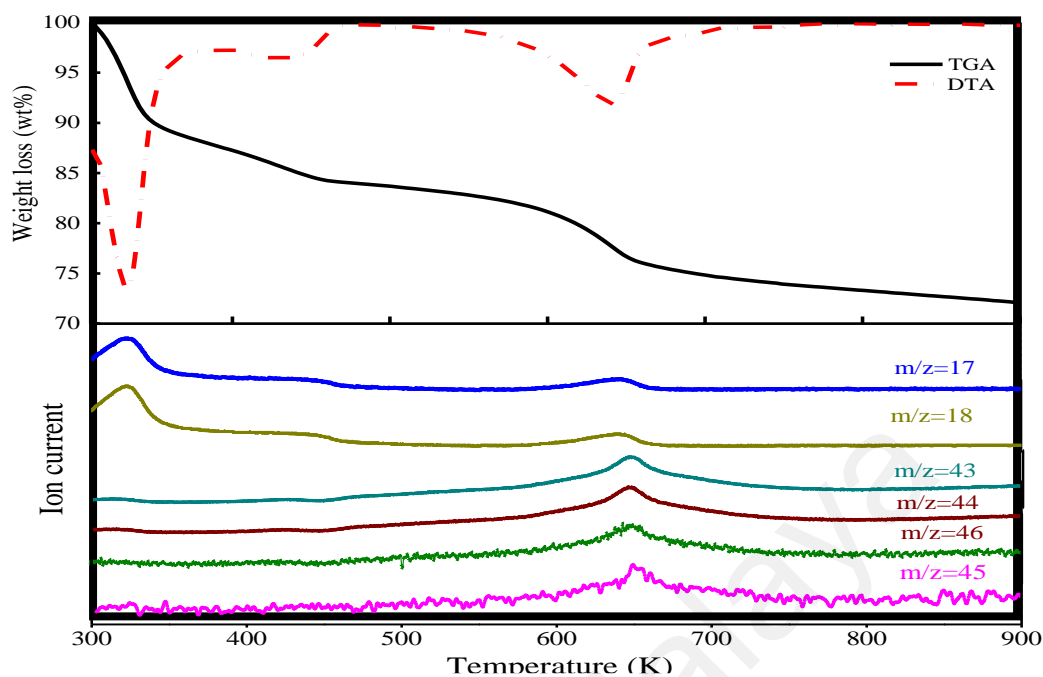


Figure 4.22: TGA-DTA combine with MS curve of 1wt% Pd/HTc-AC1

Figure 4.22 is a TGA-DTA combine with MS profiles of 1wt% Pd/HTc-AC1. The first weight loss is at temperature below 400 K, which belongs to the removal water from the sample. Second region of weight loss was attributed to the removal of crystalline water in hydrotalcite sample between 450 K to 550 K. The third region of weight loss of this sample starts at 550 K to 750 K, due to the decarbonation from hydrotalcite support. CO₂ can also be attributed to the formation of carboxyl acids as decomposition product from acetyl group in PVA (Yang, H. et al., 2012). Total weight loss of 1wt% Pd/HTc-AC1 is 27.43wt%. Other types of volatiles compound can also be identified such as chloride from preparation method from the mass spectrometry. The sample was calcined at 673 K.

4.3.2 Nitrogen Physisorption (BET)

The textural studies of palladium based supported catalysts with varying types of catalyst supports were presented in Table 4.8. There are significant differences in the pore volume and average pore diameter compared to catalyst support which indicates that introduction of the different types of support does influence the catalyst structure.

In section 4.1.4, AC1 showed high BET specific surface area of $917.9 \text{ m}^2 \cdot \text{g}^{-1}$. Different from AC1, HTc support showed relatively low BET specific surface area ($162.2 \text{ m}^2 \cdot \text{g}^{-1}$), as compared to AC1 corresponds to the different type of material and porosity. After addition of palladium to the AC1, due to the relatively low metal loadings used (1wt %), the specific surface area for 1wt% Pd/AC1 does not show significant differences from the supporting materials. The specific area for 1wt% Pd/HTc is $125.6 \text{ m}^2 \cdot \text{g}^{-1}$ which is the specific area of this catalyst shows that the amount of palladium loading did not affect the surface area but did affect in pore diameter and pore volume. However, the surface area value of 1 wt% Pd/HTc-AC1 ($632.2 \text{ m}^2 \cdot \text{g}^{-1}$) decreased after incorporation of palladium into mixture of HTc and AC1 supports as compared to 1wt% Pd/AC1. The changes of pore volume and average pore diameter indicates that palladium is incorporated into the HTc and/or AC1 framework. However, there is no regular rule and clear explanation since the bond length and angle may change during the synthesis process. Such results have been reported previously.

The N_2 -sorption isotherms of all the catalysts are shown in Figure 4.23, Figure 4.24 and Figure 4.25. Respectively, after adding the metal, the shape of N_2 isotherms remains almost the same as those of supports, and the BET value decreased slightly as compared to the supports (Table 4.8). 1wt% Pd/AC1 and 1wt% Pd/HTc/AC1 have showed the presence of mesoporous structure. The type of isotherm is a combination of type I and IV with hysteresis loop type 3 as reported in Figure 4.23 for 1wt% Pd/AC1 and in Figure

4.26 for 1wt% Pd/HTc-AC1. Differently, from 1wt% Pd/AC1 and 1wt% Pd/HTc-AC1, 1wt% Pd/HTc isotherm graph (Figure 4.24) is a Type IV with H3 type of hysteresis loop with vertical desorption branch at ($P/P_0 \leq 0.5$) with low average pore diameter 7.85 nm compared to the HTc support only. This result can be attributed to a partial blockage of the porous structure of materials upon deposition of the metallic phase (Alegre et al., 2015).

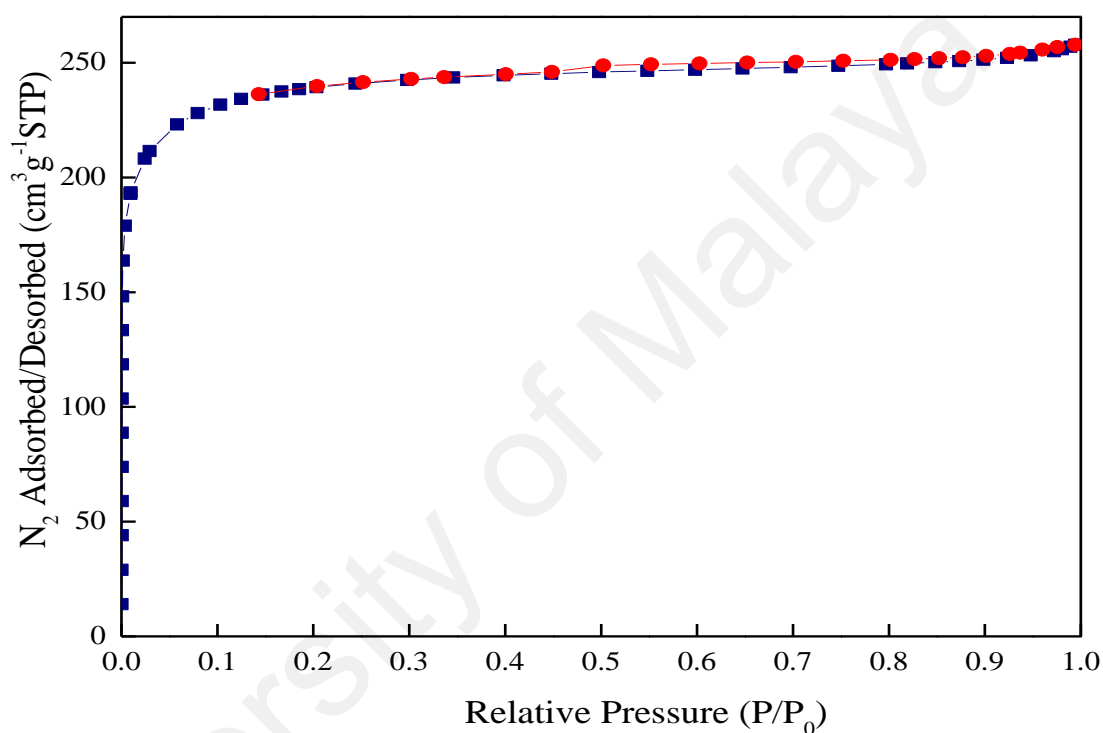


Figure 4.23: N_2 adsorption/desorption isotherms of 1wt% Pd/AC1 ; ● desorption ■ adsorption

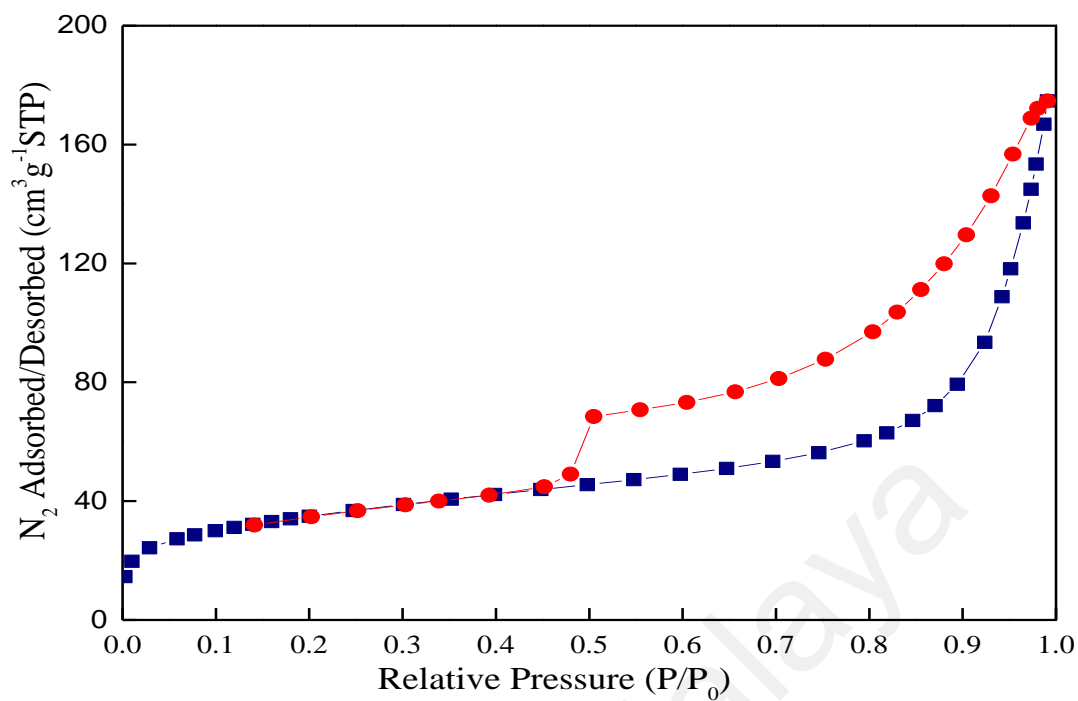


Figure 4.24: N₂ adsorption/desorption isotherms of 1wt% Pd/HTc ; ● desorption ■ adsorption

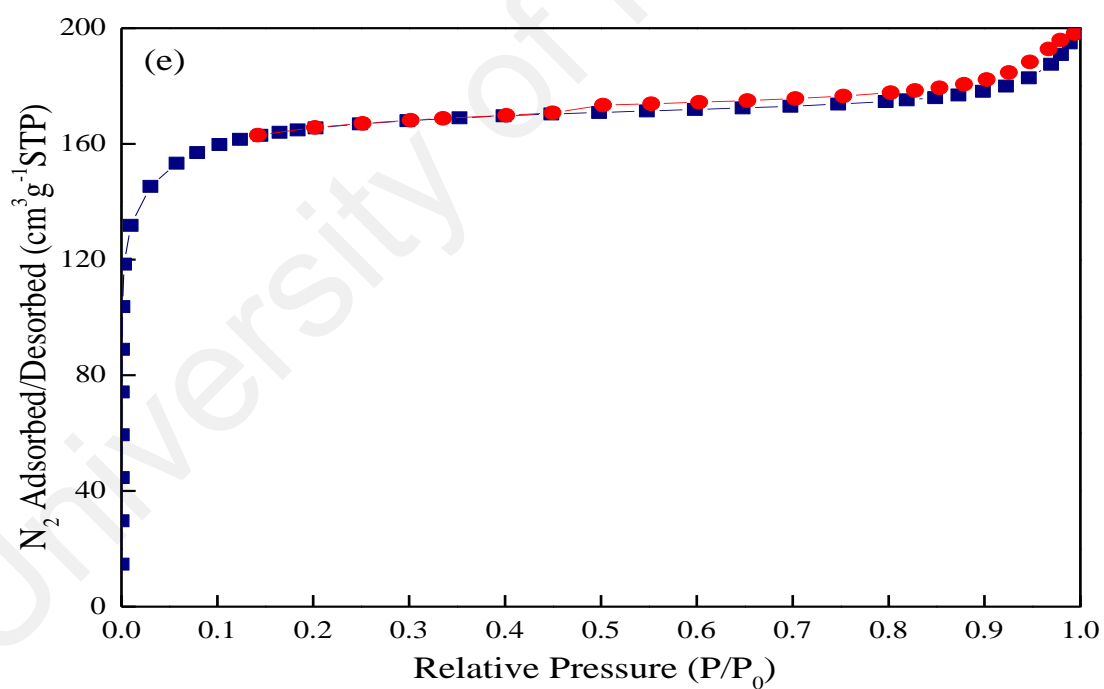


Figure 4.25: N₂ adsorption/desorption isotherms of 1wt% Pd/HTc-AC1; ● desorption ■ adsorption

Table 4.8: Nitrogen Physisorption results of palladium based supported catalysts and catalyst support

Catalyst	S_{BET} ($m^2 \cdot g^{-1}$)	Pore Volume ($cm^3 g^{-1}$)	Average pore diameter (nm)
AC1	917.90	0.47	3.59
HTc	162.20	0.03	17.38
1wt% Pd/AC1	917.10	0.03	4.45
1wt% Pd/HTc	125.60	0.28	7.85
1wt% Pd/HTc-AC1	632.20	0.05	8.11

4.3.3 X-Ray Powder Diffraction (XRD)

X-ray diffraction patterns of supports and palladium catalyst are shown in Figure 4.27. The activated carbon (AC1) pattern has a broad pure carbon peak at 26.31° and carbon oxide peak at 42.03° . This is due to the pre-treatment of nitric acid on the carbon surface. Calcined hydrotalcite (HTc) have many reflections as shown in Figure 4.26, and clearly evidenced that the structure of hydrotalcite collapsed during calcinations (773 K) (PDF 70-2152). Calcined hydrotalcite (HTc) contained Al_2O_3 peaks at 29.56° , 31.84° , 48.51° , as resulted from the calcination of the hydrotalcite (PDF 88-0107) (Tsuji et al., 2011).

For palladium catalyst, the presence of the crystalline phase corresponding to metallic palladium is confirmed at the 40.03° (PDF 88-2335) with particle shape is cubic. The pattern showed non detectable diffraction peaks correspond to crystalline PdO with Pd loading less than 2.0 wt%, which clearly indicated that the palladium oxide particles are highly dispersed (nanocrystal) or it is amorphous. However, it cannot be ruled out that the PdO crystallites might be presence as small crystallites, which is unable to be detected

by powder XRD. From the above data, it can clearly say that the palladium oxide crystallites are very fine at lower loadings and increases with the increase of palladium content (Naresh et al., 2014).

Other than that, the crystallite size of palladium metal based supported catalyst were calculated by following the Scherrer equation which utilizes the XRD data which are PDF 88-2335 for palladium crystall size. The crystall size of 1wt% Pd/AC1 is 11.00 nm, 1wt% Pd/HTc is 8.90 nm and 1wt% Pd/HTc-AC1 is 22.01 nm. 1wt% Pd/HTc-AC1 has the biggest palladium crystal diameter as compared to other catalyst. This phenomenon happened due to the agglomeration of palladium metal on surface of catalyts support (mixture of HTc and AC1).

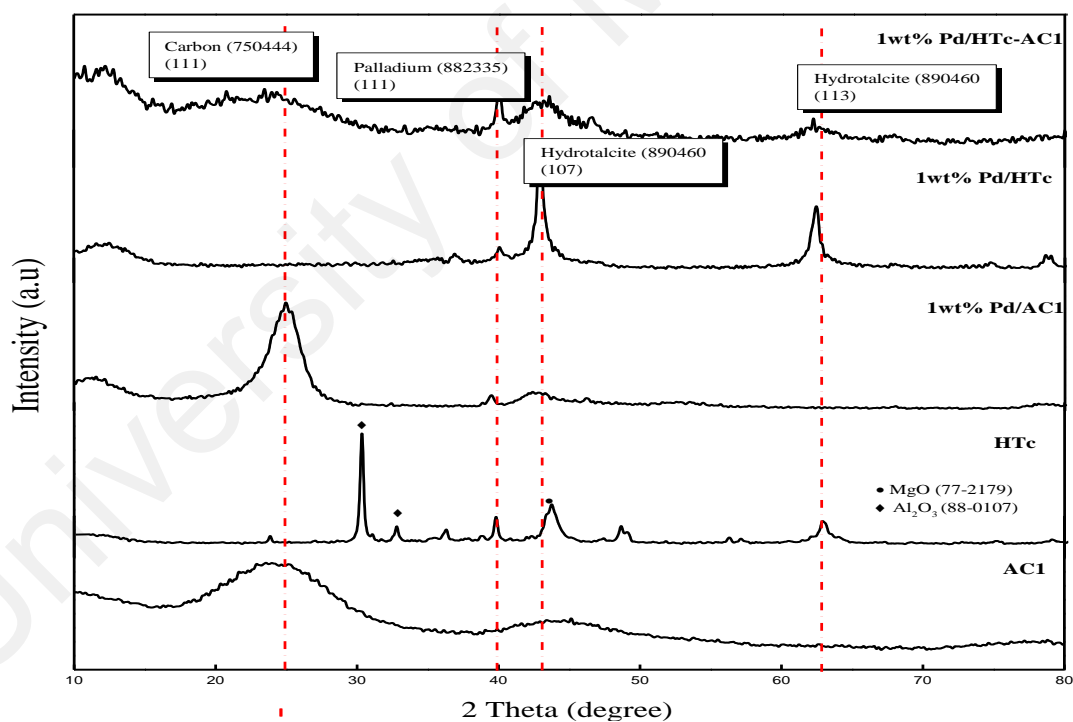


Figure 4.26: X-Ray Diffraction patterns of various catalysts

4.3.4 X-Ray Fluorescence (XRF)

The palladium based supported catalysts that had been synthesized in this studies are monometallic catalyst with fixed metal loading at 1wt%. The chemical composition of catalysts support and palladium catalyst were determined by using XRF. The elemental chemical analysis data of various catalyst were presented in Table 4.9, Table 4.10 and Table 4.11

Table 4.9: Chemical composition of 1wt% Pd/AC1

No	Element Formula	Weight %
1	O	43.08
2	Pd	1.24
3	Al	14.24
4	Si	19.09
5	P	1.65
6	S	0.70
7	Cl	3.10
8	K	2.99
9	Ca	3.76
10	Ti	0.34
12	Cr	0.27
13	Mn	0.11
14	Fe	9.33
15	Ni	0.09
Total		100

From Table 4.9, it showed that amount of palladium metal in 1wt% Pd/AC1 is 1.02% which is close with actual value (1%). The major elements in the activated carbon are silica, alumina, chloride, phosphorus and oxygen. These materials is originated from activated carbon. Other than that, the heavy metal and transition metal are produced from material. This elements plays an important role in field of catalysis (Kim, 1998)

Table 4.10: Chemical composition of 1wt% Pd/HT

No	Element Formula	Weight %
1	C	5.02
2	O	42.33
3	Pd	1.02
4	Na	0.18
5	Mg	39.41
6	Al	11.95
7	Si	0.08
Total		100

From Table 4.10, the palladium metal value of 1wt% Pd/HTc is 1.12% and it near to the actual value (1%). Hydrotalcite is consisting of Mg and Al. The calculated molar ratio hydrotalcite chemical composition is close to the actual value is 0.23. Ratio molar composition= $\text{Al}/(\text{Al}+\text{Mg})$ is equal to 0.20, (Corma et al., 2005).

Table 4.11: Chemical composition of 1wt% Pd/HTc-AC1

No	Element Formula	Weight %
1	O	44.91
2	Mg	30.87
3	Al	14.93
4	Pd	1.21
5	Si	4.54
6	P	0.87
7	S	0.15
8	Cl	0.47
9	K	0.35
10	Ca	0.63
11	Ti	0.04
12	Cr	0.03
13	Fe	1.00
Total		100

The palladium metal content of 1wt% Pd/HTc-AC1 is 1.20% as accumulated in Table 4.11, which is close with the actual value (1%). The content of Mg and Al belongs to the hydrotalcite. Furthermore, the major elements in the activated carbon are silica, alumina, chloride, phosphorus and oxygen were also detected in this sample. Other than that, the heavy metal and transition metal are produced from material. This elements plays an important role in the field of catalysis.

4.3.5 Temperature Program Desorption CO₂ (TPD-CO₂)

The basic properties of the palladium based supported catalysts were studied by TPD using CO₂. The importance of acid-base properties of catalyst for oxidation has been discussed by Ages (Katryniok et al., 2011). The acid-base property of the catalyst plays an important role in the activity as well as selectivity. Nevertheless, the formation of the product occurs mainly by the abstraction of hydrogen at alcohol functional group and addition of oxygen to the alcohol group. The adsorption-desorption of reactant and products requires an appropriate amount of acidic/basic sites as well as active metallic sites on the catalyst surface.

The CO₂ TPD profiles are found to have a different CO₂ adsorption pattern for all samples are shown in Figure 4.27. The profile showed that AC1 and 1wt% Pd/AC1 have no peaks since the surface content has no basic property.

As presented in Figure 4.28 and as tabulated in Table 4.12, 1wt% Pd/HTc, and 1wt% Pd/HTc-AC1 and HTc are found to have similar maximum peaks in the range of 600–700 K. These peaks could be related to the strong basic sites. The type of CO₂ adsorbed species is a unidentate bicarbonate, which forms strongly on basic surface O²⁻ and remained adsorbed even after evacuation at 673 K (Di Cosimo et al., 1998). Other than that, peaks that were observed at temperature below 400 K, belongs to the low basic sites of hydrotalcite (Cavani et al., 1991).

The strength of the basic properties by CO₂-TPD is depending on their desorption temperature (Naresh et al., 2014). For supported palladium catalysts, the basicity strength is lower compared to the calcined hydrotalcite (HTc), due to the formation of palladium crystallite and might be due to significance surface coverage of support palladium crystallite or substitution of basic hydroxyl groups by palladium species (DíEz et al., 2000)

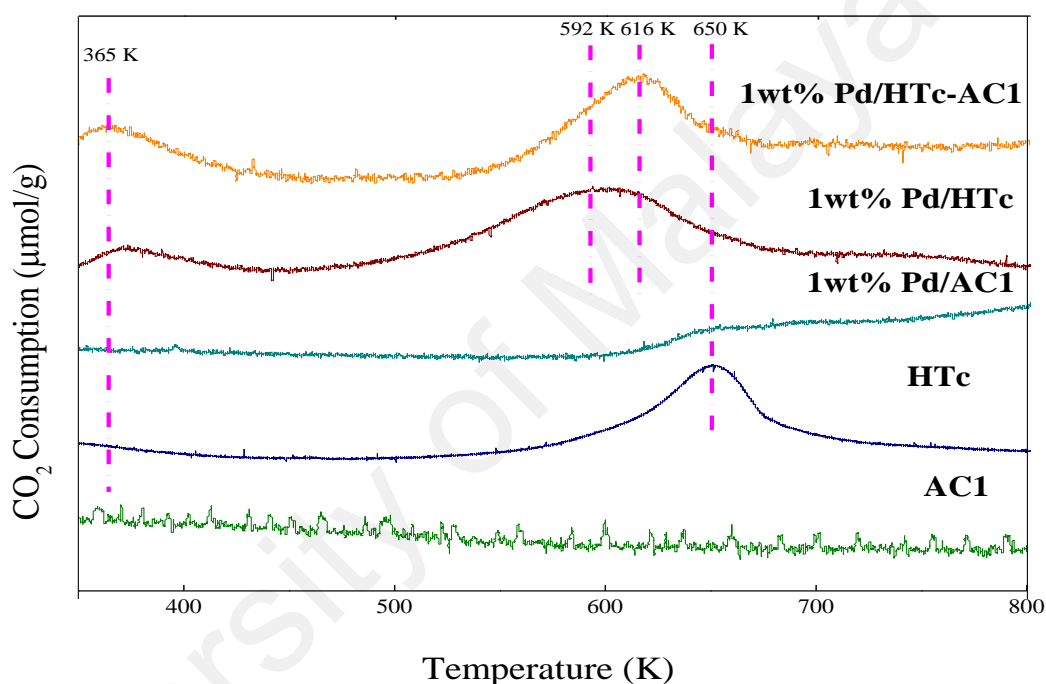


Figure 4.27: Temperature-programmed desorption of CO₂ profiles of various catalysts

Table 4.12: CO₂ adsorption of various catalysts

Entry	Catalyst	CO ₂ uptake amount (μmol/g)			Total Basicity (μmol/g)
		(390-411)K	(443-463)K	(533-553)K	
2	AC1	ND	ND	ND	ND
3	HTc	40	12	882	934
4	1wt% Pd/AC1	0	0	150	150
5	1wt%Pd/HTc	32	10	653	695
6	1wt%Pd/HTc-AC1	18	12	415	445

4.3.6 High-Resolution Transmission Electron Microscopy (HR-TEM)

The size and morphology of palladium based supported catalysts were determined by HR-TEM. The images of 1wt% Pd/AC1, 1wt% Pd/HTc and 1wt% Pd/HTc-AC1, catalysts are shown in Figure. 4.28, Figure 4.29 and Figure 4.30. In all samples, the palladium oxide crystallites are in various shapes, most of them are cubes and tetrahedrons. The shapes of palladium crystallites depend on the size of the particles. Most of the large palladium nanoparticles resulted in aggregation of the smaller seeds of spherical palladium nanoparticles (Nguyen et al., 2010). Fitting by Log-Normal function, the particle size of 1 wt% Pd/HTc-AC1 was found to have a median size of 22.0 nm, the 1wt% Pd/AC1 of 9.10 nm and the 1 wt% Pd/HTc of 8.90 nm.

All the palladium catalyst are observed in format aggregates. This clearly indicates that the palladium is reduced to metal and formed aggregates since it is not stable at metal state (+2 to 0 oxidation state). The immobilization method is the best method to solve this problem by using poly vinyl alcohol (PVA) as a stabilizing agent (Brett et al., 2011).

However, though palladium particles are big in size, palladium particles on activated carbon exhibit more homogeneous distribution. In fact, for 1wt% Pd/HTc-AC1 are observed in bigger size as compared to others. This differences could be attributed to a different and inhomogeneous distribution palladium on different types of supports. These HR-TEM results are in good agreement with the result of XRD. The crystal lattice of palladium metal is found in this analysis and the result is comparative with XRD value (d-spacing) (Figure 4.31).

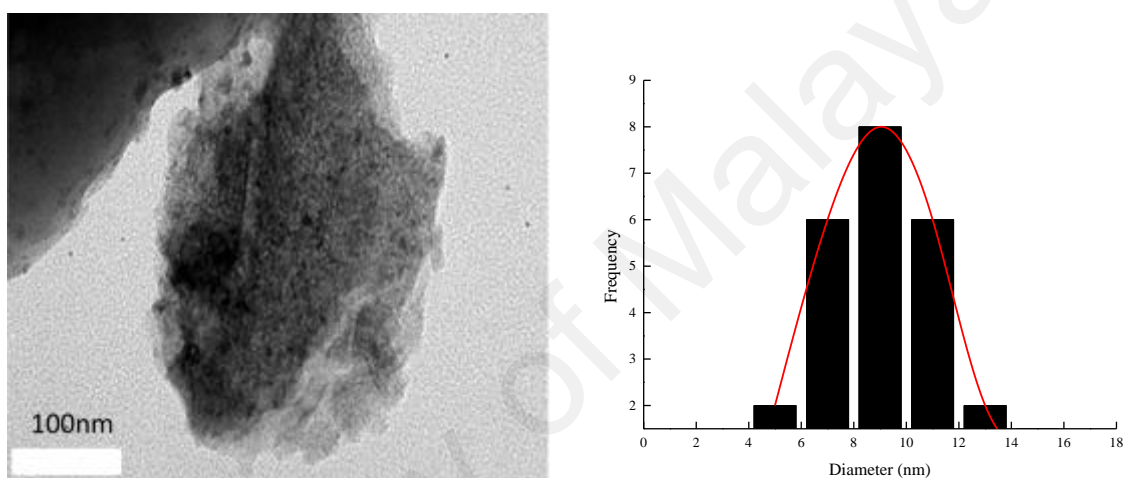


Figure 4.28: The HR-TEM overview image of 1wt% Pd/AC1 and Palladium particles distribution

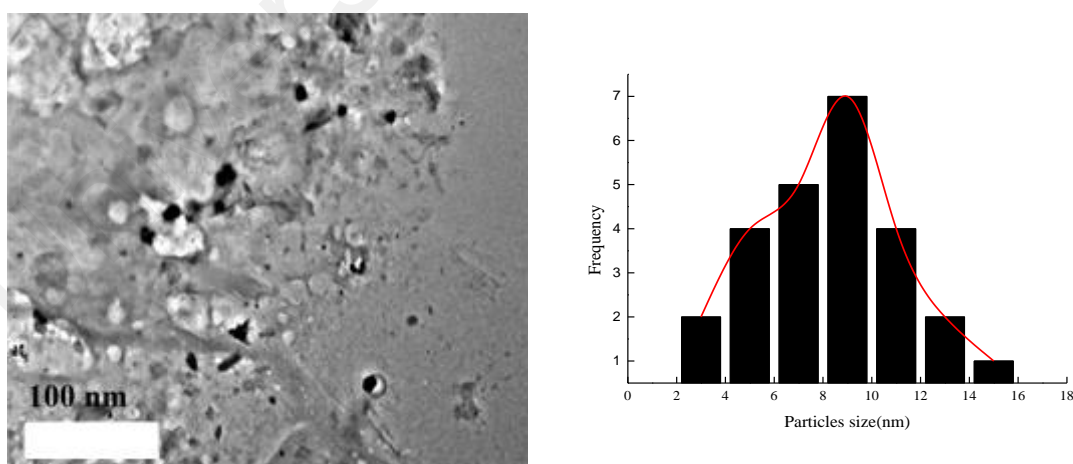


Figure 4.29: The HR-TEM overview image of 1wt% Pd/HTc and Palladium particles distribution

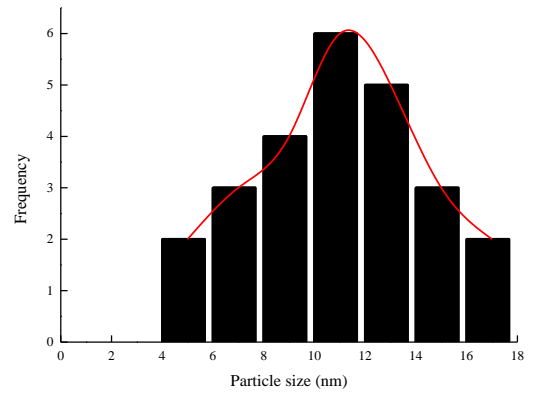
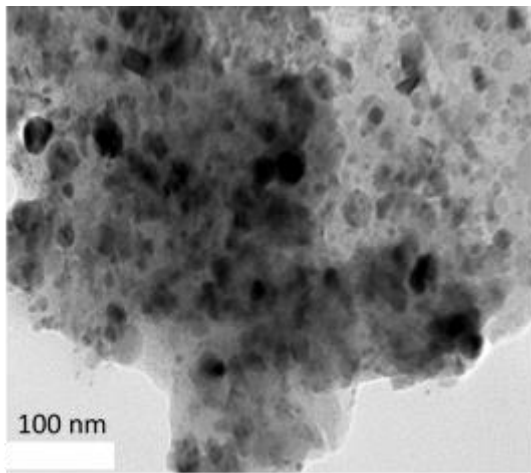


Figure 4.30: The HR-TEM overview image of 1wt% Pd/HTc-AC1 and Palladium particles distribution

University of Malaysia

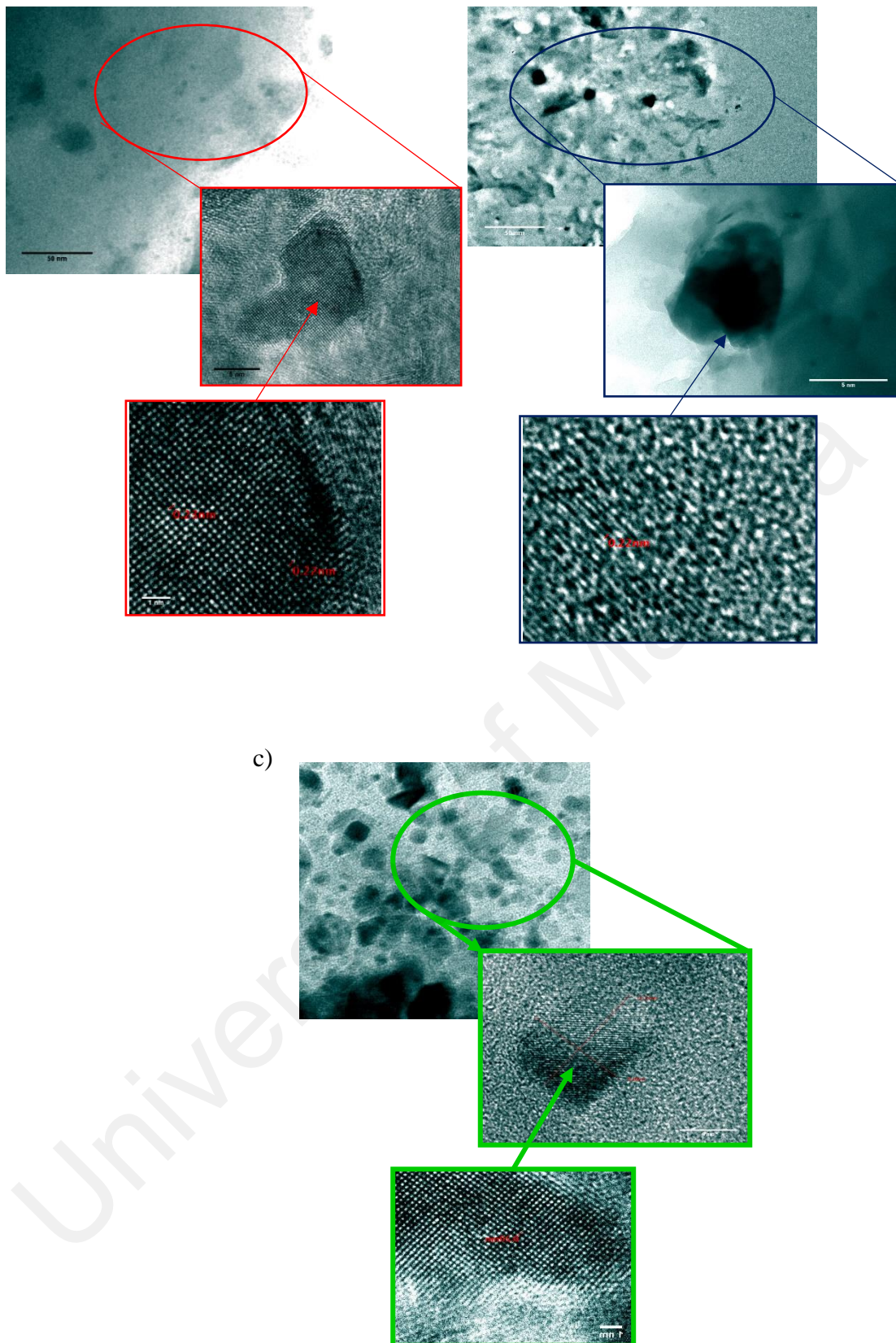


Figure 4.31: HR-TEM micrographs of a) 1wt% Pd/AC1, b) 1wt% Pd/HTc and c) 1wt% Pd/HTc-AC1, respectively with magnification of 60,000 times

4.3.7 Temperature-Programmed Reduction (TPR)

Supported palladium nanoparticles are an effective catalyst for the glycerol oxidation (Blackburn & Schwartz, 1977; Davis et al., 2013; Gallezot, 1997; Hirasawa et al., 2012; Mallat & Baiker, 2004; Nishimura et al., 2000). The catalyst activation is an important step before catalyst activity study. One of the method for palladium catalyst activation is a reduction process with H_2 .

The temperature-programmed reduction profiles of palladium catalyst supported on various type of supports is shown in Figure 4.32. Both types of supports, calcined hydrotalcite (HTc) and activated carbon (AC1), shown no major peaks for TPR profiles. HTc (Mg-Al mixed oxides) prepared by after calcinations showed reduction peak after 750 K (Takehira et al., 2004). The HTc started to reduce at high temperature as the aluminium oxide started to reduce.

1wt% Pd/AC1 showing maximum reduction peak at 519 K, which is assigned to the reduction peak. This peak is assigned to the reduction of Pd^{2+} (PdO) species to metallic Pd (Pd^0) (Naresh et al., 2014). The maximum reduction temperature of all the catalysts is varied in the temperature range 525 to 715 K, which depends on the type of supports. 1wt% Pd/HTc and 1 wt% Pd/HTc-AC1 have almost the same temperature reduction peak at 710 K and 720K. The temperature is high due to the strong interaction with support and forms metal-support interaction or highly coordinated types cause more resistance to reduce to palladium metallic state (Aznárez et al., 2015). The strong interaction is a result of the highly dispersed of the small particles on the supports (Aznárez et al., 2015). 1wt% Pd/HTc has the highest reduction peak (Figure 4.32), as the palladium loading increased due to the higher PdO content (Liu et al., 2014) compared to other catalysts. On the other hand, the increasing of the hydrogen consumption is could be due to the hydrogen spillover from metal to support or reduction of hydroxyl groups on the support (Naresh

et al., 2014). From this graph, different precursors were reduced at different temperature; 1wt% Pd/AC1 at 600 K, 1wt% Pd/HTc at 773 K and 1wt% Pd/HTc-AC1 at 750 K.

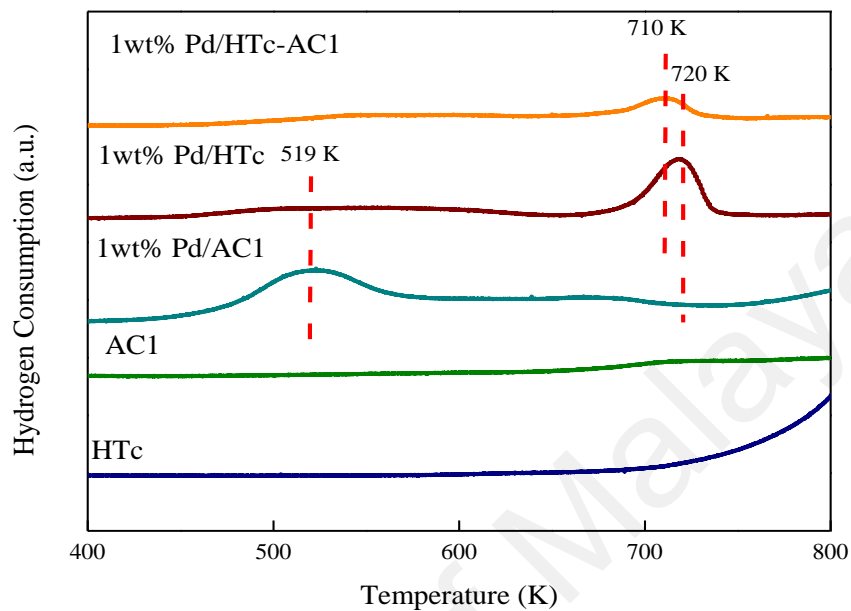


Figure 4.32: Temperature-programmed reduction profiles of palladium catalysts and supports

CHAPTER 5: LIQUID PHASE OXIDATION OF GLYCEROL

5.1 Catalyst screening for glycerol oxidation

The catalytic performances of all the prepared catalysts were tested in glycerol oxidation with the amount of active metal fixed at 1wt%. The reaction was performed in a 200 mL autoclave vessel, 3 bar O₂, for 180 min at 333 K. Among all the catalysts tested, the 1wt% Pd/HTc gave the highest conversion of 5.31% conversion with 86% selectivity to glyceric acid (Table 5.1 and Appendix). In this process, the observed major product is glyceric acid, whereas glyceraldehyde and dihydroxyacetone are the by-products. This results obtained were very encouraging despite report made by Akhiro Tsuji showed that Pd/HTc was not catalytically active for glycerol oxidation (Tsuji et al., 2011).

The glycerol oxidation reaction was carried out by two different supports, namely AC1 (activated carbon) and HTc (hydrotalcite). Under the reaction conditions (3 bar O₂, for 180 min at 333 K) used, both acidic activated carbon and basic hydrotalcite showed low activity. Conversion is less than 10% with negligible formation of DHA, GLYALD, GLYAC, and TARAC. 1wt% Pd supported on the AC1. Surprisingly, result showed low activity despite the presence of 1wt% Pd added onto the AC1. Nevertheless, presence of Pd produce GLYALD and GLYAC in line with metal catalyst oxidation.

The 1wt% Pd when loaded onto basic HTc showed an encouraging activity of 5.31% and a high selectivity to GLYAC of 86.05%. Combining both AC1 and HTc onto the 1wt% Pd shown a catalytic performance, with activity being half whilst product selectivity to GLYAC remained relatively similar to HTc supported only.

The results showed that the catalyst support (AC1 and HTc) strength is not enough to activate and convert glycerol. Glycerol conversion is catalyzed by Pd-based catalyst, and the conversion increased with increasing catalyst basicity value. These results can be related to the amount of the catalyst basicity (CO₂ desorption) as shown in Figure 4.28. Thus, the conversion of glycerol increased with increasing the base surface of the catalyst. These results suggested that the glycerol conversion may be directly proportional to the basicity, and the reaction occurs on the metal catalyst surface.

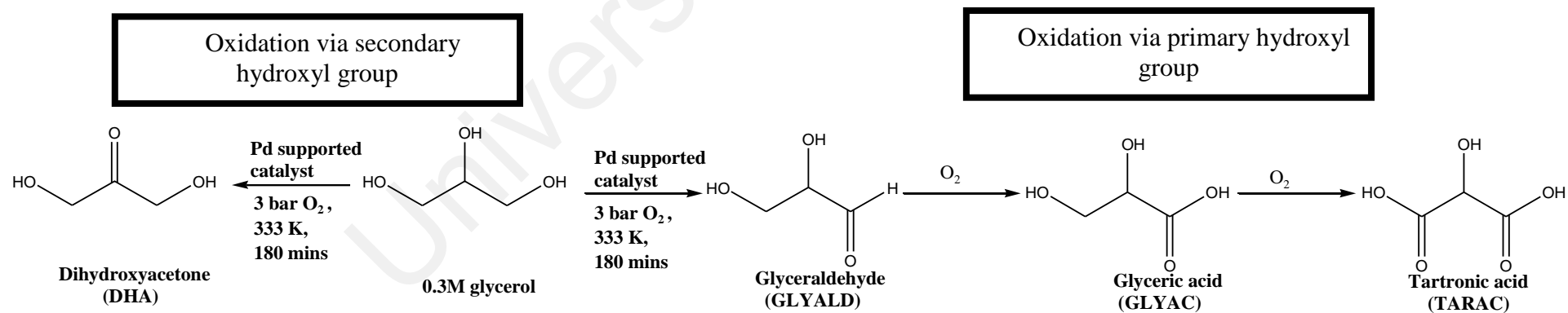
University of Malaya

Table 5.1: Glycerol oxidation over various catalyst systems

Entry	Catalyst	Total Basicity value ($\mu\text{mol.g}^{-1}$)	Conversion (%)	Selectivity (%)			
				DHA	GLYALD	GLYAC	TARAC
1	Blank	-	0.02				
2	*AC1	N/A	0.06	<0.10	<0.10	<0.10	ND
3	HTc	934.91	0.19	<0.10	<0.10	<0.10	ND
4	1wt% Pd/AC1	150.00	0.16	<0.10	33.90	66.10	ND
5	1wt%Pd/HTc	695.21	5.31	ND	<0.10	86.05	ND
6	1wt%Pd/HTc-AC1	445.94	2.50	ND	<0.10	85.01	ND

DHA: Dihydroxyacetone, GLYALD: Glyceraldehyde, GLYAC: Glyceric acid, TARAC: Tartronic acid

*Acidic value is 5.51molg^{-1} determined by titration



Scheme 5.1: Liquid phase oxidation of glycerol by palladium catalysts

5.2 Effect of catalyst supports

A comparison of catalytic activity of 1 wt% Pd supported onto HTc, AC1, and HTc-AC1 catalysts are summarized in Table 5.1. where the reactions were carried out under similar conditions. The main aim for this comparison is to assess the effect of the support on the catalytic properties of glycerol oxidation. From Table 5.1, it can be seen that the glycerol oxidation activity is catalyzed by active metal. Other than that, the basicity properties of the catalyst also has a big effect on activity as well as product selectivity.. 1wt% Pd/HTc is more active as compared with 1wt% Pd/AC1 and 1wt% Pd/HTc-AC1 catalyst. This catalyst surface properties is richer in basic sites than 1wt% Pd/AC1 and 1wt% Pd/HTc- AC1 catalysts. These results demonstrated that 1wt% Pd/HTc is a good catalyst for glycerol oxidation (Naresh et al., 2014). Similarly, the selectivity towards glyceric acid is higher than >80% for 1wt% Pd/HTc catalyst, which is due to the basic nature of HTc catalyst as compared to the other supports.

Taking into considerations the difference in textural properties as well as basicity of AC1, HTc and AC1-HTc where by:-

- AC1: 3-dimensional, high surface area ($917.87 \text{ m}^2.\text{g}^{-1}$), and microporous area is $710.38 \text{ m}^2.\text{g}^{-1}$ and mild acidic.
- HTc; 2-dimensional, moderate surface area is $162.2 \text{ m}^2.\text{g}^{-1}$ but with much higher and stronger basicity

have pronounce effect on product selectivity. The polar product such as glyceric acid is much easier to be desorbed from the surface Pd active sites. Combining AC1 and HTc does not cause positive effect to product selectivity for GLYAC, but almost reduction by 50% to its conversion. It is felt that, AC1 nor HTc do not directly change reaction mechanism for glycerol oxidation, but has a big influence on reactant sorption, and

product desorption. The complimentary support-product and support-reactant interaction have a pronounce affect onto reaction activity and selectivity.

5.3 Effect of reaction condition

It had been reported that both the conversion of glycerol and its selectivity to glyceric acid are not dependent on catalyst properties only, but it is also affected by the oxidation reaction operating conditions (Carretin et al., 2003; Gil, Marchena, et al., 2011; Villa, A. et al., 2009). In order, to carry out an in-depth study of the glycerol oxidation reaction, several operating variables were considered: oxygen pressure, temperature and NaOH/glycerol molar ratio, mol ratio of metal/glycerol and rate of stirring. All reactions were carried out using molecular oxygen as the oxidizing agent and 0.3 M aqueous glycerol solution.

5.3.1 Influence of partial oxygen pressure

The effect of oxygen pressure (PO_2), evaluated in terms of activity (TOF) and selectivity, was studied by using five different PO_2 values (1,3,5,7 and 9 bar) while keeping the other operating conditions constant: glycerol/Pd = 3500 mol/mol (8.36wt%), NaOH/glycerol = 2 mol/mol, 1000 rpm and 323 K. Palladium supported on calcined hydrotalcite (1wt% Pd/HTc), prepared by sol immobilization method was subjected to glycerol oxidation study. The development of both conversion and selectivity to glyceric acid with reaction time is shown in Figure 5.1 for the different catalysts. In all cases, an increase in the oxygen pressure did not have a dramatic effect on the catalytic conversion, which the conversion value increased less than 5% (Besson & Gallezot, 2000; Gil, Marchena, et al., 2011; Siyo, 2014). Nevertheless, a pressure increased favored the selectivity at expense production of tartronic acid. The formation of tartronic acid have been attributed as result of in situ formation of hydrogen peroxide during the reaction as described in Equation 5.1 (Dimitratos, Lopez-Sanchez, et al., 2006; Gil, Marchena, et al.,

2011; Rodrigues et al., 2012; Sobczak et al., 2010). The hydrogen peroxide formation indicates that O₂ is first reduced during the process before its dissociation (Gil, Marchena, et al., 2011). Thus, O₂ activation takes place through the formation and dissociation of peroxide (OOH*) (Equation 5.1) and hydrogen peroxide (HOOH*) intermediates (Equation 5.2) according to the following sequence of reactions:



Where * represents active site on the metal surface (Gil, Marchena, et al., 2011)

When the oxygen partial pressure is increased, the deactivation of the palladium catalyst might happen due to the palladium metal getting oxidised forming palladium oxide (Nishimura et al., 2000) which can drastically decrease the conversion and selectivity to glyceric acid (Siyo, 2014). From the experiment, we found that the conversion of glycerol at 9 bar is highest with almost 85% selectivity to glyceric acid. Table 5.2 summarize the results of influence of the partial oxygen pressure in glycerol oxidation. In summary, the presented result indicates that the addition of HTc as support prevents the catalyst from deactivation at high oxygen pressure as a result of redox capabilities of the calcined hydrotalcite (Vulic et al., 2012).

Table 5.2: Effect of the oxygen pressure on the conversion and selectivity to glyceric acid in the liquid-phase glycerol oxidation with 1wt%Pd/HTc at different oxygen pressure

*Pressure (bar)	Conversion (%)	S _{GLYAC} (%)	S _{GLYALD} (%)	S _{DHA} (%)	S _{TARAC} (%)	TOF ^{h-1}
1	0.82	83.09	0	3.12	13.76	10.75
3	5.11	83.20	0	0	12.00	22.17
5	6.31	83.74	0	0	16.26	26.44
7	7.36	85.79	0	0	14.21	28.92
9	8.51	86.88	0	0	13.13	29.55

*Reaction conditions: 0.3 M glycerol solution, glycerol/Pd =3500 mol/mol (8.36wt%), 323 K, 1000 rpm, 180 min and NaOH/glycerol = 2 mol/mol. Glyceric acid (GLYAC),Glyceraldehyde(GLYALD),Dihydroxyacetone (DHA) Tartronic acid (TARAC)

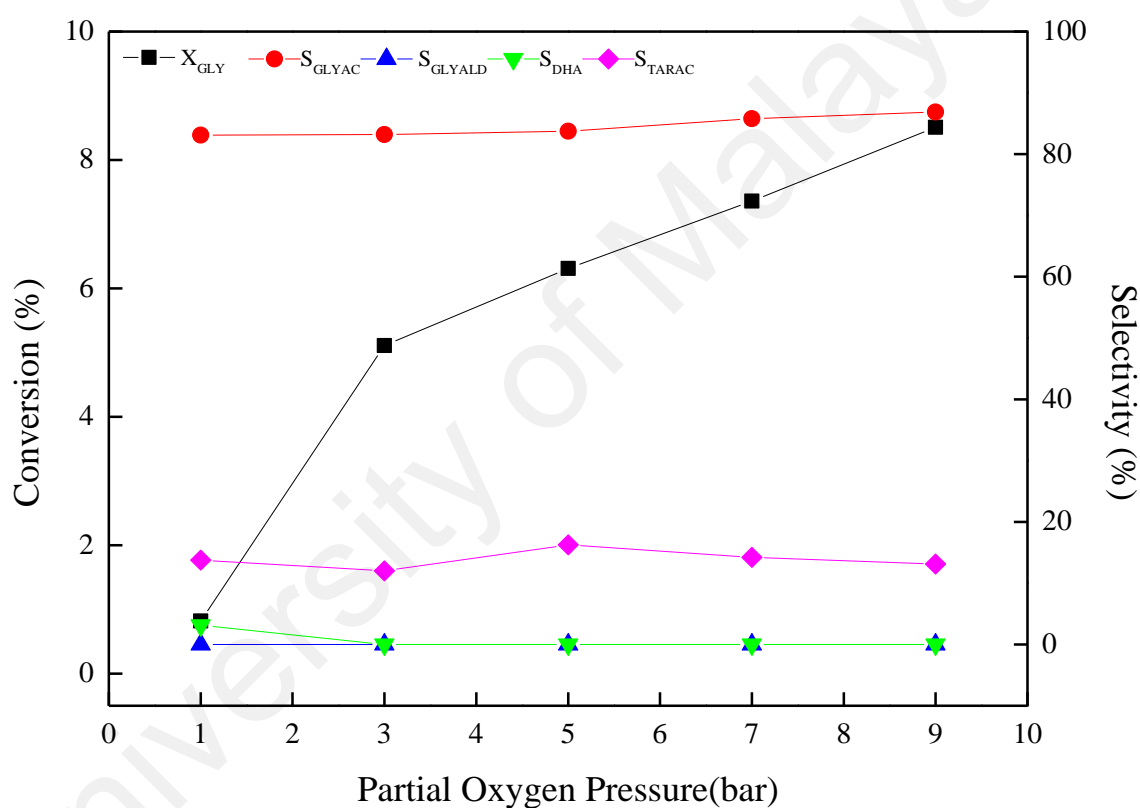


Figure 5.1: Effect of the oxygen pressure on the conversion and selectivity to glyceric acid in the liquid-phase glycerol oxidation

5.3.2 Influence of reaction temperature

The effect of reaction temperature, evaluated in terms of activity (TOF) and selectivity, was studied by varying this parameter in the range 303-383 K while keeping the other operating conditions constant: glycerol/Pd = 3500 mol/mol, NaOH/glycerol = 2 mol/mol, 1000 rpm and 9 bar O₂ for 180 min. The study was carried out with the same catalytic system used in the previous section. Figure 5.2 shows the temporal evolution of glycerol conversion and distribution of the product at different temperatures on 1wt% Pd/HTc influenced the catalytic activity to a greater extent than the oxygen pressure. Table 5.3 summarized the result of influence of reaction temperature towards glycerol oxidation. The rate of glycerol conversion is increased as the temperature increased; at 303 K, the glycerol conversion was lower than 20% even after prolonged 12 hours. Previously, it was reported that the activity of Au/C catalyst was higher than that on Pd/C at 303 K. This was attributed to a fast poisoning of palladium surface by oxygen at low temperature (Bianchi et al., 2005). However, at elevated temperatures up to 333 K, the Pd/C became more active and the effect of poisoning less pronounced (Bianchi et al., 2005). At higher temperature 363 K, the conversion is 70.35% with a selectivity of the glyceric acid is 80.34% as shown in Figure 5.2. The selectivity to the glyceric is constantly more than 75% from 303 K to 363 K, but as the temperature increased to 383 K the selectivity dropped to 60%, with 82.33% glycerol conversion. It is further observed that the formation of tartronic acid is favourable at high temperature. The formation of tartronic acid is due to the high dissociation molecular oxygen at high temperature (Brainer et al., 2014). In conclusion, high temperature of 363 K is required to produce glyceric acid with high yield by 1wt% Pd/HTc catalyst. Similarly, it was reported that the temperature has an impact on the glyceric acid selectivity in base medium (Brainer et al., 2014; Villa, A. et al., 2009; Zhu et al., 2010).

Table 5.3: Effect of the temperature on the conversion and selectivity to glyceric acid in the liquid-phase glycerol oxidation with 1wt% Pd/HTc at different reaction temperature

*Temperature (K)	Conversion (%)	S _{GLYAC} (%)	S _{GLYALD} (%)	S _{DHA} (%)	S _{TARAC} (%)	TOF ^{h-1}
303	4.60	94.43	0	0	4.59	18.26
323	8.51	86.88	0	0	13.12	29.55
343	17.17	89.48	0	0	10.52	62.58
363	70.35	80.34	0.84	0	18.79	165.58
383	82.33	60.79	1.64	14.66	22.75	234.15

*Reaction conditions: 0.3 M glycerol solution, glycerol/Pd = 3500mol/mol (8.36wt%), PO₂ = 9 bar, 1000 rpm, 180 min and NaOH/glycerol = 2 mol/mol. Glyceric acid (GLYAC), Glyceraldehyde (GLYALD), Dihydroxyacetone (DHA) Tartronic acid (TARAC)

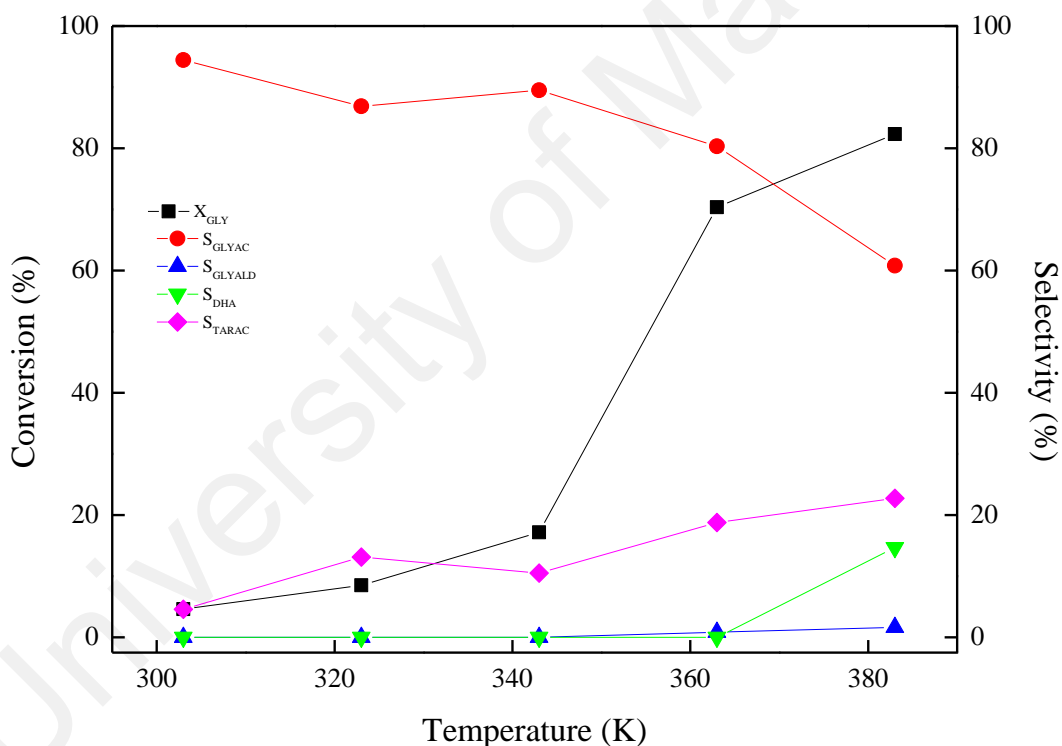


Figure 5.2: Effect of the reaction temperature on the conversion and selectivity to glyceric acid in the liquid-phase glycerol oxidation

5.3.3 Influence of Influence of NaOH/ glycerol mol ratio

The glycerol oxidation reaction using palladium-based catalysts is initiated by the presence of a base (e.g. NaOH) since the proton of the glycerol primary hydroxyl groups is readily abstracted by the hydroxyl group of the base (Besson & Gallezot, 2000; Carretin et al., 2004; Chornaja et al., 2012; Gallezot, 1997). In other words, the first step of the reaction mechanism involves dehydrogenation of the alcohol group of glycerol by the hydroxyl group of the base, and this is followed by the formation of oxidation intermediates. The influence of the base content was investigated using the 1wt% Pd/HTc catalyst, with the NaOH/glycerol mol ratio varied from 0 to 4 mol/mol and the other operating conditions kept constant: glycerol/Pd = 3500 mol/mol (8.36wt%), 363 K, 1000 rpm and 9 bar O₂. The first experiment in this study was carried out without NaOH. As expected, the glycerol conversion was low under this conditions.

The results obtained are in terms of glycerol concentration as shown in Figure 5.3. The amount of NaOH plays an important role in the catalytic activity. Conversion of glycerol increased as the NaOH/glycerol mol ratio was increased (Chornaja et al., 2012). The variation of the TOF is shown that an increase in the NaOH/ glycerol molar ratio from 1 to 2 led an increase in TOF, whereas a further increase in the NaOH/glycerol molar ratio from 3 to 4 did not induce further improvement where the TOF values remain approximately constant. In other words, the initial TOF values increased dramatically with the increment of the base content until a NaOH/glycerol mol ratio of 3 was reached. The effect of NaOH/glycerol mol ratio exceeding 3 reaching a plateau is in agreement by previous authors (Chornaja et al., 2012; Gil, Marchena, et al., 2011). Product selectivity was also found to be dependent on the NaOH concentration. At low glycerol conversion, an increase in the NaOH/glycerol mol ratio (from 1 to 2) led to a significant increase in the selectivity to glyceric acid at the expense of the tartronic acids. These results could be related to the favored hydrogen peroxide decomposition process at high NaOH

concentrations (Gil, Marchena, et al., 2011). Nevertheless, evidence for this process was not found in the present work since, although the amount of tartronic acid increased during the course of the reaction, it was not possible to observe an unusually rapid increase under the more extreme alkaline conditions. As a matter of fact, the selectivity to glyceric acid was not substantially affected by a further increase in the NaOH/glycerol mol ratio (from 3 to 4). In summary, an increase in the NaOH/glycerol molar ratio did not drastically increase the selectivity to glyceric acid. Table 5.4 summarized the results of conversion and selectivity of the product regarding to the influence of NaOH/glycerol mol ratio in this studies.

Table 5.4: Effect of the NaOH/Glycerol mol ratio on the conversion and selectivity to glyceric acid in the liquid-phase glycerol oxidation with 1wt%Pd/HTc at different mol ratio of NaOH

*NaOH/glycero l mol ratio	Conversion (%)	SGLYAC (%)	SGLYALD (%)	SDHA (%)	STARAC (%)	TOF ^{h-1}
0	1.14	100	0	0	0	7.46
1	37.42	50.79	4.49	5.17	13.12	119.70
2	70.35	80.34	0.84	0	18.79	165.58
3	74.40	65.69	6.69	8.18	19.43	248.01
4	74.50	62.22	6.33	7.29	22.43	234.15

*Reaction conditions: 0.3 M glycerol solution, glycerol/Pd 3500 mol/mol (8.36wt%), PO₂= 9 bar, 1000 rpm, 180 min, 363K. Glyceric acid (GLYAC),Glyceraldehyde(GLYALD), Dihydroxyacetone (DHA), Tartronic acid (TARAC)

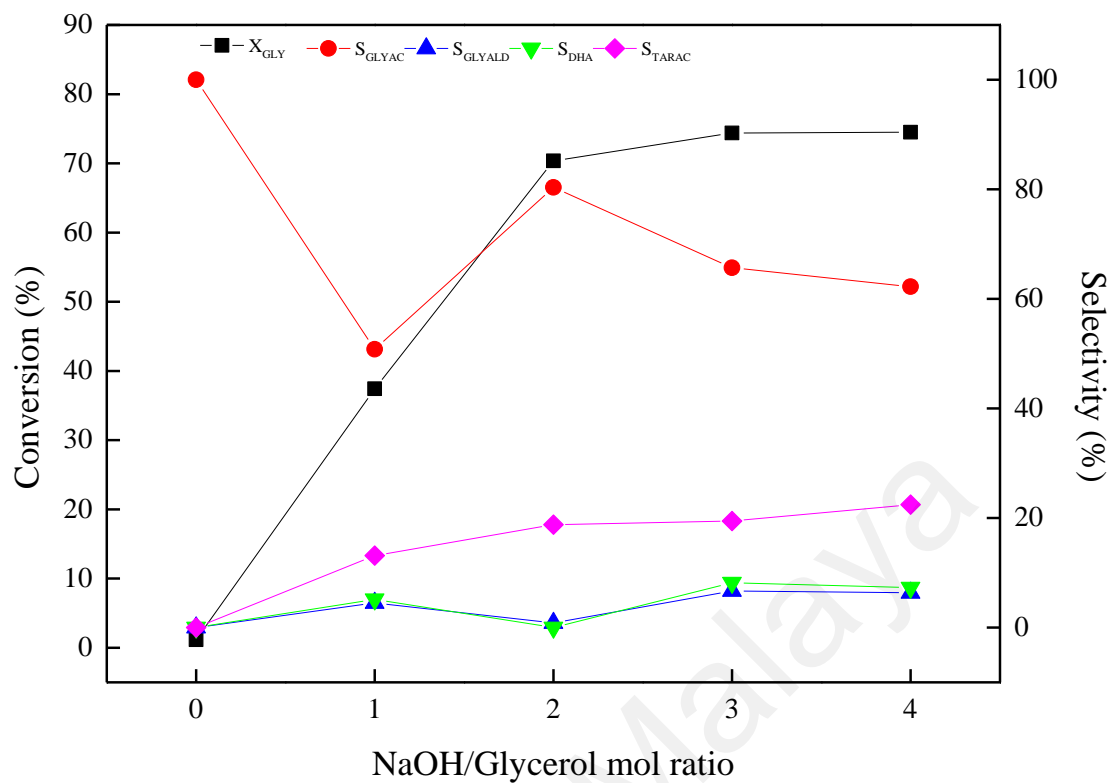


Figure 5.3: Effect of the NaOH/Glycerol molar ratio on the conversion and selectivity to glyceric acid in the liquid-phase glycerol oxidation

5.3.4 Influence of catalyst amount

The influence of catalyst amount was studied in a 200 mL stainless steel autoclave using 1wt% Pd/HTc, by varying the glycerol/Pd mol ratio from 500 to 6500 (mol/mol). Other reaction conditions were kept constant: NaOH/glycerol = 2 mol/mol, 363 K, 1000rpm and 9 bar O₂ for 180 min reaction duration.

The profiles of glycerol conversion of catalyst amount was presented in Figure 5.4, and the result was tabulated in Table 5.5. From the results, it is evident that the conversion only occurred in the presence of catalyst (Brett et al., 2011; Garcia et al., 1995; Katryniok et al., 2011). This behavior could be attributed to the reaction occurred under a rate-controlled kinetic regime (Demirel et al., 2007). As expected, glycerol conversion rate is slowly increased constant at higher catalyst amounts. The collected results indicate that incremental addition of catalyst provided additional active sites for glycerol oxidation (Brainer et al., 2014). Hence, the maximum glycerol conversion was achieved at glycerol palladium mol ratio equal 3500 mol/mol.

Furthermore, the distribution of the products was strongly dependent on the catalyst amount. The selectivity of glyceric acid decreased slightly when the glycerol/palladium molar ratio was decreased from 3500 to 2000 mol/mol. The decrease of selectivity to glyceric acid will favour the production of tartronic and glycolic acids. These behaviour indicates that by increasing the amount of catalyst, thus increasing the number of active sites, glyceric acid can be further oxidized to tartronic acid. The glycolic acid produce indicates that lower substrate to metal molar ratio enhances the C-C cleavage (Brainer et al., 2014; Dimitratos et al., 2009; Musialska et al., 2010; Skrzyńska et al., 2014; Zhang, M. et al., 2015)

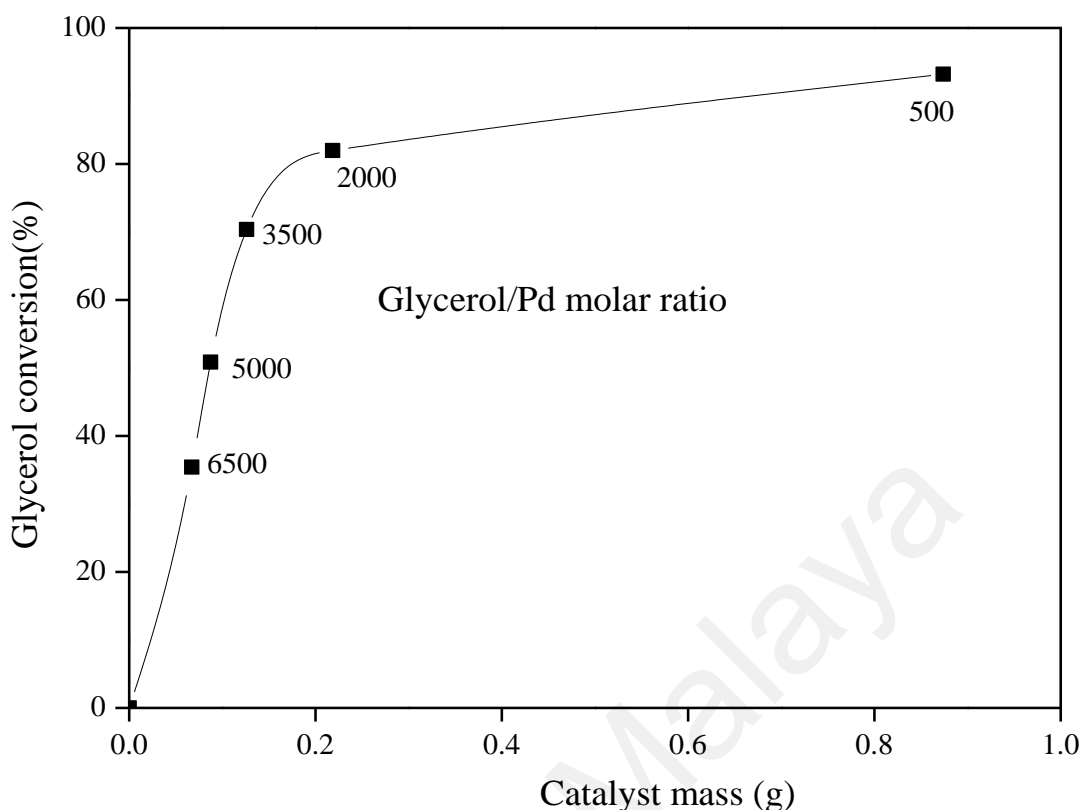


Figure 5.4: Glycerol conversion with 1wt% Pd/HTc at different catalyst amounts.

Table 5.5: Effect of the Glycerol/Pd mol ratio on the conversion and selectivity to glyceric acid in the liquid-phase glycerol oxidation with 1wt%Pd/HTc at different mol ratio of Glycerol/Pd

*Glycerol/Pd mol ratio (g)	Conversion (%)	S _{GLYAC} (%)	S _{GLYALD} (%)	S _{DHA} (%)	S _{TARAC} (%)	TOF ^{h-1}
500 (0.87)	93.21	52.30	16.87	0	22.56	276.25
2000 (0.22)	81.96	73.65	0	0	19.57	250.11
3500 (0.12)	70.35	80.37	0.84	0	18.79	165.68
5000 (0.08)	50.87	81.15	2.88	0	14.68	149.84
6500 (0.06)	35.42	84.14	1.96	0	11.45	119.07

*Reaction conditions: 0.3 M glycerol solution, NaOH/glycerol = 2 mol/mol(8.36wt%), PO₂= 9 bar, 1000 rpm,, 180 min 363K. Glyceric acid (GLYAC), Glyceraldehyde(GLYALD), Dihydroxyacetone (DHA) Tartronic acid (TARAC)

5.3.5 Influence of stirring rate

Glycerol oxidation is carried out in a three-phase system of gas and liquid in the presence of a porous solid catalyst (Zhao et al., 2014). Thus, glycerol oxidation reaction has to deal with multiple mass-transfer phenomena, e.g (i) the external mass transfer from the reaction medium to the catalyst surface and (ii) the internal mass transfer inside the porous network of the catalyst (Murzin & Salmi, 2005).

The external and internal mass transfer resistances could occur in the slurry or the fixed-bed reactor (Demirel et al., 2007). One of the conventional method to determine the resistances is by varying the stirring rate (Demirel-Gülen et al., 2005). The effect of the stirring rate was studied with 1wt% Pd/HTc in 200 mL stainless steel autoclave from 300 to 1500 rpm. Reaction conditions, glycerol/Pd mol ratio = 3500, (8.36wt%) NaOH/glycerol = 2mol/mol, 363 K, 9 bar O₂ for 180 minutes.

As shown in Table 5.6, for 1wt% Pd/HTc the lowest stirring speed gave the lowest activity and the selectivity to glyceric acid. The increase in the stirring speed from 300 to 1500 rpm resulted an increased of the catalyst activity, but lead to a decrease in the selectivity to glyceric acid. Therefore, one could suggest that the increase in catalytic activity with the increase in the stirring speed does not originate from the increase in the diffusion rate in pores but rather from the transport of products from solid to liquid. Our choice for further study was the stirring speed at 1000 rpm because it ensured the highest selectivity to glyceric acid.

Table 5.6: Effect of the stirring speed on the conversion and selectivity to glyceric acid in the liquid-phase glycerol oxidation with 1wt%Pd/HTc at different stirring speed

*Stirring speed (rpm)	Conversion (%)	SGLYAC (%)	SGLYALD (%)	SDHA (%)	STARAC (%)	TOF ^{h-1}
300	17.11	28.39	16.87	5.60	0	276.25
600	52.83	62.59	26.86	3.50	9.57	250.11
1000	70.35	80.37	0.84	0	18.79	165.68
1200	74.87	78.15	2.88	0	14.68	149.84
1500	80.42	74.14	1.96	0	11.45	119.07

*Reaction conditions: 0.3 M glycerol solution, NaOH/glycerol = 2 mol/mol (8.36wt%), PO₂= 9 bar, glycerol/Pd= 3500, 363K. Glyceric acid (GLYAC), Glyceraldehyde (GLYALD), Dihydroxyacetone (DHA) Tartronic acid (TARAC)

5.4 Catalyst Stability

Palladium catalysts are normally very sensitive to the preparation and reaction condition parameters. Thus, it is important to evaluate the catalyst stability and to determine whether the 1wt% Pd/HTc catalyst remained in its original solid form (no phase changes).

5.4.1 Filtration experiments

To determine whether the 1wt% Pd/HTc catalyst was acting purely as heterogeneous catalysts, a filtration experiment was studied. The reaction was conducted by removing the catalyst and the remaining solution was reacted for 180 min without a catalyst. The results are shown in Figure 5.5. After the catalyst was removed very little glycerol was oxidized. This indicates that the reaction is a non-heterogeneous reaction and implies that some palladium has leached from the catalyst. The reaction condition of this experiment is 363 K, NaOH/glycerol=2mol/mol, PO₂ =9 bar.

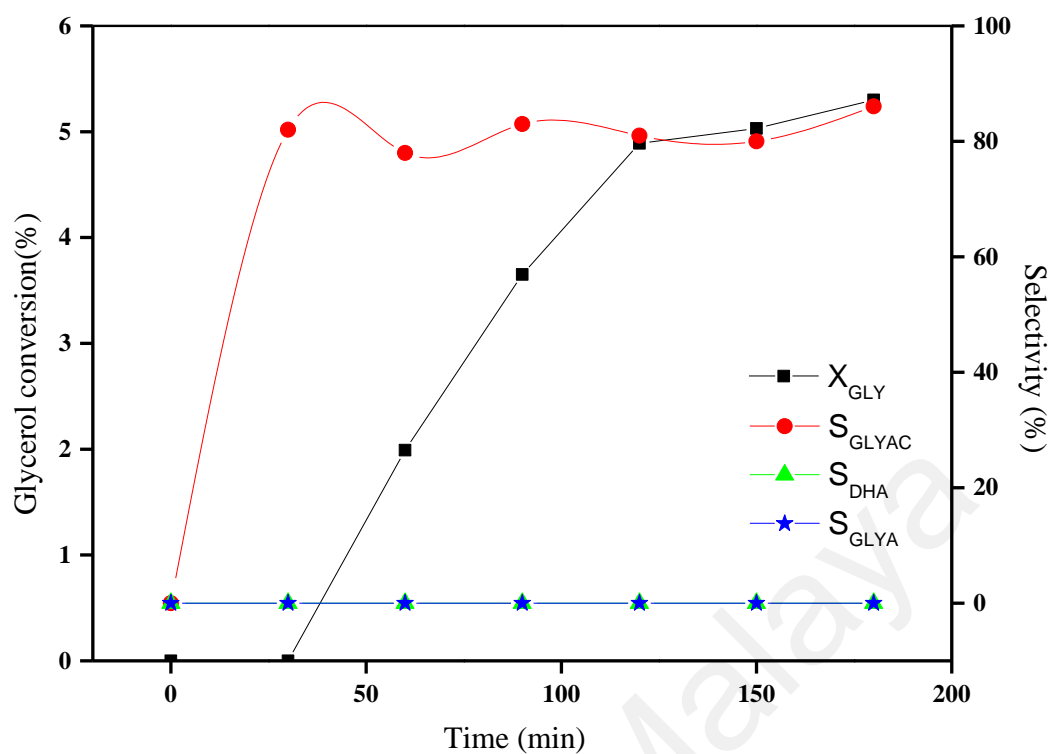


Figure 5.5: Glycerol conversion without catalyst at 3h in filtration test with 1wt% Pd/HTc catalyst.

5.4.2 Reusability

The 1wt% Pd/HTc was tested with same reaction condition for 180min, at 363 K. The catalyst was then recovered and tested under the same condition. This was repeated three times to test the reusability of the catalyst and the glycerol/Pd was calculated and fixed at 3500 mol/mol.

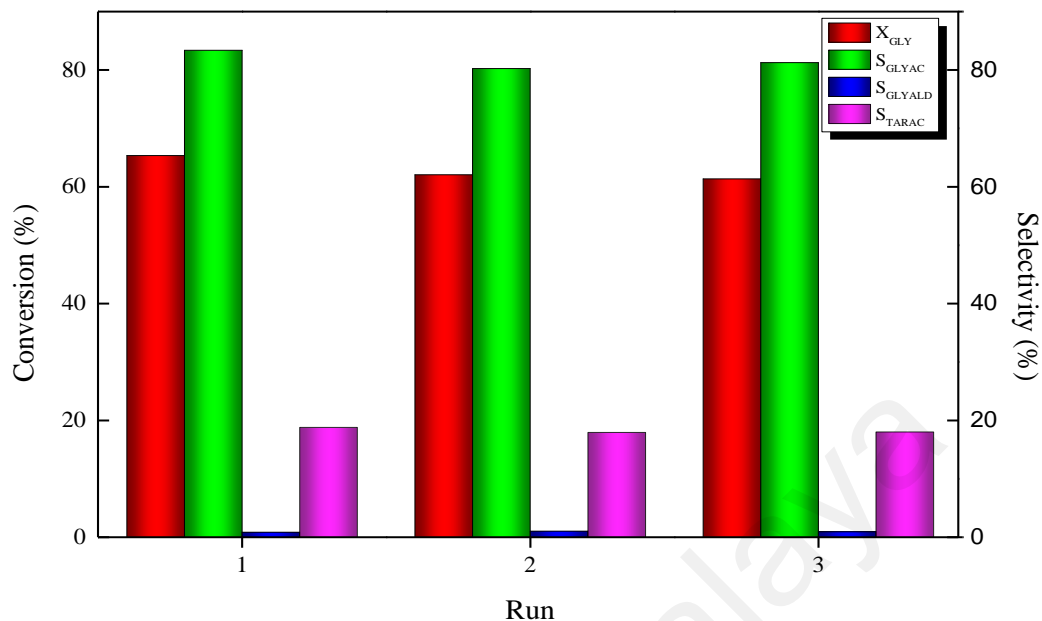


Figure 5.6: Reusability study using 1wt% Pd/HTc catalyst, reaction condition: 0.3M glycerol, glycerol/Pd=3500 mol/mol, Naoh/glycerol=2, 3 hours, 1000rpm at 363 K and 9 bar O₂.

As presented in Figure 5.6, the conversion was decreased from the 1st use to the 3rd. The 1st run conversion is 65.31%, 2nd run conversion is 62.04% and 3rd run conversion is 61.34%. The selectivity to glyceric acid was constant every time catalyst was used (83.37%, 80.25% and 81.25%). The formation of other by-products like glyceraldehyde and tartronic acid has no changes. This shows that the palladium catalyst is stable.

CHAPTER 6: CONCLUSION AND FUTURE WORKS

6.1 Conclusion

The hydrotalcite (HTc) and activated carbon were prepared in lieu of their promising catalyst support materials for supported palladium catalysts towards oxidation of glycerol. Calcined hydrotalcite is a stable mixed oxide ($MgAlO_{x3}$) that has basic properties. $Al/(Al+Mg) = 0.20$ hydrotalcite is shown as the best basic catalyst for oxidation. The surface area of calcined hydrotalcite is $162.2 \text{ m}^2.\text{g}^{-1}$ and basicity is $914.91 \mu\text{mol}.\text{g}^{-1}$.

The raw activated carbon was pre-treated with nitric acid, from which, the surface of activated carbon was functionalized from neutral to acidic. The Boehm titration used to show that the surface acidity of $5.51 \text{ mmol}.\text{g}^{-1}$ whilst TGA-MS analysis confirmed presence of carboxyl, lactonic and phenolic functional group.

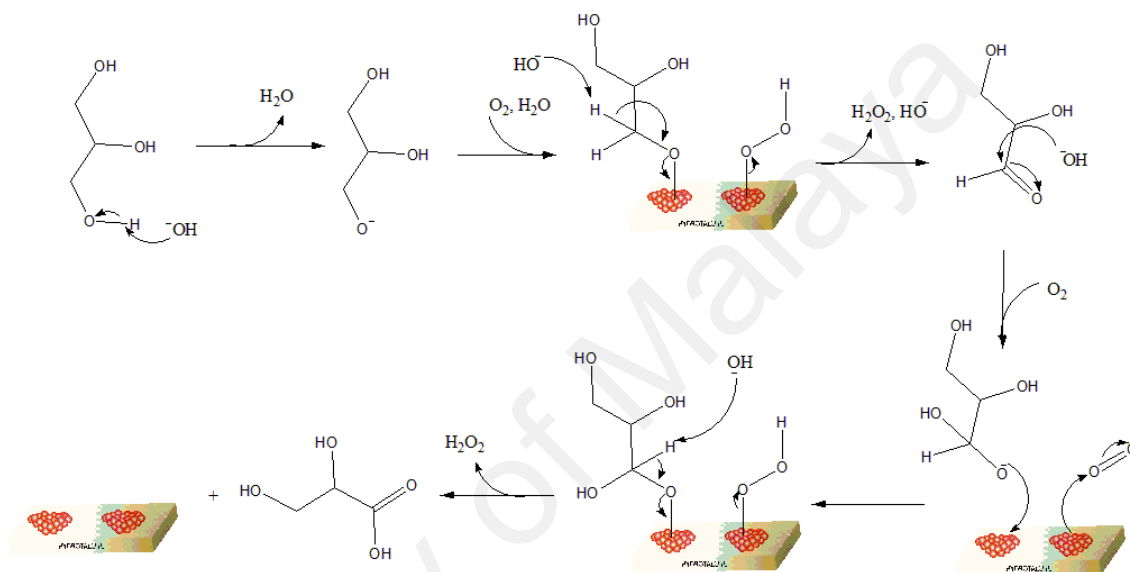
The preparation method developed benefited from PVA as a stabilizing agent prior to Pd immobilization onto hydrotalcite and activated carbon yield palladium nanoparticles are well dispersed. Its dispersion is dependent on the type of support. Results supported by TEM and XRD results. TPR results revealed that the reducibility of the palladium increased with the strong bond of the support with metal. TPD- CO_2 results apparently showed the basicity of catalyst is directly proportional to the catalyst activity.

The basicity of calcined hydrotalcite is not enough to support the oxidation of glycerol, thus the addition of base is still needed in this reaction. The 1wt% Pd/HTc catalyst showed high activity as compared to other supported palladium catalysts. The pure hydrotalcite (HTc) and activated carbon (AC1) supports were found to be inoperative for the glycerol oxidation under similar experimental conditions. Thus, this reaction is dependent on the metal particle (palladium) as the metal act as a platform for the reaction to happen. It can be established and employed as an effective catalyst for the oxidation of glycerol.

The outcomes of this study showed that the conversion glycerol and product distribution for liquid phase oxidation of glycerol are strongly dependent on the reaction conditions. The influence of oxygen pressure, reaction temperature and the molar ratio of NaOH/Glycerol, catalyst amount and stirring rate were studied by using catalytic systems based on palladium nanoparticles. They were supported on calcined hydrotalcite (HTc) prepared by sol immobilization method using PVA as a surfactant. The influenced of the oxygen pressure on the reaction was observed. From the result, small influenced was found. At low temperature, the hydrogen peroxide is formed, from the reductive of the O_2 . The selectivity to glyceric acid was well enhanced by an increase of both oxygen pressure and reaction temperature, as the palladium is fast poisoned by oxygen at low temperature (363 K). As the temperature increased, the glycerol conversion rises but the selectivity of glyceric acid decreased and show increment in the production of the tartronic acid. This is because the hydrogen peroxide from high dissociation of O_2 increased in high temperature. Glycerol conversion and glyceric acid selectivity increased when NaOH/glycerol mol ratio was raised from 1 to 3 and it remained practically unchanged at higher values. The production of tartronic acid also due to further oxidation of glyceric acid at high NaOH/glycerol molar ratio. Mechanism of oxidation of glycerol is a dehydrogenation step, hence, the pH of the reaction medium is a crucial factor in this reaction. As the catalyst amount increased, the conversion of glycerol increases too. Unfortunately, even at higher catalyst amount the glycerol conversion remained almost constant. The glyceric acid production slightly decreased at high catalyst amount due to the increased of active sites number. The mass transfer of the reaction was studied by the variation of stirring rate from 300 to 1500 rpm. As the stirring speed increases from 300 to 1500 rpm, the activity of the catalyst increased but decreased in the selectivity of glyceric acid. Therefore, one could suggest that the growth of activity with the increment

of the stirring speed does not originate from the increment of the diffusion rate in pores, but rather from the transport of products from solid to liquid.

The stability of the catalyst had been investigated by filtration experiments. From the three-time re-run of the glycerol oxidation, an inhomogeneous leaching of palladium could be observed.



Scheme 6.1: Proposed mechanism of glycerol oxidation to glyceric acid

6.2 Future works

This thesis presented a number of application of synthesized Pd-based supported catalysts on liquid phase oxidation of glycerol. The target product of this reaction is glyceric acid, which is widely used these days. It is used in medicine as metabolites in the glycolysis cycle and a precursor in the synthesis of amino acid (Comelli, 2011). Furthermore, several future directions related to this research were identified, and listed as follows:-

- Change the framework of hydrotalcite with other types of metal for example divalent metal ion (Cu²⁺, Co²⁺, Zn²⁺, Ni²⁺, Mn²⁺, Fe²⁺) and trivalent metal ion

(Al³⁺,Fe³⁺,Cr³⁺,Bi³⁺,Mn³⁺,Co³⁺) and studies the surface properties towards the glycerol oxidation.

- Synthesized the bimetallic and trimetallic catalyst with palladium metal.
- More reaction with different types of solvents, and studies the kinetic and thermodynamic properties of glycerol oxidation

University of Malaya

REFERENCES

- Aji, M. M., Gutti, B., & Highina, B. K. (2015). Production and Characterization of Activated Carbon from Groundnut Shell Sourced in Maiduguri. *Columban Journal of Life Science*, 17(1), 7.
- Al-Qodah, Z., & Shawabkah, R. (2009). Production and characterization of granular activated carbon from activated sludge. *Brazilian Journal of Chemical Engineering*, 26, 127-136.
- Alegre, C., Gálvez, M., Moliner, R., & Lázaro, M. (2015). Influence of the Synthesis Method for Pt Catalysts Supported on Highly Mesoporous Carbon Xerogel and Vulcan Carbon Black on the Electro-Oxidation of Methanol. *Catalysts*, 5(1), 392-405. doi:10.3390/catal5010392
- Alhanash, A., Kozhevnikova, E. F., & Kozhevnikov, I. V. (2010). Gas-phase dehydration of glycerol to acrolein catalysed by caesium heteropoly salt. *Applied Catalysis A: General*, 378(1), 11-18. doi:10.1016/j.apcata.2010.01.043
- Alonso, D. M., Wettstein, S. G., & Dumesic, J. A. (2012). Bimetallic catalysts for upgrading of biomass to fuels and chemicals. *Chemical Society Reviews*, 41(24), 8075-8098. doi:10.1039/C2CS35188A
- Álvarez, M. G., Chimentão, R. J., Figueras, F., & Medina, F. (2012). Tunable basic and textural properties of hydrotalcite derived materials for transesterification of glycerol. *Applied Clay Science*, 58, 16-24. doi:<http://dx.doi.org/10.1016/j.clay.2012.02.004>
- Anisuzzaman, S. M., Joseph, C. G., Taufiq-Yap, Y. H., Krishnaiah, D., & Tay, V. V. (2015). Modification of commercial activated carbon for the removal of 2,4-dichlorophenol from simulated wastewater. *Journal of King Saud University - Science*, 27(4), 318-330. doi:<http://dx.doi.org/10.1016/j.jksus.2015.01.002>
- Assouik, J., Hajji, L., Boukir, A., Herold, C., & Lagrange, P. (2016). Synthesis, structure and electrical behavior of the heavy alkali metal-arsenic alloys based graphite intercalation compounds. *Synthetic Metals*, 218, 34-42. doi:<http://dx.doi.org/10.1016/j.synthmet.2016.04.028>
- Astruc, D., Lu, F., & Aranzaes, J. R. (2005). Nanoparticles as recyclable catalysts: the frontier between homogeneous and heterogeneous catalysis. *Angewandte Chemie International Edition*, 44(48), 7852-7872. doi:10.1002/anie.200500766

- Aznárez, A., Gil, A., & Korili, S. A. (2015). Performance of palladium and platinum supported on alumina pillared clays in the catalytic combustion of propene. *Royal Society of Chemistry Advances*, 5(100), 82296-82309. doi:10.1039/c5ra15675k
- Bagheri, S., Julkapli, N. M., & Yehye, W. A. (2015). Catalytic conversion of biodiesel derived raw glycerol to value added products. *Renewable and Sustainable Energy Reviews*, 41, 113-127. doi:10.1016/j.rser.2014.08.031
- Barkauskas, J., & Dervinyte, M. (2003). An investigation of the functional groups on the surface of activated carbons. *Journal of the Serbian Chemical Society*, 69(5), 14.
- Bastiani, R., Zonno, I. V., Santos, I. A. V., Henriques, C. A., & Monteiro, J. L. F. (2004). Influence of thermal treatments on the basic and catalytic properties of Mg,Al-mixed oxides derived from hydrotalcites. *Brazilian Journal of Chemical Engineering*, 21, 193-202.
- Becker, F. (1965). Inorganic Thermogravimetric Analysis. Von C. Duval, aus d. Französ. übers. v. R. E. Oesper. Elsevier Publishing Company, Amsterdam-London-New York 1963. 2. Aufl. [1], XV, 722 S., 77 Abb., geb. DM 67.—. *Angewandte Chemie*, 77(14), 631-631. doi:10.1002/ange.19650771431
- Behr, A., Eilting, J., Irawadi, K., Leschinski, J., & Lindner, F. (2008). Improved utilisation of renewable resources: New important derivatives of glycerol. *Green Chemistry*, 10(1), 13-30. doi:10.1039/b710561d
- Bensah, E. C., & Mensah, M. (2013). Chemical Pretreatment Methods for the Production of Cellulosic Ethanol: Technologies and Innovations. *International Journal of Chemical Engineering*, 2013, 21. doi:10.1155/2013/719607
- Besson, M., & Gallezot, P. (2000). Selective oxidation of alcohols and aldehydes on metal catalysts. *Catalysis Today*, 57, 15.
- Bianchi, C. L., Canton, P., Dimitratos, N., Porta, F., & Prati, L. (2005). *Catalysis Today*, 102-103, 203-212.
- Blackburn, T. F., & Schwartz, J. (1977). Homogeneous catalytic oxidation of secondary alcohols to ketones by molecular oxygen under mild conditions. *Journal of the Chemical Society, Chemical Communications*(5), 157-158. doi:10.1039/C39770000157
- Boehm, H. P. (2002). Surface Oxides on carbon and their analysis: a critical assessment. *Carbon* 40, 5.

- Bond, G. C. (1998). Book Review: Principles and practice of heterogeneous catalysis. J. M. Thomas and W. J. Thomas, VCH, Weinheim, 1997, xxiii+669 pp., price DM88.00. ISBN 3 527 29239 X. *Journal of Chemical Technology & Biotechnology*, 73(4), 444-444. doi:10.1002/(SICI)1097-4660(199812)73:4<444::AID-JCTB968>3.0.CO;2-F
- Brainer, J. E. N., Sales, D. C. S., Medeiros, E. B. M., Lima Filho, N. M., & Abreu, C. A. M. (2014). Wet oxidation of glycerol into fine organic acids: catalyst selection and kinetic evaluation. *Brazilian Journal of Chemical Engineering*, 31(4), 913-923. doi:10.1590/0104-6632.20140314s00002655
- Brett, G. (2012). *The Selective Oxidation of Bioderived Molecules by Gold Catalysts*. (Doctor of Philosophy), Cardiff University.
- Brett, G. L., He, Q., Hammond, C., Miedziak, P. J., Dimitratos, N., Sankar, M., . . . Hutchings, G. J. (2011). Selective oxidation of glycerol by highly active bimetallic catalysts at ambient temperature under base-free conditions. *Angewandte Chemie International Edition*, 50(43), 10136-10139. doi:10.1002/anie.201101772
- Butt, J. (2012). *Activation, Deactivation, and Poisoning of Catalysts*: Elsevier Science.
- Carretin, S., McMorn, P., Johnston, P., Griffin, K., Kiely, C. J., Attard, G. A., & Hutchings, G. J. (2004). Oxidation of glycerol using supported gold catalysts. *Topics in Catalysis*, 27, 6.
- Carretin, S., McMorn, P., Johnston, P., Griffin, K., Kiely, C. J., & Hutchings, G. J. (2003). Oxidation of glycerol using supported Pt, Pd and Au catalysts. *Physical Chemistry Chemical Physics*, 5(6), 1329-1336. doi:10.1039/b212047j
- Cavani, F., Trifiro, F., & Vaccari, A. (1991). Hydrotalcite-type Anionic Clays: Preparation, Properties and Application. *Catalysis Today*, 11, 129.
- Chiari, L., & Zecca, A. (2011). Constraints of fossil fuels depletion on global warming projections. *Energy Policy*, 39(9), 5026-5034. doi:<http://dx.doi.org/10.1016/j.enpol.2011.06.011>
- Chmielarz, L., Jabłońska, M., Strumiński, A., Piwowarska, Z., Węgrzyn, A., Witkowski, S., & Michalik, M. (2013). Selective catalytic oxidation of ammonia to nitrogen over Mg-Al, Cu-Mg-Al and Fe-Mg-Al mixed metal oxides doped with noble metals. *Applied Catalysis B: Environmental*, 130-131, 152-162. doi:10.1016/j.apcatb.2012.11.004

- Chornaja, S., Dubencov, K., Kampars, V., Stepanova, O., Zhizhkun, S., Serga, V., & Kulikova, L. (2012). Oxidation of glycerol with oxygen in alkaline aqueous solutions in the presence of supported palladium catalysts prepared by the extractive-pyrolytic method. *Reaction Kinetics, Mechanisms and Catalysis*, *108*(2), 341-357. doi:10.1007/s11144-012-0516-3
- Clark, J. H., Luque, R., & Matharu, A. S. (2012). Green Chemistry, Biofuels, and Biorefinery. *Annual Review of Chemical and Biomolecular Engineering*, *3*(1), 183-207. doi:doi:10.1146/annurev-chembioeng-062011-081014
- Comelli, R. A. (2011). Glycerol, the Co-Product of Biodiesel: One Key for the Future Bio-Refinery *BIODIESEL-QUALITY, EMISSIONS AND BY-PRODUCTS* (pp. 380): InTech.
- Condon, J. B. (2006). *Surface Area and Porosity Determinations By Physisorption*: Elsevier.
- Conesa, J. C., Esteban, P., Dexpert, H., & Bazin, D. (1990). Chapter 4 Characterization of Catalyst Structures by Extended X-Ray Absorption Spectroscopy. In J. L. G. Fierro (Ed.), *Studies in Surface Science and Catalysis* (Vol. Volume 57, Part A, pp. A225-A297): Elsevier.
- Cookson, J. (2012). The Preparation of Palladium Nanoparticles. *Platinum Metals Review*, *56*(2). doi:10.1595/147106712x632415
- Corma, A., Hamid, S., Iborra, S., & Velty, A. (2005). Lewis and Brønsted basic active sites on solid catalysts and their role in the synthesis of monoglycerides. *Journal of Catalysis*, *234*(2), 340-347. doi:10.1016/j.jcat.2005.06.023
- Corma, A., Iborra, S., & Velty, A. (2007). Chemical Routes for the Transformation of Biomass into Chemicals. *Chemical Reviews*, *107*, 92.
- Costa, N. J., & Rossi, L. M. (2012). Synthesis of supported metal nanoparticle catalysts using ligand assisted methods. *Nanoscale*, *4*(19), 5826-5834. doi:10.1039/c2nr31165h
- Davis, S. E., Ide, M. S., & Davis, R. J. (2013). Selective oxidation of alcohols and aldehydes over supported metal nanoparticles. *Green Chemistry*, *15*(1), 17-45. doi:10.1039/c2gc36441g
- Demirel-Gülen, S., Lucas, M., & Claus, P. (2005). Liquid phase oxidation of glycerol over carbon supported gold catalysts. *Catalysis Today*, *102-103*, 166-172. doi:10.1016/j.cattod.2005.02.033

- Demirel, S., Lucas, M., Wärnå, J., Salmi, T., Murzin, D., & Claus, P. (2007). Reaction kinetics and modelling of the gold catalysed glycerol oxidation. *Topics in Catalysis*, *44*(1), 299-305. doi:10.1007/s11244-007-0303-y
- Di Cosimo, J., Díez, V., Xu, M., Iglesia, E., & Apesteguía, C. (1998). Structure and surface and catalytic properties of Mg-Al basic oxides. *Journal of Catalysis*, *178*(2), 499-510.
- Díez, V. K., Apesteguía, C. R., & Di Cosimo, J. I. (2000). Acid–base properties and active site requirements for elimination reactions on alkali-promoted MgO catalysts. *Catalysis Today*, *63*(1), 53-62. doi:[http://dx.doi.org/10.1016/S0920-5861\(00\)00445-4](http://dx.doi.org/10.1016/S0920-5861(00)00445-4)
- Dimitratos, N., Lopez-Sanchez, J. A., Lennon, D., Porta, F., Prati, L., & Villa, A. (2006). Effect of Particle Size on Monometallic and Bimetallic (Au,Pd)/C on the Liquid Phase Oxidation of Glycerol. *Catalysis Letters*, *108*(3-4), 147-153. doi:10.1007/s10562-006-0036-8
- Dimitratos, N., Porta, F., & Prati, L. (2005). Au, Pd (mono and bimetallic) catalysts supported on graphite using the immobilisation method. *Applied Catalysis A: General*, *291*(1-2), 210-214. doi:10.1016/j.apcata.2005.01.044
- Dimitratos, N., Villa, A., Bianchi, C. L., Prati, L., & Makkee, M. (2006). Gold on titania: Effect of preparation method in the liquid phase oxidation. *Applied Catalysis A: General*, *311*, 185-192. doi:10.1016/j.apcata.2006.06.026
- Dimitratos, N., Villa, A., & Prati, L. (2009). Liquid Phase Oxidation of Glycerol Using a Single Phase (Au–Pd) Alloy Supported on Activated Carbon: Effect of Reaction Conditions. *Catalysis Letters*, *133*(3-4), 334-340. doi:10.1007/s10562-009-0192-8
- Durán-Valle, C. J. (2012). Techniques Employed in the Physicochemical Characterization of Activated Carbons *LIGNOCELLULOSIC PRECURSORS USED IN THE SYNTHESIS OF ACTIVATED CARBON* (pp. 37).
- El-Shafey, E. I., Ali, S. N. F., Al-Busafi, S., & Al-Lawati, H. A. J. (2016). Preparation and characterization of surface functionalized activated carbons from date palm leaflets and application for methylene blue removal. *Journal of Environmental Chemical Engineering*, *4*(3), 2713-2724. doi:<http://dx.doi.org/10.1016/j.jece.2016.05.015>
- Ernst, F., & Ruhle, M. (2003). *High-resolution imaging and spectrometry of materials*. Berlin Heidelberg: Springer-Verlag.

- Fadoni, M., & Lucarelli, L. (1999). Temperature programmed desorption, reduction, oxidation and flow chemisorption for the characterisation of heterogeneous catalysts. Theoretical aspects, instrumentation and applications. *Studies in Surface Science and Catalysis*, 120, 177-225.
- Farooq, A., Mehboob, S., Chaudhry, M. M., & Irfan, N. (2009). High Concentration Preferential Adsorption of Zinc Acetate onto Acid Treated Activated Carbon for Impregnation Purposes. *The Nucleus*, 46(3), 4.
- Gallezot, P. (1997). Selective oxidation with air on metal catalysts. *Catalysis Today*, 37, 14.
- Garcia, R., Besson, M., & Gallezot, P. (1995). Chemoselective catalytic oxidation of glycerol with air on platinum metals. *Applied Catalysis A: General*, 127, 12.
- Gil, S., Cuenca, N., Romero, A., Valverde, J. L., & Sánchez-Silva, L. (2014). Optimization of the synthesis procedure of microparticles containing gold for the selective oxidation of glycerol. *Applied Catalysis A: General*, 472, 11-20. doi:10.1016/j.apcata.2013.12.008
- Gil, S., Marchena, M., Sánchez-Silva, L., Romero, A., Sánchez, P., & Valverde, J. L. (2011). Effect of the operation conditions on the selective oxidation of glycerol with catalysts based on Au supported on carbonaceous materials. *Chemical Engineering Journal*, 178, 423-435. doi:10.1016/j.cej.2011.10.048
- Gil, S., Muñoz, L., Sánchez-Silva, L., Romero, A., & Valverde, J. L. (2011). Synthesis and characterization of Au supported on carbonaceous material-based catalysts for the selective oxidation of glycerol. *Chemical Engineering Journal*, 172(1), 418-429. doi:10.1016/j.cej.2011.05.108
- Goel, A., & Rani, N. (2012). Effect of PVP, PVA and POLE surfactants on the size of iridium nanoparticles. *Open Journal of Inorganic Chemistry*, 02(03), 67-73. doi:10.4236/ojic.2012.23010
- Hirasawa, S., Nakagawa, Y., & Tomishige, K. (2012). Selective oxidation of glycerol to dihydroxyacetone over a Pd–Ag catalyst. *Catalysis Science & Technology*, 2(6), 1150. doi:10.1039/c2cy20062g
- Hirasawa, S., Watanabe, H., Kizuka, T., Nakagawa, Y., & Tomishige, K. (2013). Performance, structure and mechanism of Pd–Ag alloy catalyst for selective oxidation of glycerol to dihydroxyacetone. *Journal of Catalysis*, 300, 205-216. doi:10.1016/j.jcat.2013.01.014

- Hu, W., Knight, D., Lowry, B., & Varma, A. (2010). Selective Oxidation of Glycerol to Dihydroxyacetone over Pt-Bi/C Catalyst: Optimization of Catalyst and Reaction Conditions. *Industrial & Engineering Chemistry Research*, 49, 7.
- Hutson, N. D., & Attwood, B. C. (2008). High temperature adsorption of CO₂ on various hydrotalcite-like compounds. *Adsorption*, 14(6), 781-789. doi:10.1007/s10450-007-9085-6
- Itodo, A., Abdulrahman, F., Hassan, L., Maigandi, S., & Itodo, H. (2010). Physicochemical parameters of Adsorbents from locally sorted H₃PO₄ and ZnCl₂ modified Agricultural wastes. *New York Science Journal*, 3(5), 8.
- J.L. Figueiredo, M.F.R. Pereira, M.M.A. Freitas, & Orfao, J. J. M. (1999). Modification of the surface chemistry of activated carbons. *Carbon* 37, 11.
- Jauncey, G. E. M. (1924). The Scattering of X-Rays and Bragg's Law. *Proceedings of the National Academy of Sciences of the United States of America*, 10(2), 57-60.
- Kalijadis, A., Vukcevic, M., Jovanovic, Z., Lausevic, Z., & Lausevic, M. (2011). Characterization of surface oxygen groups on different carbon materials by the Boehm method and temperature programmed desorption. *Journal of the Serbian Chemical Society*, 76(5), 757-768. doi:10.2298/jsc091224056k
- Kanezaki, E. (1998). Thermal behavior of the hydrotalcite-like layered structure of Mg and Al-layered double hydroxides with interlayer carbonate by means of in situ powder HTXRD and DTA/TG. *Solid State Ionics*, <HT>106</HT>(<HT>3-4</HT>), 279-284. doi:[http://dx.doi.org/10.1016/S0167-2738\(97\)00494-3](http://dx.doi.org/10.1016/S0167-2738(97)00494-3)
- Katryniok, B., Kimura, H., Skrzyńska, E., Girardon, J.-S., Fongarland, P., Capron, M., . . . Dumeignil, F. (2011). Selective catalytic oxidation of glycerol: perspectives for high value chemicals. *Green Chemistry*, 13(8), 1960. doi:10.1039/c1gc15320j
- Keatch, C. J., & Dollimore, D. (1975). *An introduction to thermogravimetry*. London; New York: Heyden.
- Kim, B.-H. (2014). Supercapacitive properties of nanoporous carbon nanofibers developed from polyacrylonitrile and tetraethyl orthosilicate. *Journal of Electroanalytical Chemistry*, 734, 84-89. doi:<http://dx.doi.org/10.1016/j.jelechem.2014.09.011>
- Kim, S. C. (1998). Pore development of the activated carbon prepared by steam activation process. *Journal of Industrial and Engineering Chemistry*, 4(3), 177-184.

- Klopprogge, J. T., Krisof, J., & Frost, R. L. (2001). *Thermogravimetric analysis-mass spectrometry (TGA-MS) of hydrotalcites containing CO₃²⁻, NO₃⁻, Cl⁻, SO₄²⁻ or ClO₄*. Paper presented at the A Clay Odyssey. Proceedings of the 12th International Clay Conference Bahai-Blanca, Argentina. July 22-28. <http://eprints.qut.edu.au/924/>
- Kovanda, F., Koloušek, D., Cílová, Z., & Hulínský, V. (2005). Crystallization of synthetic hydrotalcite under hydrothermal conditions. *Applied Clay Science*, 28(1-4), 101-109. doi:10.1016/j.clay.2004.01.009
- Kuśtrowski, P., Sułkowska, D., Chmielarz, L., & Dziembaj, R. (2006). Aldol condensation of citral and acetone over mesoporous catalysts obtained by thermal and chemical activation of magnesium–aluminum hydrotalcite-like precursors. *Applied Catalysis A: General*, 302(2), 317-324. doi:<http://dx.doi.org/10.1016/j.apcata.2006.02.003>
- Lee, D. W., & Yoo, B. R. (2014). Advanced metal oxide (supported) catalysts: Synthesis and applications. *Journal of Industrial and Engineering Chemistry*, 20(6), 3947-3959. doi:<http://dx.doi.org/10.1016/j.jiec.2014.08.004>
- Lee, H. J., Seung, D., Jung, K. S., Kim, H., & Filimonov, I. N. (2010). Etherification of glycerol by isobutylene: Tuning the product composition. *Applied Catalysis A: General*, 390(1-2), 235-244. doi:<http://dx.doi.org/10.1016/j.apcata.2010.10.014>
- Li, J., Ma, L., Li, X., Lu, C., & Liu, H. (2005). Effect of Nitric Acid Pretreatment on the Properties of Activated Carbon and Supported Palladium Catalysts. *Industrial & Engineering Chemistry Research*, 44, 5.
- Li, Z. (1977). *Novel solid base catalysts for Michael additions Synthesis, Characterization and Application*. (master of science), University of Berlin.
- Liu, H., Zhang, L., Wang, N., & Su, D. S. (2014). Palladium nanoparticles embedded in the inner surfaces of carbon nanotubes: synthesis, catalytic activity, and sinter resistance. *Angewandte Chemie International Edition*, 53(46), 12634-12638. doi:10.1002/anie.201406490
- Lu, N., Tang, S., Ryu, S.-K., & Choi, H.-S. (2005). Surface characterization of the activated carbon fibers after plasma polymerization of allylamine. *Carbon Science*, 6(4), 5.
- Ma, J., Ji, Y., Sun, H., Chen, Y., Tang, Y., Lu, T., & Zheng, J. (2011). Synthesis of carbon supported palladium nanoparticles catalyst using a facile homogeneous precipitation-reduction reaction method for formic acid electrooxidation. *Applied Surface Science*, 257(24), 10483-10488. doi:10.1016/j.apsusc.2011.07.007

- Mallat, T., & Baiker, A. (2004). Oxidation of Alcohols with Molecular Oxygen on Solid Catalysts. *Chemical Reviews*, *104*, 3037-3058.
- Mallesham, B., Sudarsanam, P., Reddy, B. V. S., & Reddy, B. M. (2016). Development of cerium promoted copper–magnesium catalysts for biomass valorization: Selective hydrogenolysis of bioglycerol. *Applied Catalysis B: Environmental*, *181*, 47-57. doi:<http://dx.doi.org/10.1016/j.apcatb.2015.07.037>
- Medford, A. J., Vojvodic, A., Hummelshøj, J. S., Voss, J., Abild-Pedersen, F., Studt, F., . . . Nørskov, J. K. (2015). From the Sabatier principle to a predictive theory of transition-metal heterogeneous catalysis. *Journal of Catalysis*, *328*, 36-42. doi:<http://dx.doi.org/10.1016/j.jcat.2014.12.033>
- Meryemoglu, B., Irmak, S., & Hasanoglu, A. (2016). Production of activated carbon materials from kenaf biomass to be used as catalyst support in aqueous-phase reforming process. *Fuel Processing Technology*, *151*, 59-63. doi:<http://dx.doi.org/10.1016/j.fuproc.2016.05.040>
- Mokhtar, M., Inayat, A., Ofili, J., & Schwieger, W. (2010). Thermal decomposition, gas phase hydration and liquid phase reconstruction in the system Mg/Al hydrotalcite/mixed oxide: A comparative study. *Applied Clay Science*, *50*(2), 176-181. doi:<http://dx.doi.org/10.1016/j.clay.2010.07.019>
- Moteki, T., Murakami, Y., Noda, S., Maruyama, S., & Okubo, T. (2011). Zeolite Surface As a Catalyst Support Material for Synthesis of Single-Walled Carbon Nanotubes. *The Journal of Physical Chemistry C*, *115*(49), 24231-24237. doi:10.1021/jp207930m
- Murzin, D., & Salmi, T. (2005). *Catalytic Kinetics*: Elsevier Science & Technology Books.
- Musialska, K., Finocchio, E., Sobczak, I., Busca, G., Wojcieszak, R., Gaigneaux, E., & Ziolk, M. (2010). Characterization of alumina- and niobia-supported gold catalysts used for oxidation of glycerol. *Applied Catalysis A: General*, *384*(1-2), 70-77. doi:10.1016/j.apcata.2010.06.006
- Namdeo, A., Mahajani, S. M., & Suresh, A. K. (2016). Palladium catalysed oxidation of glycerol—Effect of catalyst support. *Journal of Molecular Catalysis A: Chemical*, *421*, 45-56. doi:<http://dx.doi.org/10.1016/j.molcata.2016.05.008>
- Naresh, D., Kumar, V. P., Harisekhar, M., Nagaraju, N., Putrakumar, B., & Chary, K. V. R. (2014). Characterization and functionalities of Pd/hydrotalcite catalysts. *Applied Surface Science*, *314*, 199-207. doi:10.1016/j.apsusc.2014.06.156

- Nguyen, V. L., Nguyen, D. C., Hirata, H., Ohtaki, M., Hayakawa, T., & Nogami, M. (2010). Chemical synthesis and characterization of palladium nanoparticles. *Advances in Natural Sciences: Nanoscience and Nanotechnology*, 1(3), 035012. doi:10.1088/2043-6262/1/3/035012
- Nishimura, T., Kakiuchi, N., Inoue, M., & Uemura, S. (2000). Palladium(ii)-supported hydrotalcite as a catalyst for selective oxidation of alcohols using molecular oxygen. *Chemical Communications*(14), 1245-1246. doi:10.1039/b002447n
- Nwabanne, J., & Igbokwe, P. (2011). Preparation of activated carbon from Nipa palm nut: Influence of preparation conditions. *Research Journal of Chemical Sciences*, 1(6), 53-58.
- Omonmhenle, S. I., & Shannon, I. J. (2016). Synthesis and characterisation of surfactant enhanced Mg–Al hydrotalcite-like compounds as potential 2-chlorophenol scavengers. *Applied Clay Science*, 127–128, 88-94. doi:<http://dx.doi.org/10.1016/j.clay.2016.03.033>
- Ozbek, M. O., Onal, I., & Van Santen, R. A. (2011). Why silver is the unique catalyst for ethylene epoxidation. *Journal of Catalysis*, 284(2), 230-235. doi:<http://dx.doi.org/10.1016/j.jcat.2011.08.004>
- Pagliari, M., Ciriminna, R., Kimura, H., Rossi, M., & Della Pina, C. (2007). From glycerol to value-added products. *Angewandte Chemie International Edition*, 46(24), 4434-4440. doi:10.1002/anie.200604694
- Pagliari, M., & Rossi, M. (2010). *The Future of Glycerol*. Milan: RSC Publishing.
- Palmer, S. J., Frost, R. L., & Nguyen, T. (2009). Hydrotalcites and their role in coordination of anions in Bayer liquors: anion binding in layered double hydroxides. *Coordination Chemistry Reviews*, 253(1), 250-267.
- Pendem, C., Gupta, P., Chaudhary, N., Singh, S., Kumar, J., Sasaki, T., . . . Bal, R. (2012). Aqueous phase reforming of glycerol to 1,2-propanediol over Pt-nanoparticles supported on hydrotalcite in the absence of hydrogen. *Green Chemistry*, 14(11), 3107. doi:10.1039/c2gc36019e
- Pérez, C. N., Monteiro, J. L. F., López Nieto, J. M., & Henriques, C. A. (2009). Influence of basic properties of Mg, Al-mixed oxides on their catalytic activity in knoevenagel condensation between benzaldehyde and phenylsulfonylacetonitrile. *Química Nova*, 32(9), 2341-2346.
- Prati, L., Villa, A., Porta, F., Wang, D., & Su, D. (2007). Single-phase gold/palladium catalyst: The nature of synergistic effect. *Catalysis Today*, 122(3-4), 386-390. doi:10.1016/j.cattod.2006.11.003

- Prinetto, F., Manzoli, M., Ghiotti, G., Martinez Ortiz, M. d. J., Tichit, D., & Coq, B. (2004). Pd/Mg(Al)O catalysts obtained from hydrotalcites: investigation of acid–base properties and nature of Pd phases. *Journal of Catalysis*, 222(1), 238-249. doi:10.1016/j.jcat.2003.10.014
- Purushothaman, R. K. P. (2014). *Oxidation of glycerol to biobased chemicals using supported mono- and bimetallic noble metal catalysts*. (PhD research), University of Groningen.
- Rashidi, N. A., Yusup, S., Ahmad, M. M., Mohamed, N. M., & Hameed, B. H. (2012). Activated Carbon from the Renewable Agricultural Residues Using Single Step Physical Activation: A Preliminary Analysis. *APCBEE Procedia*, 3, 84-92. doi:10.1016/j.apcbee.2012.06.051
- Reyero, I., Velasco, I., Sanz, O., Montes, M., Arzamendi, G., & Gandía, L. M. (2013). Structured catalysts based on Mg–Al hydrotalcite for the synthesis of biodiesel. *Catalysis Today*, 216, 211-219. doi:10.1016/j.cattod.2013.04.022
- Rodrigues-Reinoso, F. (1998). The Role of Carbon Materials in The Heterogeneous Catalysis. *Carbon*, 36(3), 17.
- Rodrigues, E. G., Carabineiro, S. A. C., Delgado, J. J., Chen, X., Pereira, M. F. R., & Órfão, J. J. M. (2012). Gold supported on carbon nanotubes for the selective oxidation of glycerol. *Journal of Catalysis*, 285(1), 83-91. doi:10.1016/j.jcat.2011.09.016
- Rodrigues, E. G., Pereira, M. F. R., Chen, X., Delgado, J. J., & Órfão, J. J. M. (2013). Selective Oxidation of Glycerol over Platinum-Based Catalysts Supported on Carbon Nanotubes. *Industrial & Engineering Chemistry Research*, 52(49), 17390-17398. doi:10.1021/ie402331u
- Rouquerol, J., Avnir, D., Fairbridge, C., Everett, D., Haynes, J., Pernicone, N., . . . Unger, K. (1994). Recommendations for the characterization of porous solids (Technical Report). *Pure and Applied Chemistry*, 66(8), 1739-1758.
- Sariođlan, Ő. (2013). Recovery of Palladium from Spent Activated Carbon-Supported Palladium Catalysts. *Platinum Metals Review*, 57(4), 289-296. doi:10.1595/147106713x663988
- Sawoo, S., Srimani, D., Dutta, P., Lahiri, R., & Sarkar, A. (2009). Size controlled synthesis of Pd nanoparticles in water and their catalytic application in C–C coupling reactions. *Tetrahedron*, 65(22), 4367-4374. doi:10.1016/j.tet.2009.03.062

Schwengber, C. A., Alves, H. J., Schaffner, R. A., da Silva, F. A., Sequinel, R., Bach, V. R., & Ferracin, R. J. (2016). Overview of glycerol reforming for hydrogen production. *Renewable and Sustainable Energy Reviews*, 58, 259-266. doi:<http://dx.doi.org/10.1016/j.rser.2015.12.279>

Serwicka, E. M. (2000). Surface area and porosity, X-ray diffraction and chemical analyses. *Catalysis Today*, 56(4), 335-346. doi:[http://dx.doi.org/10.1016/S0920-5861\(99\)00293-X](http://dx.doi.org/10.1016/S0920-5861(99)00293-X)

Shaarani, F. W., & Hameed, B. H. (2011). Ammonia-modified activated carbon for the adsorption of 2,4-dichlorophenol. *Chemical Engineering Journal*, 169(1-3), 180-185. doi:<http://dx.doi.org/10.1016/j.cej.2011.03.002>

Shen, W., Li, Z., & Liu, Y. (2007). China Patent No. Bentham Science Publishers Ltd: C. Engineeing.

Siyo, B. (2014). *Development of Palladium Nanoparticles Based Catalysts for Aerobic Oxidation of 5-Hydroxymethylfurfural and Glycerol*. (doctoral degree), University of Rostock.

Skrzyńska, E., Wondolowska-Grabowska, A., Capron, M., & Dumeignil, F. (2014). Crude glycerol as a raw material for the liquid phase oxidation reaction. *Applied Catalysis A: General*, 482, 245-257. doi:10.1016/j.apcata.2014.06.005

Sobczak, I., Jagodzinska, K., & Ziolk, M. (2010). Glycerol oxidation on gold catalysts supported on group five metal oxides—A comparative study with other metal oxides and carbon based catalysts. *Catalysis Today*, 158(1-2), 121-129. doi:10.1016/j.cattod.2010.04.022

Sobrino, F. H., & Monroy, C. R. (2009). Critical analysis of the European Union directive which regulates the use of biofuels: An approach to the Spanish case. *Renewable and Sustainable Energy Reviews*, 13(9), 2675-2681. doi:10.1016/j.rser.2009.05.003

Srirangan, K., Akawi, L., Moo-Young, M., & Chou, C. P. (2012). Towards sustainable production of clean energy carriers from biomass resources. *Applied Energy*, 100, 172-186. doi:<http://dx.doi.org/10.1016/j.apenergy.2012.05.012>

Stefenelli, M., Todt, J., Riedl, A., Ecker, W., Müller, T., Daniel, R., . . . Keckes, J. (2013). X-ray analysis of residual stress gradients in TiN coatings by a Laplace space approach and cross-sectional nanodiffraction: a critical comparison. *Journal of applied crystallography*, 46(5), 1378-1385.

- Sudarsanam, P., Mallesham, B., Prasad, A. N., Reddy, P. S., & Reddy, B. M. (2013). Synthesis of bio-additive fuels from acetalization of glycerol with benzaldehyde over molybdenum promoted green solid acid catalysts. *Fuel Processing Technology*, *106*, 539-545. doi:<http://dx.doi.org/10.1016/j.fuproc.2012.09.025>
- Takehira, K., Shishido, T., Wang, P., Kosaka, T., & Takaki, K. (2004). Autothermal reforming of CH₄ over supported Ni catalysts prepared from Mg–Al hydrotalcite-like anionic clay. *Journal of Catalysis*, *221*(1), 43-54. doi:10.1016/j.jcat.2003.07.001
- Tan, H. W., Abdul Aziz, A. R., & Aroua, M. K. (2013). Glycerol production and its applications as a raw material: A review. *Renewable and Sustainable Energy Reviews*, *27*, 118-127. doi:<http://dx.doi.org/10.1016/j.rser.2013.06.035>
- Teng, H., Lin, Y.-C., & Hsu, L.-Y. (2000). Production of Activated Carbons from Pyrolysis of Waste Tires Impregnated with Potassium Hydroxide. *Journal of the Air & Waste Management Association*, *50*(11), 1940-1946. doi:10.1080/10473289.2000.10464221
- Tessonnier, J.-P., Rosenthal, D., Hansen, T. W., Hess, C., Schuster, M. E., Blume, R., . . . Schlögl, R. (2009). Analysis of the structure and chemical properties of some commercial carbon nanostructures. *Carbon*, *47*(7), 1779-1798. doi:10.1016/j.carbon.2009.02.032
- Titiladunayo, I., & Fapetu, O. (2011). Selection of appropriate clay for furnace lining in a pyrolysis process.
- Toebes, M. L., van Dillen, J. A., & de Jong, K. P. (2001). Synthesis of supported palladium catalysts. *Journal of Molecular Catalysis A: Chemical*, *173*(1–2), 75-98. doi:[http://dx.doi.org/10.1016/S1381-1169\(01\)00146-7](http://dx.doi.org/10.1016/S1381-1169(01)00146-7)
- Tongsakul, D., Nishimura, S., Thammacharoen, C., Ekgasit, S., & Ebitani, K. (2012). Hydrotalcite-Supported Platinum Nanoparticles Prepared by a Green Synthesis Method for Selective Oxidation of Glycerol in Water Using Molecular Oxygen. *Industrial & Engineering Chemistry Research*, *51*(50), 16182-16187. doi:10.1021/ie3020507
- Tongsakul, D., Wongravee, K., Thammacharoen, C., & Ekgasit, S. (2012). Enhancement of the reduction efficiency of soluble starch for platinum nanoparticles synthesis. *Carbohydrate Research*, *357*, 90-97. doi:10.1016/j.carres.2012.04.012
- Tsuji, A., Rao, K. T., Nishimura, S., Takagaki, A., & Ebitani, K. (2011). Selective oxidation of glycerol by using a hydrotalcite-supported platinum catalyst under atmospheric oxygen pressure in water. *ChemSusChem*, *4*(4), 542-548. doi:10.1002/cssc.201000359

- Uprety, B. K., Chaiwong, W., Ewelike, C., & Rakshit, S. K. (2016). Biodiesel production using heterogeneous catalysts including wood ash and the importance of enhancing byproduct glycerol purity. *Energy Conversion and Management*, 115, 191-199. doi:<http://dx.doi.org/10.1016/j.enconman.2016.02.032>
- Vermani, O. P. (2003). *Applied Chemistry: Theory and Practice*: New Age International.
- Villa, A., Janjic, N., Spontoni, P., Wang, D., Su, D. S., & Prati, L. (2009). Au–Pd/AC as catalysts for alcohol oxidation: Effect of reaction parameters on catalytic activity and selectivity. *Applied Catalysis A: General*, 364, 221-228.
- Villa, A., Wang, D., Dimitratos, N., Su, D., Trevisan, V., & Prati, L. (2010). Pd on carbon nanotubes for liquid phase alcohol oxidation. *Catalysis Today*, 150(1-2), 8-15. doi:10.1016/j.cattod.2009.06.009
- Villa, A., Wang, D., Su, D. S., & Prati, L. (2009). Gold sols as catalysts for glycerol oxidation: The role of stabilizer. *ChemCatChem*, 1(4), 510-514.
- Villa, A., Wang, D., Veith, G. M., & Prati, L. (2012). Bismuth as a modifier of Au–Pd catalyst: Enhancing selectivity in alcohol oxidation by suppressing parallel reaction. *Journal of Catalysis*, 292, 73-80. doi:10.1016/j.jcat.2012.04.021
- Voll, M., & Boehm, H. P. (1971). Basische Oberflächenoxide auf Kohlenstoff—IV. Chemische Reaktionen zur Identifizierung der Oberflächengruppen. *Carbon*, 9(4), 481-488. doi:[http://dx.doi.org/10.1016/0008-6223\(71\)90028-5](http://dx.doi.org/10.1016/0008-6223(71)90028-5)
- Vulic, T. J., Reitzmann, A. F. K., & Lázár, K. (2012). Thermally activated iron containing layered double hydroxides as potential catalyst for N₂O abatement. *Chemical Engineering Journal*, 207-208, 913-922. doi:10.1016/j.cej.2012.06.152
- Wang, J., & Chen, B. (2015). Adsorption and coadsorption of organic pollutants and a heavy metal by graphene oxide and reduced graphene materials. *Chemical Engineering Journal*, 281, 379-388. doi:<http://dx.doi.org/10.1016/j.cej.2015.06.102>
- Wen, G., Xu, Y., Ma, H., Xu, Z., & Tian, Z. (2008). Production of hydrogen by aqueous-phase reforming of glycerol. *International Journal of Hydrogen Energy*, 33(22), 6657-6666. doi:<http://dx.doi.org/10.1016/j.ijhydene.2008.07.072>
- Williams, D. B., & Carter, C. B. (1996). *Transmission Electron Microscopy*.
: Springer US.

- Wu, G., Wang, X., Guan, N., & Li, L. (2013). Palladium on graphene as efficient catalyst for solvent-free aerobic oxidation of aromatic alcohols: Role of graphene support. *Applied Catalysis B: Environmental*, 136-137, 177-185. doi:10.1016/j.apcatb.2013.01.067
- . X-ray Fluorescence (XRF) and Particle-Induced X-ray Emission (PIXE). (2007) *Atomic and Nuclear Analytical Methods: XRF, Mössbauer, XPS, NAA and B63Ion-Beam Spectroscopic Techniques* (pp. 1-90). Berlin, Heidelberg: Springer Berlin Heidelberg.
- Xie, W., Peng, H., & Chen, L. (2006). Calcined Mg–Al hydrotalcites as solid base catalysts for methanolysis of soybean oil. *Journal of Molecular Catalysis A: Chemical*, 246(1-2), 24-32. doi:10.1016/j.molcata.2005.10.008
- Y. Zhang, Z. Tang, Maroto-Valer, M. M., & Andrésen, J. M. (2003). Development of Microporous Activated Carbons from Unburned Carbon in Fly Ash. *Fuel Chemistry Division Preprints*, 48(1), 2.
- Yang, F., Hanna, M. A., & Sun, R. (2012). Value-added uses for crude glycerol--a byproduct of biodiesel production. *Biotechnol Biofuels*, 5, 13. doi:10.1186/1754-6834-5-13
- Yang, H., Xu, S., Jiang, L., & Dan, Y. (2012). Thermal Decomposition Behavior of Poly (Vinyl Alcohol) with Different Hydroxyl Content. *Journal of Macromolecular Science, Part B*, 51(3), 464-480. doi:10.1080/00222348.2011.597687
- Yang, H., Yan, R., Chen, H., Lee, D. H., & Zheng, C. (2007). Characteristics of hemicellulose, cellulose and lignin pyrolysis. *Fuel*, 86(12–13), 1781-1788. doi:<http://dx.doi.org/10.1016/j.fuel.2006.12.013>
- Yang, W., Kim, Y., Liu, P. K., Sahimi, M., & Tsotsis, T. T. (2002). A study by in situ techniques of the thermal evolution of the structure of a Mg–Al–CO₃ layered double hydroxide. *Chemical Engineering Science*, 57(15), 2945-2953.
- Yang, X., Yang, L., Lin, S., & Zhou, R. (2014). Effects of the addition of small quantities of ceria on the catalytic behavior of Pd-only close-coupled catalysts during automobile exhaust elimination. *Chinese Journal of Catalysis*, 35(8), 1267-1280. doi:[http://dx.doi.org/10.1016/S1872-2067\(14\)60157-1](http://dx.doi.org/10.1016/S1872-2067(14)60157-1)
- Yu, B., Chang, Z., & Wang, C. (2016). The key pre-pyrolysis in lignin-based activated carbon preparation for high performance supercapacitors. *Materials Chemistry and Physics*, 181, 187-193. doi:<http://dx.doi.org/10.1016/j.matchemphys.2016.06.048>

- Zhang, M., Liang, D., Nie, R., Lu, X., Chen, P., & Hou, Z. (2012). Oxidation of Biodiesel Glycerol over Pt Supported on Different Sized Carbon Supports in Base-Free Solution. *Chinese Journal of Catalysis*, 33(7-8), 1340-1346. doi:10.1016/s1872-2067(11)60411-7
- Zhang, M., Nie, R., Wang, L., Shi, J., Du, W., & Hou, Z. (2015). Selective oxidation of glycerol over carbon nanofibers supported Pt catalysts in a base-free aqueous solution. *Catalysis Communications*, 59, 5-9. doi:10.1016/j.catcom.2014.09.036
- Zhang, Q., Ma, L., Lu, C., Xu, X., Lyu, J., & Li, X. (2015). Solvent-free selective hydrogenation of o-chloronitrobenzene over large palladium particles on oxygen-poor activated carbon. *Reaction Kinetics, Mechanisms and Catalysis*, 114(2), 629-638. doi:10.1007/s11144-014-0826-8
- Zhang, Z., & Yang, Z. (2013). Theoretical and practical discussion of measurement accuracy for physisorption with micro- and mesoporous materials. *Chinese Journal of Catalysis*, 34(10), 1797-1810. doi:[http://dx.doi.org/10.1016/S1872-2067\(12\)60601-9](http://dx.doi.org/10.1016/S1872-2067(12)60601-9)
- Zhao, B., Li, C., & Xu, C. (2012). Insight into the catalytic mechanism of glycerol hydrogenolysis using basal spacing of hydrotalcite as a tool. *Catalysis Science & Technology*, 2(9), 1985-1994. doi:10.1039/C2CY20144E
- Zhao, Y., Jia, L., Medrano, J. A., Ross, J. R. H., & Lefferts, L. (2013). Supported Pd Catalysts Prepared via Colloidal Method: The Effect of Acids. *ACS Catalysis*, 3(10), 2341-2352. doi:10.1021/cs4004479
- Zhao, Z., Arentz, J., Pretzer, L. A., Limpornpipat, P., Clomburg, J. M., Gonzalez, R., . . . Wong, M. S. (2014). Volcano-shape glycerol oxidation activity of palladium-decorated gold nanoparticles. *Chemical Science*, 5(10), 3715. doi:10.1039/c4sc01001a
- Zhou, C. H., Beltramini, J. N., Fan, Y. X., & Lu, G. Q. (2008). Chemoselective catalytic conversion of glycerol as a biorenewable source to valuable commodity chemicals. *Chemical Society Reviews*, 37(3), 527-549. doi:10.1039/b707343g
- Zhu, Y., Qian, H., & Jin, R. (2010). An atomic-level strategy for unraveling gold nanocatalysis from the perspective of Au(n)(SR)m nanoclusters. *Chemistry*, 16(37), 11455-11462. doi:10.1002/chem.201001086
- Zope, B. N., Davis, S. E., & Davis, R. J. (2012). Influence of Reaction Conditions on Diacid Formation During Au-Catalyzed Oxidation of Glycerol and Hydroxymethylfurfural. *Topics in Catalysis*, 55(1-2), 24-32. doi:10.1007/s11244-012-9777-3

LIST OF PUBLICATIONS AND PAPERS PRESENTED

Proceeding Paper

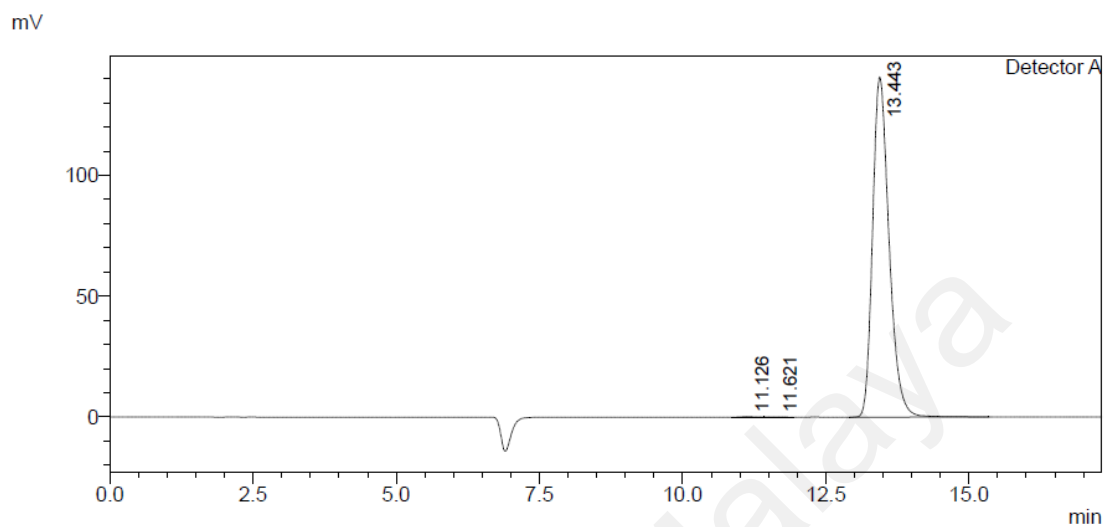
Norfatehah Basiron, Sharifah Bee Abdul Hamid, Wageeh A. Yehya, Selective Oxidation of Glycerol under Base-Free Condition over Supported Palladium Metal-Based Catalysts, 1st ICRIL-INternatioanl Conference on Innovation in Science and Technology (IICIST 2015), April 2015, UTM Kuala Lumpur

ISI Paper (Published)

Hamid, S. B. A., N. Basiron, W. A. Yehya, P. Sudarsanam and S. K. Bhargava "Nanoscale Pd-based catalysts for selective oxidation of glycerol with molecular oxygen: Structure-activity correlations." Polyhedron.

APPENDIX

HPLC calculation for 1wt% Pd/AC1



No	Name	Retention time	Area	Height
1	Glyceraldehyde GLYALD	11.621	1559	95
2	Glyceic acid (GLYAC)	11.126	3040	174
3	Glycerol (GLY)	13.443	2827544	140718
4	water	18.901	110764	50031

Conversion of glycerol (X_{GLY}):

$$X_{GLY} = \frac{y}{x} \quad x = \text{Total area of the peaks} - \text{area of the solvent peak}$$

$$y = x - \text{area of starting material peaks}$$

$$x = (1559 + 3040 + 2827544 + 110764) - 110764$$

$$= 2832143$$

y = x — area of starting material peaks

$$y = 2832143 - 2827544$$

$$= 4599$$

$$X_{\text{GLY}} = \frac{y}{x} \times 100$$

$$= \frac{4599}{2832143} \times 100$$

$$= 0.16\%$$

$$\text{Selectivity}_{\text{GLYAC}} = S_{\text{products}} = \frac{\text{area of the product peaks}}{\text{total peak area of the products}} \times 100$$

$$= \frac{3040}{3040+1559} \times 100$$

$$= 66.10\%$$

$$\text{TOF} = \frac{\text{mmol of converted glycerol}}{\text{mmol of total Pd} \times \text{Reaction time (hour)}}$$

$$: \text{mol} = \text{RF} \times \text{area}$$

$$\text{RF} = \frac{1}{m} \quad m = \text{slope of calibration curve}$$

$$: \text{slope of glycerol calibration curve} = 351328$$

$$: \text{RF} = \frac{1}{351328} = 2.8463 \times 10^{-6}$$

$$\text{mol of converted glycerol} = 2.8463 \times 10^{-6} \times (\text{Glycerol}_{\text{in}} - \text{Glycerol}_{\text{out}})$$

$$= 2.8463 \times 10^{-6} \times (2942907 - 2827544)$$

$$= 3.2836 \times 10^{-4} \text{ mol}$$

$$\text{TOF} = \frac{3.2836 \times 10^{-4}}{(4.2857 \times 10^{-6}) \times 3}$$

$$= 25.54 \text{ h}^{-1}$$